TESI

PRESENTATA A CONCLUSIONE DEL CORSO DI PERFEZIONAMENTO IN "SCIENZE DEI MATERIALI" FINANZIATO DALLA SOCIETÀ MAPEI S.P.A.

Chain entanglements and fracture energy in interfaces between immiscible polymers

Leonardo Silvestri

SUPERVISORS: *Chiar.^{mo} Prof. Franco Bassani*
Chiar.^{mo} Prof. Sergio Carrà

August 4, 2003

To Camelia

Abstract

Entanglements are the ultimate source of toughness in glassy polymers, in fact at molecular weights lower than the critical molecular weight for entanglements they become quite brittle. Similarly, the strength of an interface between two immiscible glassy polymers is determined by the density of entangled strands that cross it, usually denoted by Σ_{eff}. This is a microscopic quantity that cannot be measured or controlled directly, except in very special cases, and therefore it is important to relate it to some significative macroscopic parameter characterizing the interface. In recent years many experimental works proved that there is a clear correlation between the toughness of an interface between glassy polymers and its width, so that models of entanglements at interfaces have become necessary to interpret the data. Some theoretical approaches have been proposed in the last few years, but their agreement with experimental data cannot be considered completely satisfactory.

In this thesis we propose a new model to describe entanglements at interfaces, that relates the fracture energy of an interface between immiscible polymers to its width [1]. The role of other important parameters, first of all the molecular weight of the polymers, is also investigated.

The starting point is a study of the interfaces between immiscible polymers at thermodynamical equilibrium. To this end we use a Self Consistent Field approach, which is suitable for the strong and intermediate segregation regime, to numerically derive concentration profiles and mean fields.

The central part of this work is devoted to the calculation of Σ_{eff}, with a method, based on a mean field approximation, that it is a generalization of the stochastic

approach successfully applied by Mikos and Peppas [2] to symmetric interfaces. Numerical results are obtained using the Self Consistent mean fields and the dependence of Σ_{eff} on the interface width and polymers molecular weights is shown. Following previous literature descriptions, possible fracture mechanisms, depending on the values of Σ_{eff}, are then discussed and a new fracture regime is introduced, called "partial crazing", to account for the intermediate situation in which a craze starts in one of the two materials but it cannot fully develop. Numerical results for the fracture energy as a function of interface width and polymers molecular weights are compared with literature experimental data, showing good agreement. In the case of PMMA/P(S-r-MMA) interfaces, the dependence of the fracture energy on the interfacial width could be reproduced very well over the whole range of investigated widths, more satisfactory than in previous literature works.

The last chapter of this work is focused on the calculation of the molecular weight of entanglements M_e, which influences greatly the value of Σ_{eff}. This quantity has been measured in bulk polymers, but, to our knowledge, never at a polymer-polymer interface. Moreover, theories that clarify the nature of entanglements and allow speculations on the value of M_e in inhomogeneous systems, have been proposed only recently. In this work the packing model for entanglements is adopted to estimate the value of M_e at polymer-polymer interfaces and in thin polymer films. Our numerical results show that the molecular weight of entanglement of chains near an interface is larger than in the bulk, leading to appreciable corrections in the Σ_{eff} and fracture energy calculations. We also compute the average molecular weight of entanglements in thin films, and predict that it should increase as the thickness of the film decreases below the entanglement length.

Acknowledgements

This Ph.D Thesis concludes a three years research at the Scuola Normale Superiore in Pisa financially supported by MAPEI S.p.A., that the author wishes to thank.

There are a number of people who assisted in preparation of this thesis. First of all I wish to thank my supervisors, Prof. Franco Bassani and Prof. Sergio Carrà, who have been a constant source of encouragement and guidance throughout my whole Ph.D studies. Thanks also goes to Stefano Carrà for his precious suggestions and for being always ready to offer his help in both scientific and everyday matters.

I'm also grateful to Prof. Hugh Brown, with whom I have had the pleasure of collaborating at the University of Wollongong. I will never be able to thank him enough for the time he has dedicated to me and for the enlightening discussions we had. I would also like to thank Robert Oslanec for his help with the numerical calculations and for sharing with me his computer programs.

This work wouldn't have been possible without the support of my family, who backed me during the frantic days of its preparation.

The final lines are for Camelia, who listened to my endless talking about polymers and spent her summer days checking the final manuscript with me. To her this thesis is dedicated.

Contents

Chapter 1

Introduction

The adhesion of polymers is relevant in many scientific and technological areas and has become in recent years a very important field of study [3]-[7]. Its main application is bonding by adhesives, but adhesion is also involved whenever two polymers are brought into contact, as in coatings, paints, polymer blends, filled polymers or composite materials. Even the toughness of a bulk polymer, for example, can be viewed as a problem of adhesion between two pieces of the same material. In general the final performance of these materials depends significantly on the quality of the interfaces formed inside them; it is therefore understandable that a better knowledge of adhesion is very important for many practical applications. Yet only 50 years ago adhesion became a scientific subject in its own right. The reason is probably that the understanding of adhesion requires a knowledge in many different fields, ranging from macromolecular science and physical chemistry of surfaces and interfaces to materials science, mechanics and rheology. It is well known for example that adhesive properties of polymeric materials rely not only on the strength of interfaces they can form, that have to sustain the stress, but most of all on their ability to dissipate energy in the bulk. A full comprehension of both aspects of the problem involves then many different research fields, as we will see for glassy polymers systems.

The first subtle question that needs to be answered when studying this subject is probably how toughness is measured. In fact it is not obvious what is the best physical quantity to characterize the strength of an interface. One could say that it

is the maximum stress that the interface can sustain, called "fracture strength", but this is not the best choice. In real systems there are always flaws and cracks leading to values of the local stress much higher than the average applied stress. The result is that interfaces usually fail much earlier than expected. A more useful approach is to invoke an energy criterion: an interface fails if a pre-existing crack can grow. This happens when the strain energy released by the failure of the interface is greater than the energy needed to create two new surfaces. The strength of an interface in practical cases is therefore related to the latter quantity, that is called "fracture energy" and is indicated with G_c.

The problem that we face now is how to estimate G_c for glassy polymers. If we could separate two surfaces A and B in a thermodynamically reversible way, then the fracture energy would be equal to the work of adhesion $W_{AB} = \sigma_A + \sigma_B - \sigma_{AB}$, where σ_A and σ_B are the surface tensions and σ_{AB} is the interfacial tension. For an interface between two identical material the above formula gives a work of cohesion of twice the surface tension. With such an approach we would obtain for glassy polymers a fracture energy of about 0.1 J/m^2 [8], while measured fracture energies of many glassy polymers reach values four order of magnitude higher and are strongly dependent on the polymer molecular weight [9]-[12]. In particular a transition is observed at molecular weights close to the critical molecular weight for entanglement M_c, after which the fracture energy increases abruptly and then reaches a plateau at infinite molecular weight, as shown in Figure 1.1. High fracture energies are also known to be associated with the intermediate formation of a craze, that is a plastic deformation, localized around the crack zone, capable of dissipating a great amount of energy [13]-[15]. These experimental observations make it immediately clear that entangled chains are essential to improve cohesion and to obtain crazing in the bulk; nevertheless a quantitative explanation of the experimental results has not been achieved for many years.

It is easy to imagine that, when trying to propagate a crack inside a glassy polymer, all the chains that are entangled at both sides of the crack will oppose some resistance. Such a chain coupling across the interface can be described by the areal density of entangled strands that cross it, indicated by Σ_{eff}, which is

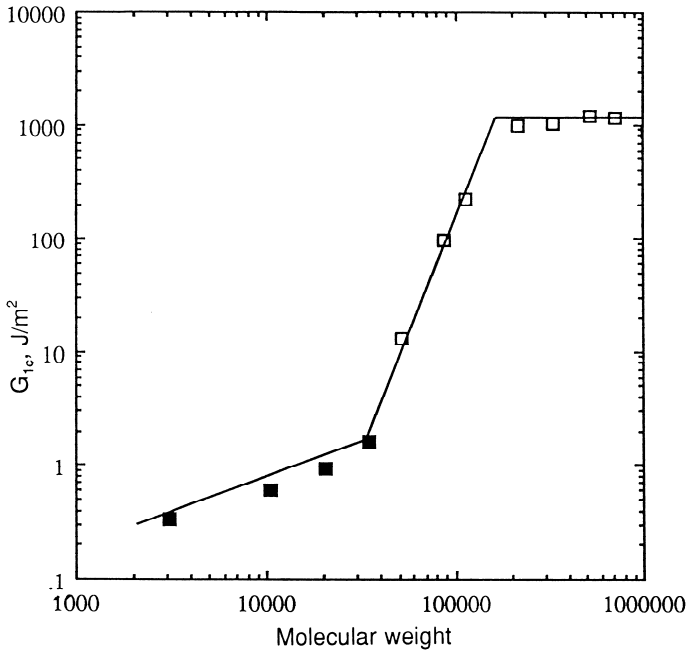

Figure 1.1: Fracture energy G_{1c} versus molecular weight, for PS in the virgin state. The fracture energy starts to increase very quickly at $M_c \approx 32000$, and reaches a plateau at $M \approx 8M_c$. After R.P. Wool [6].

proportional to the maximum stress an interface can withstand. For symmetric interfaces a simple model, similar to Lake and Thomas theory of elastomers [16], predicts $\Sigma_{\text{eff}} = \rho_e L_e/2$, where ρ_e is the density of entanglements and L_e is the root mean square end to end distance between them [13]. Such an expression is correct in the limit of infinite molecular weights, but can not explain the molecular weight dependence of the fracture strength found experimentally. A more accurate expression was derived by Mikos and Peppas [2], who used a stochastic approach to count the number of coupling strands across a fracture plane in bulk polymers and included chain end effects in their analysis. They subdivided each chain in segments of N_e monomers and assumed that each of them formed an entanglement, except the first and last ones. In this way they could take into account the fact that dangling ends do not contribute to entanglements, and predicted that the infinite molecular weight Σ_{eff} should be scaled by a factor $1 - 2M_e/M$. This agrees with the normalized experimental data and with the observation that usually $M_c \approx 2M_e$. Yet

the connection between Σ_{eff} and the fracture energy still posed problems, because of the difficulties in describing crazing. Crazed material was believed to be made of parallel load-bearing fibrils running perpendicularly to the interface, so that any theory predicted a fracture energy proportional to Σ_{eff}. The problem was that, in order to reproduce experimental results, the energy needed to break C-C bonds should have been one order of magnitude higher than the measured values. The solution was found by Brown [17], who first recognized the importance of the cross-tie fibrils that connects primary fibrils and are capable of transferring load. He modelled the craze as an elastic continuum and computed the stress amplification at the crack tip, demonstrating that $G_c \propto \Sigma_{\text{eff}}^2$, as described in detail in section 3.3. This scaling law has been confirmed since then by a number of experiments performed on interfaces reinforced by block copolymers, and could finally explain the high fracture energies of glassy polymers. A summary of the mentioned experimental data is presented in Figure 1.2, while experimental details are discussed further down in this section.

In technology the use of pure materials is rare, because usually people need to combine in a single mixture the properties of different materials. Unfortunately, in the absence of specific interactions, most of polymers are immiscible so that in mixing them you end up with a number of coarse domains of the pure materials. Moreover the interfaces between such domains are very weak, with the result that the final composite material is useless. For these reasons a knowledge of the interfacial properties is often very important from a technological point of view.

The starting point of any study of the strength of an interface is a knowledge of the equilibrium properties of the interphase between them, and the most interesting quantity to know is probably the degree of interpenetration between species, or in other words the concentration profiles. The two general theoretical approaches for describing interfacial properties of polymer system are based on Self Consistent Field (SCF) [18]-[29] and Density Functional methods [30]-[39]. The latter approach consists in writing the free energy of an inhomogeneous system as a functional of the unknown densities, that are then found by minimization of such a free energy. The free energy functional is generally written as a functional expansion around the

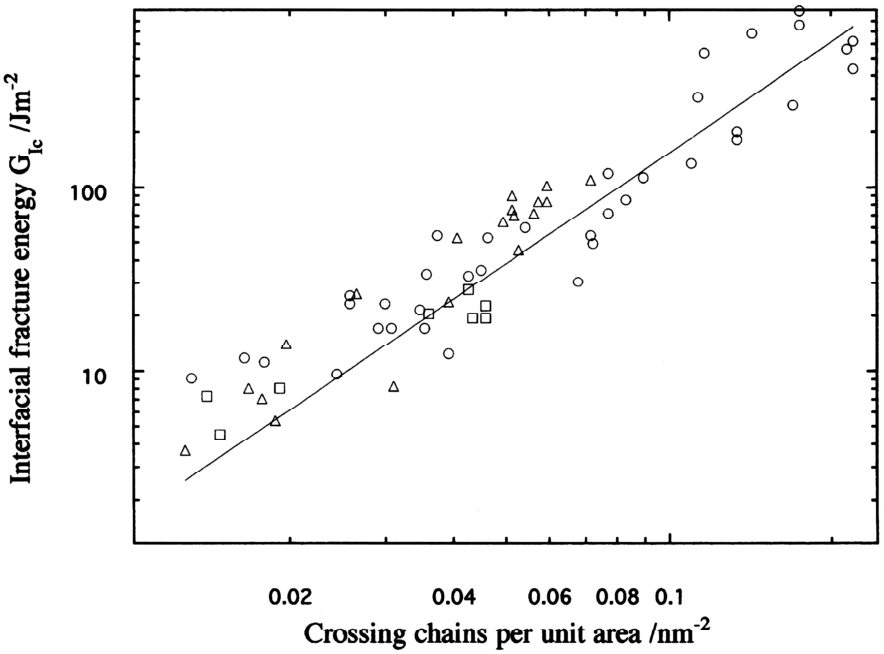

Figure 1.2: Fracture energy of interfaces reinforced with block copolymers as a function of the effective areal density of chains crossing the interface. Triangles and squares are for polystyrene/poly(2-vinyl pyridine) interfaces reinforced with styrene-2-vinyl pyridine block copolymers [56]. Circles are for poly(xylenyl ether)/poly(methyl methacrylate) interfaces reinforced with styrene-methyl methacrylate block copolymers [17],[57]. After Creton et al. [56].

homogeneous blend expression. Due to its nature this method is appropriate only for weakly immiscible polymer pairs and wide interfaces, when the square gradient term alone is sufficient, but it has the great advantage that analytical results can be often obtained. Self Consistent Field approaches require instead computer intensive calculations, but can also be used in the intermediate and strong segregation regimes. The SCF method is the one we adopted and will be described in detail in chapter 2; we only recall here briefly recall how this method works. Mean fields are expressed as functionals of the densities, that in turn can be computed from a probability density satisfying a modified diffusion equation with a potential term given by the above mean fields. The corresponding coupled equations for fields and densities are then solved numerically by a self-consistent algorithm.

Both of the above described approaches are usually based on a simple incom-

pressible Flory-Huggins expression for the homogeneous polymer blend [3], that is sufficiently detailed for our study of the interface toughness. However it is worth mentioning that more sophisticated expressions are available, to include the effects of compressibility, specific interactions, block copolymers, grafted chains, etc.. [40]-[41]. An interesting improvement in this sense is the Lattice Cluster Theory (LCT) by Dudowicz and Freed [41]. It is a lattice based model, where monomers are allowed to occupy more than one site and to have different structures, while compressibility is taken into account by adding voids as non-interacting particles occupying only one site. Corrections to the mean field approximation are then systematically added to the free energy expression through a double power expansion in the microscopic interaction energies and in the inverse lattice coordination number. With this approach Freed and coworkers could explain effects due to monomer structures, as the temperature independent term in the effective interaction parameter χ, that is due to non-combinatorial entropy of mixing, or the miscibility of polyolefin blends [42].

The theories described above have been extensively tested against experimental results for interfacial widths and tensions, displaying a good agreement within their range of validity [43]-[49].

The toughness of interfaces between immiscible polymers instead has started to be investigated only recently, raising new questions about the concept of entanglement. The typical experiments on these systems are set up as follows. Two immiscible glassy polymers are annealed at a temperature T above the glass transition temperatures, T_g, of the two species, for a time that is long enough to reach thermodynamical equilibrium. Then the system is cooled down very quickly to room temperature and the fracture energy of the glassy joint is measured. This measurement is usually performed by an asymmetric double cantilever beam test, in which two welded polymer bars of different thicknesses are driven apart by a razor blade of known width, as illustrated in Figure 1.3. The length of the crack ahead of the blade is then measured and the fracture energy is computed from the known geometric and elastic properties of the beams. In such experiments the ratio of bar thicknesses is chosen to obtain the smallest value of the fracture energy; in this situation the crack propagates at the interface and the applied stress is purely tensile. The cor-

responding fracture is usually referred to as mode I, and the corresponding energy is sometimes indicated with G_{Ic}. Mode I failure gives the lowest values of fracture energy and it is also better understood from a theoretical point of view. These experiments have been performed for a range of different materials and experimental conditions [50]-[58], so that some data are now available in the literature, allowing theoretical models to be tested.

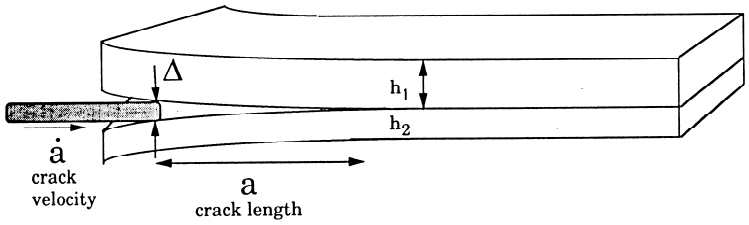

Figure 1.3: Asymmetric Double Cantilever Beam Test. The arrangement is asymmetric to compensate for differences in elastic and crazing properties between the two materials, as discussed in the text. After Creton et al. [56].

The first conclusion that can be drawn is that entanglements are essential in strengthening the interfaces between immiscible polymers. Many experimental groups have measured, for instance, the interfacial fracture energy between polystyrene (PS) and poly(methyl methacrylate) (PMMA) finding values between 10 and 20 J/m^2 [50]-[52], much less than bulk fracture energy of both polymers, but substantially greater than the ideal work of adhesion. Moreover they found that, similarly to what happens in bulk glassy polymers, at low molecular weights, G_c drops below 3 J/m^2 [52]. A qualitative explanation of such results is not difficult: the extent of entanglement is much smaller in interfaces than in the bulk. In fact the interface between PS and PMMA has a width of only 3 nm, while the distance between entanglements in polystyrene is about three times greater.

Applying the same concepts valid for bulk glassy polymers, one can describe the

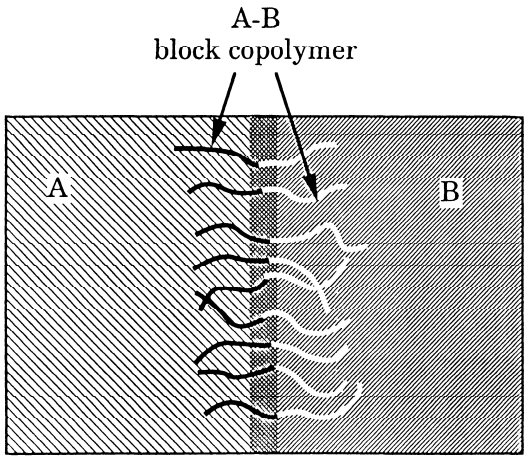

Figure 1.4: Schematic of a layer of A-B block copolymer chains segregated at a A/B interface. After Creton et al. [56].

chain coupling across the interface by Σ_{eff}, which is also the quantity determining the failure mechanism. Important information about this aspect can be obtained from experiments on interfaces reinforced with block copolymers. We know that when a diblock copolymer AB is placed at an A/B interface, each block will mix with its homopolymer, as shown schematically in Figure 1.4. It is then possible to assume that all the copolymer chains will cross the interface, and to compute the contribute to Σ_{eff} due to the copolymer from its density. Moreover for strongly immiscible pairs the homopolymer contribution can be neglected, so that for such systems Σ_{eff} is perfectly known. Creton et al. [56] studied an interface between PS and poly(2-vinylpiridine) (PVP) reinforced with block copolymers of PS and PVP. They showed that different failure mechanisms occur depending on the molecular weight of the blocks and on Σ_{eff}. Short blocks, that are not long enough to be entangled with their homopolymers, can be easily pulled out from their surroundings and only small increases of fracture energy can be obtained. At higher molecular weights, i.e. when $M > M_c$, and low Σ_{eff}, the active failure mechanism is chain scission, as proved by surface analysis that measured the fraction of blocks on each side of the interface after failure. At high molecular weights and high Σ_{eff}, crazing is the

preferred mechanism and fracture energies are very high. Similar conclusions were confirmed also by Dai et al. [58], who investigated the same system with similar techniques, and by Creton et al. [59] who studied interfaces between PMMA and poly(phenylene oxide) (PPO) homopolymers reinforced with varying amounts of a PMMA-PS block copolymer. A useful picture of the transition between different failure modes is given in Figure 1.5, where we report experimental results from Kramer [60], showing how the fracture mechanism changes from chain scission, in which $G_c \propto \Sigma_{\text{eff}}$, to crazing, in which $G_c \propto \Sigma_{\text{eff}}^2$, when Σ_{eff} increases.

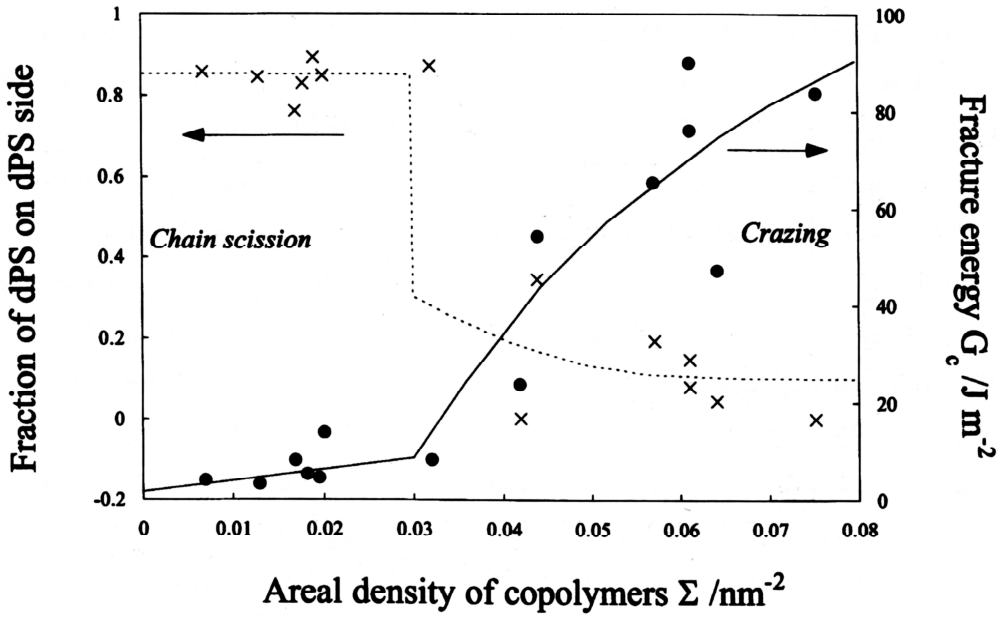

Figure 1.5: Reinforcement of a PS/poly(vinyl pyridine) interface by a deuterated styrene (dPS)-vinyl pyridine block copolymer. Circles (right-hand axes) show the measured fracture energy, and crosses the fraction of dPS found on the PS side of the interface after fracture, both as a function of the copolymer chain density. The discontinuity of the curves at $\Sigma = 0.03$ nm^{-2} indicates a transition from chain scission to crazing. After Kramer et al. [60].

The cited experiments allowed to determine the relation between Σ_{eff} and the

toughness of an interface, but in non reinforced systems Σ_{eff} cannot be measured. It would be therefore desirable to link it to measurable parameters of the interface. We can start from the observation we made on PS/PMMA systems: if the width is much lower than the distance between entanglements then they are not very effective in reinforcing the interface. This simple prediction has been investigated in some recent experiments. Schnell et al. [53] measured the fracture energy of bilayers of PS and poly(para-methyl styrene) (PpMS), for a wide range of interfacial widths, obtained by changing the annealing temperature of the samples. In this way, they were able to demonstrate that there is a clear correlation between the width, measured by neutron reflectivity, and the fracture energy of the interface. The results were confirmed in another work of the same authors on interfaces between PS and the statistical copolymer of poly(bromostyrene-styrene)(PBr$_x$S) [54]. The same correlation has been found by Brown [55], who measured the toughness of the interface between a random copolymer P(S-r-PMMA) and pure PMMA, for different fractions of PS in the copolymer. In order to show how G_c depends on the interfacial width, we reproduce in Figure 1.6 a plot in which several experimental results are reported together.

It would be of great importance to establish a quantitative relation between width and toughness, because it would allow easier predictions of the strength of interfaces and would clarify the concept of entanglement. For weakly immiscible polymer pairs, De Gennes [61] proposed a scaling law for the dependence of Σ_{eff} on the interface width through the Flory-Huggins interaction parameter χ. However, his result is based on energetic considerations, and it does not take into account properly the effect of inhomogeneous polymer densities at the interface. In recent years a new approach has been proposed by Brown [55], in which Σ_{eff} depends only on the concentration profile of the polymer. He assumed that the probability that a strand starting from x might end in x' is proportional to the ratio of the polymer volume fractions at the two points, but we will see in chapter 3 that this is not correct. As a result, his model predicts a variation of the density of effective entangled chains that is too slow with respect to the changes in the interface width. Both models are discussed in detail in section 3.2.

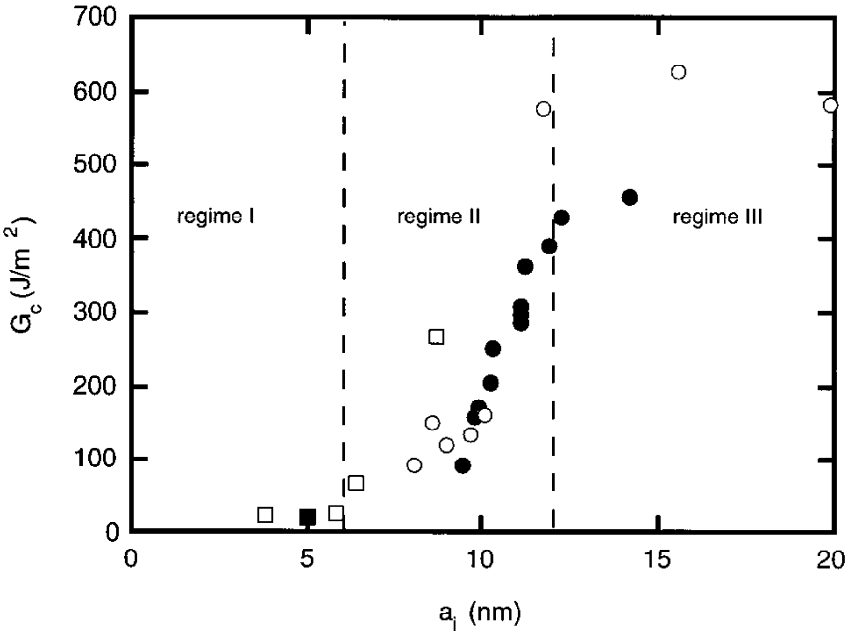

Figure 1.6: Fracture energy G_c plotted as a function of the interfacial width a_I for different samples: PS-PBr$_x$S (open squares) [54], PS-PMMA (filled squares) [44][50], PS-PpMS (filled circles) [53], and PS-PS (open circles) [53]. After Schnell et al. [54].

More generally, we believe that the main limitation of all available descriptions of the strength of interfaces is the scarce knowledge of entanglements. A great step forward in this direction has been done in the last fifteen years, when some new models have been proposed to link the molecular weight of entanglements to conformational characteristics of the polymer chains [62]-[69]. Recent experiments [67],[70] seem to confirm the validity of a particular the so called "packing models" for bulk glassy polymers, and some authors have already attempted to apply the same concepts to entanglements at interfaces and surfaces [71]-[73]. Unfortunately it is not clear how to determine experimentally the molecular weight of entanglement in interfaces, so that for these systems the predictions of different models cannot be tested. A possible way of measuring M_e in thin films has been instead proposed by Brown and Russell [71], and experiments are currently being performed.

In this thesis we present a new model for entanglements at interfaces, that can

account for the experimentally found dependence of the toughness on the interfacial width. The work is organized as follows. In chapter 2 we study the thermodynamics of polymer blends, describing in detail the Self Consistent Field (SCF) approach and the numerical calculations we performed to obtain concentration profiles and mean fields at polymer-polymer interfaces. In chapter 3 a new model is presented that allows to compute the density of entangled strands across the interface. Our model, supplemented with an appropriate description of the fracture mechanisms and the introduction of a new fracture regime, describes very well the available experimental data. In particular it reproduces very well the dependence of the toughness on the interface width over the whole range of experimental widths. In the final part of this work, chapter 4, we adopt a packing model for entanglements and apply it to inhomogeneous systems in order to estimate M_e. Numerical results show that the molecular weight of entanglement of chains near an interface is larger than in the bulk, and the corrections to the fracture energy calculations due to this effect are discussed. We compute also the average molecular weight of entanglements in thin films, showing how it increases as the thickness of the film decreases below the entanglement length. Conclusions and ideas for future developments are the subject of chapter 5.

Chapter 2

Self Consistent Field method for polymer interfaces

The main goal of this work is to predict the strength of a joint as a function of its interfacial properties, and it is therefore natural to start from the thermodynamics of polymer mixtures. In particular we are interested in the equilibrium concentration profiles of the two joined polymers and in the mean fields that chains experience at the interface. As we will see in chapter 3 our model of entanglements is in fact based on a mean field approximation.

As already pointed out in the introduction two methods are commonly used to study inhomogeneous systems, that have different ranges of validity. Density Functional methods [30]-[39] can give some accurate analytic predictions for wide interfaces, but they are not very useful in the case of the strongly immiscible systems we want to study. A Self Consistent Field approach [18]-[29] is more suitable for strong and intermediate segregation and, even if it requires computer intensive calculations, it allows to compute at the same time the densities and the corresponding mean fields. For these reasons we will adopt a SCF method to obtain the needed equilibrium properties of interfaces.

The origins of the SCF approach can be dated back to the mid-1960s, when Edwards pointed out the analogy between the classical problem of interacting electrons and the "new" problem of interacting polymers [74]. Many methods were available at the time to deal with many body systems and they proved immediately success-

ful when first applied to polymers by Helfand and Tagami [18]. The problem was initially presented from a mean field point of view and only later a more comprehensive theory, based on a functional integral approach, showed the connection between that intuition and fundamental statistical mechanics [20]. In his works Helfand studied in detail the interface between two immiscible polymers that he assumed incompressible, and soon recognized the importance of avoiding fluctuations of the overall density. He therefore added to the free energy an "ad hoc" term proportional to the square of the deviation from the average density and to the inverse of bulk compressibility, to restrict such fluctuations. Some years later Hong and Noolandi [24] developed instead a truly compressible theory, that was derived from an earlier work on incompressible multi component polymer systems [23], by simply assuming one of the small molecule components to be vacancies.

We performed SCF calculations on interfaces with both methods and checked that, in the incompressible limit, they give the same results within the numerical errors. For convenience however we adopted the approach by Helfand [20], and followed the work by Shull et al. [25]-[28] to perform numerical calculations.

In this section we first derive correct SCF equations for inhomogeneous polymer systems following the work by Hong and Noolandi [23], and then describe in detail how we solved them in the case of interfaces, paying particular emphasis on the approximations of Helfand's approach. We hope in this way to give a clear picture of the physics involved.

2.1 SCF equations for inhomogeneous polymer systems

The index $p = 1, 2, ..., n$ labels the polymeric species, while we will indicate with the subscript 0 the voids. Summations involving also the vacancies will be denoted with the index $k = 0, 1, ..., n$. In this section, for consistency with the work of Hong and Noolandi [23], the number of chains of type p is denoted by $\tilde{N}_p = N_p/Z_p$, where N_p is the number of monomer units and Z_p is the degree of polymerization. Of course $Z_0 = 1$, so that we will use either N_0 or $\tilde{N}_0$. Moreover we will assume that

each vacancy occupies the same volume, that we will call v and that can be in fact regarded as the lattice cell volume.

Our derivation starts from the grand partition function for a system with fixed number of particles, but a variable number of vacancies

$$\mathbf{Z} = \left(\prod_k \frac{\mathcal{Z}_k^{\tilde{N}_k}}{\tilde{N}_k!} \right) \int \left(\prod_{i=1}^{N_0} \delta \mathbf{r}_{0i}(\cdot) \right) \left(\prod_p \prod_{i=1}^{\tilde{N}_p} \delta \mathbf{r}_{pi}(\cdot) P\left[\mathbf{r}_{pi}(\cdot) \right] \right) \exp(-\beta V), \tag{2.1}$$

where $\mathcal{Z}_k$ is the partition function due to the kinetic energy and V is the intermolecular potential. It is clear that a vacancy cannot have a kinetic energy, so that $\mathcal{Z}_0$ is to be interpreted as a normalization constant that will be determined later. We also assume that vacancies don't interact, and therefore they do not enter the intermolecular potential V. Connectivity of polymer chains is accounted for by writing

$$P\left[\mathbf{r}_{pi}(\cdot) \right] \propto \exp\left[-\frac{3}{2b_p^2} \int_0^{Z_p} dt \dot{\mathbf{r}}_{pi}^2(t) \right]. \tag{2.2}$$

In this chapter we will use $k_B T$ as the unit of energy and prefer to define a nondimensional potential $\hat{W} = V/k_B T$, that can be expressed in terms of the microscopic particle densities

$$\hat{\rho}_p(\mathbf{r}) = \hat{\rho}_p(\mathbf{r}; \{\mathbf{r}_{pi}(\cdot)\}) = \sum_{i=1}^{\tilde{N}_p} \int_0^{Z_p} dt \delta\left[\mathbf{r} - \mathbf{r}_{pi}(t) \right], \tag{2.3}$$

as

$$\hat{W} = \frac{1}{2} \sum_{pp'} \int d\mathbf{r} \int d\mathbf{r}' \hat{\rho}_p(\mathbf{r}) W_{pp'}\left(\mathbf{r} - \mathbf{r}' \right) \hat{\rho}_{p'}(\mathbf{r}'). \tag{2.4}$$

Now we use a δ functional identity to introduce the real density fields $\rho_k(\mathbf{r})$ and write

$$\exp\left(-\hat{W} \right) = \int \left[\prod_p \delta \rho_p(\cdot) \right] \prod_p \delta\left[\rho_p(\cdot) - \hat{\rho}_p(\cdot) \right] \exp(-W), \tag{2.5}$$

where

$$W = W\left(\{\rho_p(\cdot)\} \right) = \frac{1}{2} \sum_{pp'} \int d\mathbf{r} \int d\mathbf{r}' \rho_p(\mathbf{r}) W_{pp'}\left(\mathbf{r} - \mathbf{r}' \right) \rho_{p'}(\mathbf{r}'). \tag{2.6}$$

Another set of fields, ω_k, can be introduced by using the exponential representation

$$\delta\left[\rho_k(\cdot)-\hat{\rho}_k(\cdot)\right]=\mathcal{N}'\int_{-i\infty}^{i\infty}\delta\omega_k(\cdot)\exp\left\{\int d\mathbf{r}\omega_k(\mathbf{r})\left[\rho_k(\mathbf{r})-\hat{\rho}_k(\mathbf{r})\right]\right\}, \tag{2.7}$$

where $\mathcal{N}'$ is a normalization constant and the limits of integration are $-i\infty$ and $i\infty$.

The partition function is finally obtained as

$$\mathbf{Z}=\left(\prod_k\frac{\mathcal{Z}_k^{\tilde{N}_k}}{\tilde{N}_k!}\right)\mathcal{N}\int\left[\prod_k\delta\omega_k(\cdot)\delta\rho_k(\cdot)\right]\prod_k\mathcal{Q}_k^{\tilde{N}_k}\exp\left\{\sum_k\int d\mathbf{r}\omega_k(\mathbf{r})\rho_k(\mathbf{r})-W\right\}, \tag{2.8}$$

where $\mathcal{N}$ is another normalization constant and

$$\mathcal{Q}_k=\int\delta\mathbf{r}(\cdot)P[\mathbf{r}(\cdot)]\exp\left\{-\int_0^{Z_k}dt\omega_k[\mathbf{r}(t)]\right\}=\int d\mathbf{r}d\mathbf{r}_0Q_k(\mathbf{r}_0,\mathbf{r};Z_k). \tag{2.9}$$

For the vacancies it is easy to verify that

$$\mathcal{Q}_0=\int d\mathbf{r}e^{-\omega_0(\mathbf{r})}. \tag{2.10}$$

In summary, the above procedure allowed to eliminate particle-particle interactions and replace them with the interactions between individual particles and the fluctuating fields ω_k.

Before proceeding further we note that, for a polymer, the function $Q_p(\mathbf{r}_0,\mathbf{r};Z_p)$ is nothing but its Green function, and, at thermodynamic equilibrium, it represents the statistical weight of chains starting at $\mathbf{r}_0$ and ending at $\mathbf{r}'$ in Z_p steps, normalized with respect to the value it assumes in absence of external fields. Moreover it can be shown to satisfy the Modified Diffusion Equation (MDE)

$$\left[\frac{\partial}{\partial t}-\frac{b_p^2}{6}\nabla^2+\omega_p\right]Q_p\left(\mathbf{r}_0,\mathbf{r};t\right)=0, \tag{2.11}$$

with boundary condition

$$Q_p\left(\mathbf{r}_0,\mathbf{r};0\right)=\delta\left(\mathbf{r}-\mathbf{r}_0\right). \tag{2.12}$$

It is also useful to define the quantities

$$q_p(\mathbf{r},t) = \int d\mathbf{r}_0 Q_p\left(\mathbf{r}_0,\mathbf{r};t\right), \tag{2.13}$$

representing the probability of finding the end of a chain of length t at $\mathbf{r}$. It is easy to verify that they satisfy the relations

$$q_p(\mathbf{r},0) = 1, \tag{2.14}$$

and

$$\mathcal{Q}_p = \int d\mathbf{r} q_p(\mathbf{r},Z_p). \tag{2.15}$$

We will make extensive use of the Green function and of probabilities q in chapter 3, where the former quantity will be denoted with G instead of $\mathcal{Q}$.

If we use Stirling's approximation for large $\tilde{N}_k$ ($\ln \tilde{N}_k! \approx \tilde{N}_k(\ln \tilde{N}_k - 1)$) in equation (2.8) we obtain

$$\mathbf{Z} = \mathcal{N} \int \left[\prod_k \delta\omega_k(\cdot)\delta\rho_k(\cdot)\right] \exp\left[-\mathcal{F}(\{\rho_k(\cdot)\},\{\omega_k(\cdot)\})\right], \tag{2.16}$$

where the free energy functional is given by

$$\begin{aligned}\mathcal{F}(\{\rho_k(\cdot)\},\{\omega_k(\cdot)\}) = \\ = W(\{\rho_k(\cdot)\}) - \sum_k \int d\mathbf{r}\omega_k(\mathbf{r})\rho_k(\mathbf{r}) + \sum_k \int d\mathbf{r}\frac{\rho_k(\mathbf{r})}{Z_k}\left[\ln\left(\frac{N_k}{Z_k\mathcal{Z}_k\mathcal{Q}_k}\right) - 1\right].\end{aligned} \tag{2.17}$$

We now know the free energy $\mathcal{F}$ as a functional of the densities ρ_k and of the external fields ω_k, that can be obtained by the saddle function method. It consists in minimizing the functional $\mathcal{F}$ with respect to both densities and external fields, obtaining a set of coupled equations. This procedure corresponds to a mean field approximation, so that the self consistent ω_k are exactly the mean fields we will need in chapter 3 to compute Σ_{eff}. The minimization is performed under two constraints, that are added in order to model physical properties of the polymers. The first derives from the fact that there is an excluded volume effect due to hard-core repulsion, and it states that there is no volume change upon mixing. Mathematically this is modelled by imposing

$$\sum_k \rho_k(\mathbf{r})/\rho_k^* = 1, \tag{2.18}$$

where $\rho_0^* = 1/\upsilon$, and ρ_p^* are the densities of the pure polymers in monomer segments per unit volume. The above condition can also be interpreted by thinking that chains are placed on a lattice, where each cell has to be occupied by monomers or voids. In this picture ρ_0^*/ρ_p^* gives the number of lattice cells occupied by one monomer of polymer p. The second constraint is that the number of monomers of each polymeric component is fixed

$$\int d\mathbf{r}\rho_p(\mathbf{r}) = N_p. \tag{2.19}$$

Denoting the Lagrangian multipliers corresponding to constraints (2.18) and (2.19) respectively by $\eta(\mathbf{r})$ and μ_k, we write the variational equations as

$$\rho_k(\mathbf{r}) + \frac{\tilde{N}_k}{\mathcal{Q}_k}\frac{\delta\mathcal{Q}_k}{\delta\omega_k(\mathbf{r})} = 0, \tag{2.20}$$

$$\frac{\delta W}{\delta\rho_0(\mathbf{r})} - \omega_0(\mathbf{r}) + \left[\ln\left(\frac{N_0}{\mathcal{Z}_0\mathcal{Q}_0}\right) - 1\right] + \frac{\eta(\mathbf{r})}{\rho_0^*} = 0, \tag{2.21}$$

$$\frac{\delta W}{\delta\rho_p(\mathbf{r})} - \omega_p(\mathbf{r}) + \frac{1}{Z_p}\left[\ln\left(\frac{N_p}{Z_p\mathcal{Z}_p\mathcal{Q}_p}\right) - 1\right] + \frac{\eta(\mathbf{r})}{\rho_p^*} - \mu_p = 0. \tag{2.22}$$

Equation (2.20) leads immediately to

$$\rho_0(\mathbf{r}) = \frac{N_0}{\mathcal{Q}_0}e^{-\omega_0(\mathbf{r})} \tag{2.23}$$

for the vacancies, and to

$$\rho_p(\mathbf{r}) = \frac{N_p}{Z_p\mathcal{Q}_p}\int_0^{Z_p} dt q_p(\mathbf{r},t)q_p(\mathbf{r},Z_p-t), \tag{2.24}$$

for polymers. We are then left with equations (2.21)-(2.24) in which Lagrangian multipliers have still to be determined. Since all the fields ω_k are defined up to a

constant, we decide to choose those constants in such a way that

$$\mathcal{Q}_p = N_p/\rho_p^*. \tag{2.25}$$

For the vacancies $\mathcal{Z}_0$ can be determined by

$$\frac{\mathcal{Z}_0^{N_0}}{N_0!} = \frac{1}{V_0^{N_0}}, \tag{2.26}$$

which gives, using Stirling's formula,

$$\mathcal{Z}_0 e = N_0/V_0 = \rho_0^*, \tag{2.27}$$

where V_0 is the total volume available to the vacancies.

In order to write the final equations in a more usual notation, it is better to express the potential W, with the help of eq.(2.18), in the form

$$W = W\left(\{\rho_k(\cdot)\}\right) = \frac{1}{2}\sum_p \rho_p^* N_p \epsilon_{pp} + \frac{1}{2}\sum_{kk'}\int d\mathbf{r}\int d\mathbf{r}'\rho_k(\mathbf{r})U_{kk'}\left(\mathbf{r}-\mathbf{r}'\right)\rho_{k'}(\mathbf{r}'), \tag{2.28}$$

where

$$U_{kk'}(\mathbf{r}) = W_{kk'}(\mathbf{r}) - \frac{1}{2\rho_k^*\rho_{k'}^*}\left(\rho_k^{*2}W_{kk}(\mathbf{r}) + \rho_{k'}^{*2}W_{k'k'}(\mathbf{r})\right), \tag{2.29}$$

and

$$\epsilon_{pp'} = \int d\mathbf{r} W_{pp'}(\mathbf{r}). \tag{2.30}$$

In practice $W_{kk'}$ represents the van der Waals interaction between monomers and vanishes when $k = 0$ or $k' = 0$, while $U_{kk'}$ is an exchange energy and vanishes when $k = k'$.

It is finally possible to find the Lagrangian multiplier $\eta(\mathbf{r})$ from equation (2.21) as

$$\frac{\eta(\mathbf{r})}{\rho_0^*} = -\frac{\delta W}{\delta\rho_0(\mathbf{r})} - \ln\frac{\rho_0(\mathbf{r})}{\rho_0^*}, \tag{2.31}$$

and rewrite all the relevant SCF equations in the more explicit form

$$\frac{\delta W}{\delta \rho_p(\mathbf{r})} - \frac{\rho_0^*}{\rho_p^*}\frac{\delta W}{\delta \rho_0(\mathbf{r})} - \omega_p(\mathbf{r}) + \frac{1}{Z_p}\left[\ln\left(\frac{\rho_p^*}{Z_p \mathcal{Z}_p}\right) - 1\right] - \frac{\rho_0^*}{\rho_p^*}\ln\frac{\rho_0(\mathbf{r})}{\rho_0^*} = \mu_p \tag{2.32}$$

$$\rho_0(\mathbf{r}) = \rho_0^* e^{-\omega_0(\mathbf{r})}, \tag{2.33}$$

$$\rho_p(\mathbf{r}) = \frac{\rho_p^*}{Z_p}\int_0^{Z_p} dt q_p(\mathbf{r}, t) q_p(\mathbf{r}, Z_p - t). \tag{2.34}$$

The physical meaning of the above equations is now clear. The last two merely give the densities as functionals of the fields, while equations (2.32) express the constance of the chemical potentials. In fact the Lagrangian multipliers μ_p are nothing but the chemical potentials for species p.

Equations (2.32)-(2.34) are the core of the Self Consistent method, and allow to explicitly find the fields ω_p and the densities ρ_p.

We can check the above results by applying them to a homogeneous system. The interaction potential per unit volume is given by

$$\frac{W^h}{V} = \frac{1}{2}\sum_p \epsilon_{pp}\rho_p^*\rho_p + \frac{1}{2}\sum_{kk'} U_{kk'}\rho_k\rho_{k'}, \tag{2.35}$$

where

$$U_{kk'} = \int U_{kk'}(\mathbf{r}) d\mathbf{r}. \tag{2.36}$$

The probabilities q and the fields ω_p are constant and given respectively by

$$q_p^h(t) = e^{-\omega_p^h t} \tag{2.37}$$

and

$$\omega_k^h = -\frac{1}{Z_k}\ln\frac{\rho_k}{\rho_k^*}. \tag{2.38}$$

The specific free energy in the homogeneous case is then found in the standard Flory-Huggins form

$$f^h = \rho_0 \ln\frac{\rho_0}{\rho_0^*} + \sum_{kk'}\frac{1}{2}U_{kk'}\rho_k\rho_{k'} + \sum_p \frac{\rho_p}{Z_p}\ln\frac{\rho_p}{\rho_p^*} + \sum_p \rho_p\mu_{0p}, \tag{2.39}$$

where we have included all the linear terms in the definition of the chemical potential of the pure polymer μ_{0p}

$$\mu_{0p} = \frac{1}{2}\epsilon_{pp}\rho_0^* + \frac{1}{Z_p}\left[\ln\left(\frac{\rho_p^*}{Z_p \mathcal{Z}_p}\right) - 1\right]. \tag{2.40}$$

The chemical potentials appearing in the SCF equations can be determined from the polymer densities $\{\rho_p^I, \rho_p^{II}\}$ in the two uniform bulk phases, denoted as I and II, by applying the results for the homogeneous system. The equations to find the densities are obtained from the equality of the chemical potentials in the two bulk regions

$$\mu_p^I = \mu_p^{II}, \tag{2.41}$$

and by fixing the pressure,

$$P(\mathbf{r}) = \sum_p \rho_p(\mathbf{r})\mu_p - f(\mathbf{r}), \tag{2.42}$$

in the two bulk phases.

Before ending the section we recall that a very useful approximation is possible if the interaction energy is supposed to be short ranged. In that case we can perform the expansion

$$\begin{aligned} W &= \frac{1}{2}\sum_p \rho_p^* N_p \epsilon_{pp} + \frac{1}{2}\sum_{k,k'}\int\int d\mathbf{r}d\mathbf{r}' U_{kk'}(\mathbf{r}-\mathbf{r}')\rho_k(\mathbf{r})\rho_{k'}(\mathbf{r}') \approx \\ &\frac{1}{2}\sum_p \rho_p^* N_p \epsilon_{pp} + \frac{1}{2}\sum_{kk'} U_{kk'}\int d\mathbf{r}\rho_k(\mathbf{r})\rho_{k'}(\mathbf{r}) - \frac{1}{12}\sum_{kk'} V_{kk'}\int d\mathbf{r}\nabla\rho_k(\mathbf{r})\cdot\nabla\rho_{k'}(\mathbf{r}), \end{aligned} \tag{2.43}$$

with

$$V_{kk'} = \int d\mathbf{r} r^2 U_{kk'}(\mathbf{r}). \tag{2.44}$$

Retaining only the first two terms of the expansion represents the random mixing approximation.

2.2 Numerical solution of SCF equations at interfaces

At an interface between two immiscible polymers the fields vary only in one direction, that we will denote with x, and $k = 0, 1, 2$, where 0 denotes the vacancies as above. We will work with the volume fractions

$$\phi_k(x) = \frac{\rho_k(x)}{\rho_k^*}, \tag{2.45}$$

that are equal to the reduced densities if there is no volume change upon mixing, and satisfy

$$\phi_0(x) = 1 - \phi_1(x) - \phi_2(x). \tag{2.46}$$

Using relations (2.32) the compressible mean fields for a binary blend are given in the random mixing approximation by

$$\omega_1(x) = \frac{\rho_0^*}{\rho_1^*}\left[\chi_{12}\phi_2(x) + \chi_{01}(\phi_0(x) - \phi_1(x)) - \chi_{02}\phi_2(x) - \ln\phi_0(x)\right] + \mu_{01} - \mu_1, \tag{2.47}$$

$$\omega_2(x) = \frac{\rho_0^*}{\rho_2^*}\left[\chi_{12}\phi_1(x) + \chi_{02}(\phi_0(x) - \phi_2(x)) - \chi_{01}\phi_1(x) - \ln\phi_0(x)\right] + \mu_{02} - \mu_2, \tag{2.48}$$

where

$$\chi_{0p} = U_{0p}\rho_p^* \tag{2.49}$$

and

$$\chi_{12} = U_{12}\frac{\rho_1^*\rho_2^*}{\rho_0^*} \tag{2.50}$$

are the usual Flory-Huggins interaction parameters. Please note that, as in the whole chapter, k_BT is the unit of energy and that in the mean fields the kinetic terms, i.e. terms inversely proportional to Z_p, cancel exactly.

Our goal is to find the self consistent inhomogeneous concentration profiles $\phi_p(x)$ and mean fields $\omega_p(x)$, and we present in this section our method of solution and the approximations we adopted. The first and most important regards the compressibility of the system. We have seen that the SCF method can account properly for a finite compressibility, but the real polymers we study in this work, i.e. PS, PMMA and PpMS, are quite stiff. Moreover in a compressible system three different

interaction energies, χ_{01}, χ_{02} and χ_{12}, need to be determined, and it is difficult to extract meaningful values from the experiments. This is why we preferred to consider the incompressible limit, that in Hong and Noolandi formulation is equivalent to fixing a very high pressure $P \to \infty$. In this limit $\phi_0 \to 0$, and the term $\ln \phi_0$ increases indefinitely but tends to be constant across the interface. From all these considerations it follows also that there is only one interaction energy entering the incompressible equations.

An alternative approach is the one by Helfand [20], that is not rigorous but gives the correct incompressible limit. Helfand derived the mean fields from a "special, but realistic, free energy", which, expressed in k_BT units, reads

$$\Delta f^* = \int d\mathbf{r} \left[\rho_0^* \chi \frac{\rho_1(\mathbf{r})}{\rho_1^*} \frac{\rho_2(\mathbf{r})}{\rho_2^*} + \frac{1}{2\kappa} \left(\frac{\rho_1(\mathbf{r})}{\rho_1^*} + \frac{\rho_2(\mathbf{r})}{\rho_2^*} - 1 \right)^2 \right], \tag{2.51}$$

where κ is an average compressibility. Mean fields are obtained from equations

$$\omega_p(\mathbf{r}) = \frac{\delta \Delta f^*}{\delta \rho_p(\mathbf{r})}, \tag{2.52}$$

which in the case of an interface give

$$\omega_p(x) = \frac{\rho_0^*}{\rho_p^*} \left[\chi \phi_{p'}(x) + \frac{1}{\rho_0^* \kappa} \left(\phi_1(x) + \phi_2(x) - 1 \right) \right]. \tag{2.53}$$

This expressions should be compared with equations (2.47) and (2.48). Apart from the fact that there is only one interaction energy χ, as expected from the incompressible theory, the most serious difference is in the treatment of the density fluctuations. In the correct fields (2.47) and (2.48) the overall density is maintained constant by the logarithmic term related to the pressure of the system that arises naturally from the entropy of vacancies. In Helfand formulation an extra term is added to the free energy for purely practical reasons. This term can be seen as a quadratic expansion of the correct logarithm term about the incompressible system where $\phi_0 = 0$, containing an indeterminate coefficient. In fact the incompressible limit is achieved by letting the compressibility κ tend to 0, thus imposing a constant overall density through the interface.

In our numerical calculations we use the Helfand expression (2.53) for the mean fields with $\rho_p^* = \rho_0^*$ and proceed as follows. We start by fixing a small compressibility $\kappa \ll \chi^{-1}$, and then compute the equilibrium volume fractions $\{\phi_1(\pm\infty), \phi_2(\pm\infty)\}$ from equations (2.41), using the Flory-Huggins expression for the chemical potentials. As the first step of the iterative procedure we need an initial guess for the concentration profiles $\phi_1^0(x)$ and $\phi_2^0(x)$, that interpolates between the two homogeneous phases. The corresponding fields $\omega_1(x)$ and $\omega_2(x)$ are then computed using the relations (2.53).

From the initial fields we compute the new densities in two steps. First we solve the differential equation for $q(x,t)$, that can be derived from the MDE (2.11) and reads

$$\left[\frac{\partial}{\partial t} - \frac{b_p^2}{6}\frac{\partial^2}{\partial x^2} + \omega_p(x)\right] q_p(x,t) = 0, \tag{2.54}$$

with initial conditions

$$q_p(x,0) = 1. \tag{2.55}$$

Then we use the relation

$$\phi_p(x) = \frac{1}{Z_p}\int_0^{Z_p} dt q_p(x,t) q_p(x, Z_p - t), \tag{2.56}$$

which is obtained from equation (2.34).

The spatial boundary conditions of equations (2.54) can be found by noting that at $x = \pm\infty$, if there is no actual external field, the system is homogeneous, so that we obtain from equations (2.37) and (2.38)

$$q_p(\pm\infty, t) = \exp\left[-\omega_p(\pm\infty)t\right] = \exp\left[\frac{t}{Z_p}\ln\phi_p(\pm\infty)\right]. \tag{2.57}$$

The new densities are then used to obtain image fields $\omega_p^{(1)}(x)$ from equations (2.53). In order to achieve convergence we don't use the image fields as the next guess in the iterative procedure, but we prefer to use the expression

$$\omega_p^{\text{new}}(x) = \omega_p(x) + \lambda\left[\omega_p^{(1)}(x) - \omega_p(x)\right], \tag{2.58}$$

where λ is some relaxation parameter. With the new fields, a new iteration is started by computing new volume fractions and so on, until the self consistency condition

$$\max_x \left|\omega_p(x) - \omega_p^{(1)}(x)\right| < \epsilon \tag{2.59}$$

is achieved for both polymers. In our calculations we usually set $\epsilon \approx 10^{-4}$ and $\lambda \approx 1/Z_p$. In order to improve convergence we sometimes considered separately the two terms of the fields (2.53) and used two different relaxation parameters λ_1 and λ_2.

The differential equations are numerically solved by means of a standard discrete approximation [25]-[28] that we briefly report. The two variables x and t are treated as discrete, through the relations

$$x = (i - N)\Delta x \ ; \ i = 0, ..., 2N \tag{2.60}$$

and

$$t = j\Delta t \ ; \ j = 0, ..., M, \tag{2.61}$$

with $\Delta t = Z_p/M$ and Δx depending on the width of the interface. The discrete MDE for $q_p(i,j)$, derived from equation (2.54), is solved by the recursion relation

$$\begin{aligned} q_p(i,j) = & \\ = & \left[\frac{1-\lambda_0}{2} q_p(i-1,j-1) + \lambda_0 q_p(i,j-1) + \frac{1-\lambda_0}{2} q_p(i+1,j-1)\right] \exp\left[-\omega_p(i)\right], \end{aligned} \tag{2.62}$$

with discrete boundary conditions

$$q_p(i,0) = 1, \tag{2.63}$$

$$q_p(0,j) = \exp\left[\frac{j}{M} \ln \phi_p(-\infty)\right], \tag{2.64}$$

and

$$q_p(2N,j) = \exp\left[\frac{j}{M} \ln \phi_p(+\infty)\right]. \tag{2.65}$$

The parameter λ_0 is the probability that a monomer is found in the same layer j as the preceding one along the chain, and depends on the lattice type. In the limit $\Delta x \to 0$ and $\omega_p \to 0$, it can be proved that $q_p(i,j)$ satisfies

$$\left[\frac{\partial}{\partial t} - \frac{(1-\lambda_0)\Delta x^2}{2}\frac{\partial^2}{\partial x^2} + \omega_p(x)\right] q_p(x,t) = 0, \tag{2.66}$$

which is the same equation as in (2.54), provided that $\Delta x = b_p/\sqrt{3(1-\lambda_0)}$. We therefore proceed as follows. We first choose a cubic lattice, for which $\lambda_0 = 2/3$, and fix a Δx sufficiently small with respect to the investigated interface. Then we consider equivalent chains with $b_1^* = b_2^* = \Delta x$ and, accordingly,

$$Z_p^* = Z_p \frac{b_p^2}{\Delta x^2} \tag{2.67}$$

$$\omega_p^* = \omega_p \frac{Z_p}{Z_p^*}. \tag{2.68}$$

As a matter of fact it can be verified that, using the new parameters, we obtain the correct $\phi_p(x)$. Moreover if Δx is chosen smaller than b_p, as we always did, then also the corresponding mean fields ω_p^* decrease with respect to the original ones and the continuous limit is approached. Another advantage of using equivalent chains with the same Kuhn segment length is that it can be assumed that vacancies and monomers of both species occupy the same volume Δx^3, thus simplifying all the equations. The scaled mean fields that we obtain can then be used in the MDE (2.11), together with the other scaled parameters to obtain numerically the Green functions of real chains.

We performed self consistent calculations on all the samples studied in chapter 3, but, in order to show the essential features of our results, we first apply the SCF method to a simple illustrative system, simulating an interface between two materials with bulk parameters equal to those of PS. In particular we used $b = 6.7$ Å as the Kuhn segment length, and the same molecular weight of 300k for both polymers. The interfacial width is changed by choosing an appropriate interaction parameter χ. This symmetric system will be used through the whole thesis to test our model and to show its most important predictions. In Figure 2.1 we plot the volume fractions calculated numerically with the above described SCF method for $\chi = 0.013$ (squares and circles). Applying the theory of Helfand and Tagami [18] in the long chain limit, we would predict hyperbolic tangent profiles with an interfacial width of $a_I = 2b/\sqrt{6\chi} = 5$ nm. In order to compare the two results we also plotted

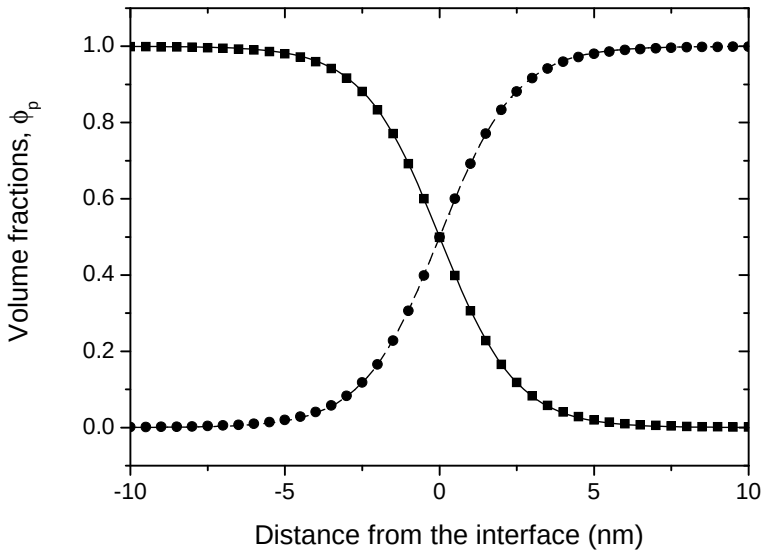

Figure 2.1: Computed volume fractions for the illustrative system described in the text in the incompressible limit (symbols). Solid and dashed lines represent hyperbolic tangent profiles with $a_I = 5$ nm.

in the same figure (solid and dashed lines) the profiles predicted by this theory, that seem to agree very well with our numerical results.

The corresponding mean fields are reported in Figure 2.2. Two wells can be distinguished close to the interface, that are consistent with the condition of a constant total density across the interface. Since the system is strongly immiscible we have $\phi_1(-\infty) = \phi_2(+\infty) \approx 1$ and $\phi_1(\infty) = \phi_2(-\infty) \approx 0$, from which follows $\omega_1(-\infty) = \omega_2(+\infty) \approx 0$ and $\omega_1(\infty) = \omega_2(-\infty) \approx \chi$.

We also show in Figure 2.3 a contour plot of the Green function $Q(x, x'; n)$, relative to polymer 1, whose bulk phase is at $x = -\infty$. In the calculations we used $n = 128$, that corresponds to the mean spacing between entanglements in PS, so that the scale length over which the function changes is $b\sqrt{n} \approx 7.6$ nm. The presence of the interface is responsible for the well pronounced asymmetry in space, that corresponds to higher probabilities for the chains of being at $x < 0$. The function is instead symmetric with respect to the exchange of x with x', as expected.

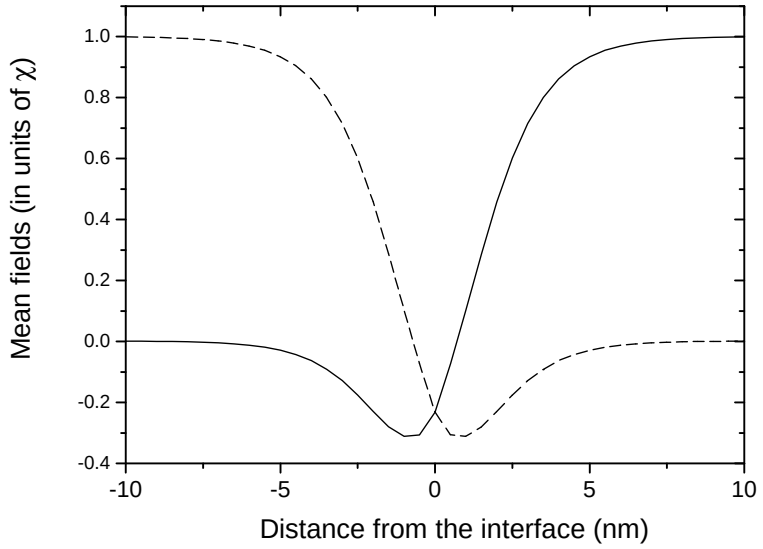

Figure 2.2: Mean fields computed by the SCF method for the same system as in figure 2.1.

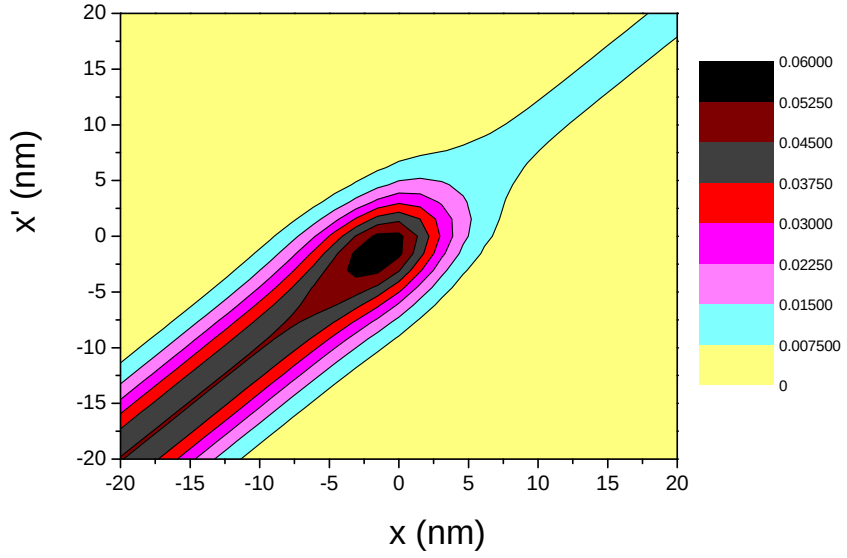

Figure 2.3: Contour plot of the Green function $Q(x, x'; n = 128)$, computed from the mean field given in figure 2.2 as the solid line.

Chapter 3

Chain entanglements and fracture energy

In this chapter a new method is proposed to compute the fracture energy of an interface between immiscible glassy polymers. It is based on a microscopic model of entanglements that is very simple, but capable of capturing the essential features of the problem, as described in section 1. In section 2 we find an explicit expression for Σ_{eff}, and evaluate it numerically by using the SCF method of the previous chapter. The dependence of Σ_{eff} from the interfacial width and the molecular weight is discussed and a comparison with other approaches is also presented. A useful approximation, valid in the case of long chains is given, that allows a simple and fast calculation of Σ_{eff}, and an alternative description of our method using a stochastic language is presented. Fracture energy is explicitly found as a function of Σ_{eff} in section 3, where all the relevant fracture regimes are taken into account. Numerical results are finally obtained for real systems and compared with available experimental data in section 4.

3.1 Model of entanglements

We assume that the two polymers are in thermodynamic equilibrium at an annealing temperature above their T_g, and we will use, in our derivation, a mean field approximation, that is suitable for melts [4]. Each polymer chain is therefore viewed as an

ideal Gaussian chain, submitted to the mean external field created by all the other chains. Consider a polymer chain of molecular weight M, made of N repeating units of molecular weight M_0. In order to account for chain stiffness, in our derivation we will take into consideration the equivalent Gaussian chain of the actual macromolecule. Statistical units of the equivalent chain have molecular weight M_0 and length b, given by

$$b = l\sqrt{C_\infty j}, \tag{3.1}$$

where j is the number of backbone bonds of the original repeating unit, C_∞ is the chain stiffness and l the bond length, which is 1.54 Å for C-C bonds.

Each chain will form entanglements, and we can imagine them as more or less localized where two chains crosses. To carry on the calculations we need to assume something about their positions along the chain. In principle they can be described as an independent stochastic process, but at present not much is known about such a process. What is known is the average molecular weight between entanglements along the chain, M_e, for bulk polymers. As a zero order approximation we can assume that each segment of molecular weight M_e, containing $N_e = M_e/M_0$ monomers, forms exactly one entanglement. Chain end effects can be taken into account by assuming that entanglements are localized at the end of each segment excluding the final one, as already done by Mikos and Peppas [2]. A chain with molecular weight M therefore has on average $n = M/M_e$ segments and $n - 1$ entanglements. Due to the mean field approximation, in our derivation we will solve a single chain problem, and, to perform the calculations, it is necessary to assume that the exact number and position of the entanglements along the chain is known. What we can do is consider a real chain that has two dangling ends and forms an integer number of entanglements, given by $n_e = [n] - 1$, where $[x]$ denotes the integer part of x. Since the two ends of a chain are completely equivalent, it can be safely assumed that, on the average, entanglements are symmetrically distributed with respect to the chain center. Entanglements are therefore located at positions $i_k = kN_e + \Delta$ along the chain, where $\Delta = (N - N_e[n])/2$ and $k = 1, \ldots, n_e$, as shown in Figure 3.1a.

Rigorously, the mean value of every physical quantity depending on the entanglement positions should be an appropriate average over all the possible configurations

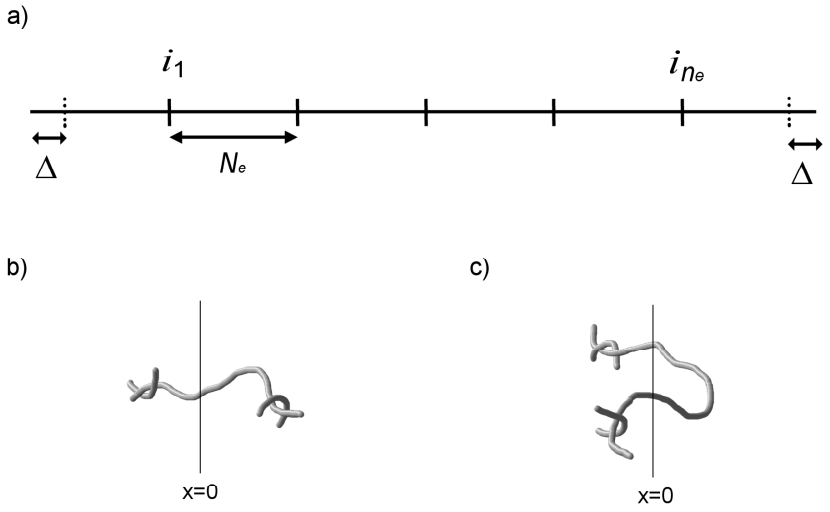

Figure 3.1: (a) Position of the n_e entanglements along the chain. Continuous bars represent entangled chains crossings while dashed ones are just an aid to the eye. Distances are expressed in number of monomer units. (b,c) Schematic representation of an effective (b) and a not effective (c) entanglement; the planar interface is defined by x=0.

$\{i_k\}$, but as a first approximation we treat the entanglement as fixed along the chain. This is done in the belief that, with an appropriate choice of the fixed configuration, a good approximation of the correct mean values can be obtained. To support this conclusion we will also show that Σ_{eff} changes little if the positions of all entanglements are translated along the chain. Unfortunately the configuration we chose has a number of entanglement n_e that is different from their average number per chain n, so that in the numerical calculation we will need to normalize the computed Σ_{eff}. An alternative continuous approach that is able to directly consider the correct average number of monomers per chain is presented in chapter 4. Another hypothesis assumed in our derivation is that the molecular weight of entanglement stays constant throughout the whole interface; this approximation is also discussed in chapter 4.

3.2 Calculation of the effective entanglement density for asymmetric interfaces

Chain coupling across the interface is described by the areal density of effectively entangled strands, Σ_{eff}. A strand is said to be effectively entangled if it connects two subsequent entanglements placed on different sides of the interface, and is therefore able to transfer stress across the interface, as shown in Figures 3.1b and 3.1c.

In an asymmetric interface we assume that Σ_{eff} can be written as the sum of the effective entanglements formed by the two polymers:

$$\Sigma_{\text{eff}} = \Sigma_{\text{eff}}^{(A)} + \Sigma_{\text{eff}}^{(B)}. \tag{3.2}$$

Calculations will be carried out for polymer A, and we will always refer to this species, unless otherwise stated. Derivations would obviously be the same for polymer B.

In order to solve the problem we introduce the Green function formalism. At thermodynamic equilibrium, the Green function $G(\mathbf{r}, \mathbf{r}'; N)$, that we have already introduced in chapter 2, represents the statistical weight of chains starting at $\mathbf{r}$ and ending at $\mathbf{r}'$ in N steps, normalized with respect to the value it assumes in absence of external fields. The Green function of a Gaussian chain in the presence of an external field U_e satisfies the following differential equation [5]

$$\left(\frac{\partial}{\partial N} - \frac{b^2}{6}\frac{\partial^2}{\partial \mathbf{r}^2} + \frac{1}{k_B T}U_e(\mathbf{r})\right) G(\mathbf{r}', \mathbf{r}; N) = \delta(\mathbf{r} - \mathbf{r}')\delta(N), \tag{3.3}$$

where the right hand side term is set so that it can satisfy the proper boundary conditions. We remark that the above formulation is completely equivalent to the Modified Diffusion Equation (2.11). For $U_e = 0$, the Green function gives the well known Gaussian distribution function

$$G_0(\mathbf{r}, \mathbf{r}'; N) = \left(\frac{2\pi N b^2}{3}\right)^{-3/2} \exp\left(-\frac{3(\mathbf{r} - \mathbf{r}')^2}{2Nb^2}\right). \tag{3.4}$$

The mean values of any physical quantity depending on the position $\mathbf{r}_n$ of the nth monomer is given by [5]

$$\langle A(\mathbf{r}_n)\rangle = \frac{\int d\mathbf{r}_0 d\mathbf{r}_n d\mathbf{r}_N G(\mathbf{r}_0,\mathbf{r}_n;n)G(\mathbf{r}_n,\mathbf{r}_N;N-n)A(\mathbf{r}_n)}{\int d\mathbf{r}_0 d\mathbf{r}_N G(\mathbf{r}_0,\mathbf{r}_N;N)}. \tag{3.5}$$

If a quantity depends on the position of two monomers the corresponding expression for its mean value is

$$\langle A(\mathbf{r}_n,\mathbf{r}_m)\rangle = \frac{\int d\mathbf{r}_0 d\mathbf{r}_n d\mathbf{r}_m d\mathbf{r}_N G(\mathbf{r}_0,\mathbf{r}_n;n)G(\mathbf{r}_n,\mathbf{r}_m;m-n)G(\mathbf{r}_m,\mathbf{r}_N;N-m)A(\mathbf{r}_n,\mathbf{r}_m)}{\int d\mathbf{r}_0 d\mathbf{r}_N G(\mathbf{r}_0,\mathbf{r}_N;N)}, \tag{3.6}$$

with $m > n$ [5].

Since in the case of a plane interface the external potential depends only on one coordinate, that we identify as x, we can integrate on the other two and work in one dimension. The Green function G_0 becomes

$$G_0(x,x';N) = \frac{\beta_N}{\sqrt{\pi}} \exp\left[-\beta_N^2 (x-x')^2\right] \tag{3.7}$$

with

$$\beta_N = \frac{\sqrt{3/2}}{N^{1/2}b}. \tag{3.8}$$

To compute Σ_{eff} it is necessary to count every strand that connects two subsequent entanglements placed on different sides of the interface, that we assume to be at $x = 0$. Working in a mean field approximation, it is sufficient to consider the single chain problem and then multiply the result by the number of chains. The operator that counts the total number of the coupling strands across the interface per unit area is

$$\begin{aligned}\hat{\Sigma}_{\text{eff}} &= \frac{\nu}{A}\sum_{k=1}^{n_e-1}\left[\int_{x<0} d\mathbf{r}\int_{x>0} d\mathbf{r}'\delta(\mathbf{r}_{i_k}-\mathbf{r})\delta(\mathbf{r}_{i_{k+1}}-\mathbf{r}')\right. \\ &\quad \left.+\int_{x>0} d\mathbf{r}\int_{x<0} d\mathbf{r}'\delta(\mathbf{r}_{i_k}-\mathbf{r})\delta(\mathbf{r}_{i_{k+1}}-\mathbf{r}')\right],\end{aligned} \tag{3.9}$$

where the sum over k counts entanglements along the chain, A is the system area and ν is the total number of chains. The density of effective entanglements per unit area can be expressed as the mean value of the above defined operator

$$\Sigma_{\text{eff}} = \langle \hat{\Sigma}_{\text{eff}} \rangle. \tag{3.10}$$

From eq.(3.6) we then obtain

$$\Sigma_{\text{eff}} = \frac{\nu}{A} \frac{1}{\int\int d\mathbf{r}_0 d\mathbf{r}_N G(\mathbf{r}_0, \mathbf{r}_N; N)} \times \tag{3.11}$$
$$\sum_{k=1}^{n_e-1} \left[\int_{x<0} d\mathbf{r} \int_{x>0} d\mathbf{r}' \int\int d\mathbf{r}_0 d\mathbf{r}_N G(\mathbf{r}_0, \mathbf{r}; i_k) G(\mathbf{r}, \mathbf{r}'; N_e) G(\mathbf{r}', \mathbf{r}_N; N - i_{k+1}) + \right.$$
$$\left. \int_{x<0} d\mathbf{r}' \int_{x>0} d\mathbf{r} \int\int d\mathbf{r}_0 d\mathbf{r}_N G(\mathbf{r}_0, \mathbf{r}; i_k) G(\mathbf{r}, \mathbf{r}'; N_e) G(\mathbf{r}', \mathbf{r}_N; N - i_{k+1}) \right].$$

Integrating over y and z we obtain

$$\Sigma_{\text{eff}} = \frac{\nu}{A} \frac{1}{\int q(x; N) dx} \times \tag{3.12}$$
$$\sum_{k=1}^{n_e-1} \left[\int_{-\infty}^{0} dx \int_{0}^{\infty} dx' q(x; i_k) G(x, x'; N_e) q(x'; N - i_{k+1}) + \right.$$
$$\left. \int_{-\infty}^{0} dx' \int_{0}^{\infty} dx q(x; i_k) G(x, x'; N_e) q(x'; N - i_{k+1}) \right].$$

where the notation

$$q(x; n) \equiv \int G(x, x'; n) dx', \tag{3.13}$$

has been introduced.

Expression (3.12) can be simplified by noting that $G(x, x'; m) = G(x', x; m)$ and that, since we assumed entanglements symmetrically distributed with respect to the chain center, $N - i_{k+1} = i_{n_e-k}$. Using these relationships it is possible to write

$$\int_{-\infty}^{0} dx' \int_{0}^{\infty} dx \sum_{k=1}^{n_e-1} q(x; i_k) G(x, x'; N_e) q(x'; N - i_{k+1}) = \tag{3.14}$$

$$= \int_{-\infty}^{0} dx' \int_{0}^{\infty} dx \sum_{k=1}^{n_e-1} q(x'; i_k) G(x', x; N_e) q(x; N - i_{k+1}),$$

and finally

$$\Sigma_{\text{eff}} = \frac{\nu}{A} \frac{2}{\int_L q(x; N) dx} \times \sum_{k=1}^{n_e-1} \left[\int_{-\infty}^{0} dx \int_{0}^{\infty} dx' q(x; i_k) G(x, x'; N_e) q(x'; N - i_{k+1}) \right], \tag{3.15}$$

where L is the dimension of the system in the x direction. The total number of chains can be written as

$$\nu = \frac{1}{N} \int_V \rho(\mathbf{r}) d\mathbf{r} = \frac{\rho_b A}{N} \int_L \phi(x) dx, \tag{3.16}$$

where $\rho(\mathbf{r})$ is the total density of monomers, $\phi(x) = \frac{\rho(x)}{\rho_b}$ is the polymer volume fraction, ρ_b is the bulk monomer density and V is the system volume. Substituting equation (3.16) into equation (3.15) one derives

$$\Sigma_{\text{eff}} = \frac{2\rho_b}{N} \frac{\int_L \phi(x) dx}{\int_L q(x; N) dx} \times \sum_{k=1}^{n_e-1} \left[\int_{-\infty}^{0} dx \int_{0}^{\infty} dx' q(x; i_k) G(x, x'; N_e) q(x'; N - i_{k+1}) \right]. \tag{3.17}$$

Finally observe that in the homogeneous phases $\phi(\pm\infty) = q(\pm\infty; N)$, as follows from equation (2.57), so that for a system where L is much greater than the interface width we have

$$\lim_{L \to \infty} \frac{\int_L \phi(x) dx}{\int_L q(x; N) dx} = 1. \tag{3.18}$$

The final expression for Σ_{eff} is therefore

$$\Sigma_{\text{eff}} = \frac{2\rho_b}{N} \sum_{k=1}^{n_e-1} \left[\int_{-\infty}^{0} dx \int_{0}^{\infty} dx' q(x; i_k) G(x, x'; N_e) q(x'; N - i_{k+1}) \right]. \tag{3.19}$$

This equation gives the density of effective entanglements formed by one polymer across the interface. The total density is the sum of the contributions by both species. Expression (3.19) is the main result of this section.

In the case of an A/A interface, $U_e = 0$, $\phi(x) \equiv 1$, $G(x, x'; N_e) = G_0(x, x'; N_e)$ and $q(x; i) \equiv 1\ \forall i$, so that from equation (3.19) it holds

$$\Sigma_{\text{eff}} = \frac{2\rho_b}{N}(n_e - 1)\left[\int_{-\infty}^{0} dx \frac{1}{2}\left[1 + \text{Erf}(\beta_{N_e} x)\right]\right]. \tag{3.20}$$

If the total number of entanglements is the real number $n_e = n - 1$, then the final result in the symmetric case reads

$$\Sigma_{\text{eff}} = \frac{\rho_b(n-2)}{N\beta_{N_e}\sqrt{\pi}} = \frac{\rho_e L_e}{\sqrt{3\pi/2}}\left(1 - \frac{2M_e}{M}\right), \tag{3.21}$$

where we used $\rho_e = \rho_b/N_e$ and $L_e = b\sqrt{N_e}$. Equation (3.21) is exactly the same result that was obtained by Mikos and Peppas [2]. We also note that, except for chain end effects, the result is very similar to the one obtained with the simple Lake and Thomas approach, since $\sqrt{3\pi/2} \approx 2.17$.

3.2.1 Long chains approximation

Expression (3.19) is quite lengthy to evaluate and it may obscure the essential features of our model. Nevertheless it is possible to derive an excellent approximation in the case of long chains.

In a ν chains system, the density of the nth monomers along the chains is given by

$$\rho_n(x) = \nu\langle\delta(x - x_n)\rangle = \frac{\rho_b}{N} q(x; n) q(x; N - n). \tag{3.22}$$

In general the density profiles $\rho_n(x)$ are not uniform and are functions of n, that indicates the position along the chain, through $q(x; n)$. For infinite chains, we can neglect the chain end effects and we can imagine that all the monomers are infinitely distant from the chain ends, so that $q(x; n)$ approaches a function $q(x; \infty)$

not depending on n. For the same reason all the monomers will have the same density distribution

$$\frac{\rho_n(x)}{\rho_b} \equiv \frac{\phi(x)}{N}, \tag{3.23}$$

leading to

$$q(x;\infty) = \sqrt{\phi(x)}. \tag{3.24}$$

Notice that the approximation (3.24) is the same used in the classical work of Helfand and Tagami [18].

Substituting every $q(x;n)$ with $q(x;\infty)$ in eq. (3.19) and considering a real $n_e = n - 1$, we finally obtain

$$\Sigma_{\text{eff}} = \frac{2\rho_b}{N}(n-2)\left[\int_{-\infty}^{0} dx \int_{0}^{\infty} dx' \sqrt{\phi(x)} G_0(x,x';N_e)\sqrt{\phi(x')}\right], \tag{3.25}$$

where in addition we used G_0 as a rough approximation of the complete Green function. Expression (3.25) is surprisingly good in approximating the accurate results for the entire range of interfacial width, as shown in Figures 3.2 and 3.3. We also checked it for all the samples we studied, finding a comparable agreement.

We observe that in expression (3.25) the effective density Σ_{eff}, normalized with respect to its bulk value, is a universal function of a_I/L_e, at least if we assume that volume fractions follow the incompressible hyperbolic tangent profile. This is only approximately true for the complete expression (3.19), in which the molecular weights and other polymer parameters enter the self consistent probability distributions.

3.2.2 An alternative point of view

Expression (3.19) for $\langle\Sigma_{\text{eff}}\rangle$ can also be obtained in the following way. The number of effective entanglements is given by the mean density of the kth monomers times the probability that the following entanglement is on the other side of the interface. This can be represented as

$$\Sigma_{\text{eff}} = 2\sum_{k=1}^{n_e-1}\left[\int_{-\infty}^{0} dx_{i_k}\rho_{i_k}(x_{i_k}) \int_{0}^{\infty} dx_{i_{k+1}} p(x_{i_k}, x_{i_{k+1}};N_e)\right], \tag{3.26}$$

where the symmetry of entanglement positions with respect to the chain center is used, see eq.(3.14), and we denoted by $p(x_n, x_m; m-n)$ the probability of finding the mth monomer in x_m given that the nth is in x_n. In terms of the Green function we have

$$p(x_n, x_m; m-n) = G(x_n, x_m; m-n)\frac{q(x_m; N-m)}{q(x_n; N-n)}, \tag{3.27}$$

wherefrom expression (3.19) can be recovered.

In the approximation of very long chains we can rewrite eq.(3.25) as

$$\Sigma_{\text{eff}} = \frac{2\rho_b}{N}(n-2)\int_{-\infty}^{0} dx\phi(x)\int_{0}^{\infty} dx'\sqrt{\frac{\phi(x')}{\phi(x)}}G_0(x, x'; N_e), \tag{3.28}$$

and identify the expression in the second integral as an approximation for $p(x, x'; N_e)$.

3.2.3 Comparison with other approaches

Before exposing our numerical results it is useful to report in more detail two previous approaches for the calculation of Σ_{eff}, due respectively to Brown [55] and de Gennes [61].

The approach proposed by Brown is very similar in spirit to the stochastic description given above, but contains some simplifying assumptions. In particular, Brown neglected chain end effects and assumed that the probability that a strand starting from x might end in x' is proportional to the ratio of the polymer volume fractions at the two points. In this way he obtained the density of effective entanglements formed by one polymer as

$$\Sigma_{\text{eff}} = 2\rho_e\int_{-L_e}^{0} dx\phi(x)\int_{0}^{L_e+x} dx'\frac{\phi(x')}{2L_e\phi(x)}, \tag{3.29}$$

which in the homogeneous case, $\phi \equiv 1$, gives $\Sigma_{\text{eff}} = \rho_e L_e/2$ as predicted by the simple model resembling Lake and Thomas theory. In order to clarify the comparison with

our model, and in particular with equation (3.28), we also rewrite Brown's formula (3.29) as

$$\Sigma_{\text{eff}} = 2\rho_e \int_{-\infty}^{0} dx\phi(x) \int_{0}^{\infty} dx' \frac{\phi(x')}{\phi(x)} \frac{\theta(L_e - |x' - x|)}{2L_e}, \tag{3.30}$$

where $\theta(x)$ is the step function

$$\theta(x) = \begin{cases} 1 & \text{if } x > 0 \\ 0 & \text{if } x < 0. \end{cases} \tag{3.31}$$

Recalling that

$$\frac{2\rho_b}{N}(n-2) = 2\rho_e \left(1 - 2\frac{M_e}{M}\right), \tag{3.32}$$

a comparison between the two expressions is even clearer. In Brown's approach chain end effects are neglected, which is correct in the long chain limit, and chain connectivity is taken into account with a step function $\theta(L_e - |x' - x|)/2L_e$ that approximates the usual Gaussian $G_0(x, x'; N_e)$. The main difference, producing the bigger discrepancies in the numerical results, is that for long chains the probability scales as $\sqrt{\phi(x')/\phi(x)}$ while in his model it is linear in volume fractions ratio.

De Gennes used instead the following scaling arguments to predict the dependence of Σ_{eff} from the interaction parameter χ. If m monomers of polymer A are on the B side of the interface then the free energy involved is of the order $\Delta F = mk_BT\chi$. At equilibrium $\Delta F \approx k_BT$, so that the average number of monomers that penetrate the interface should be $\bar{m} = \chi^{-1}$. The corresponding width of the interface is related to the degree of interpenetration, so that we can say $a_I = b\sqrt{\bar{m}} = b\chi^{-1/2}$, in agreement with the main theories of inhomogeneous systems [18]. He then assumes that only arcs of chain of length greater than N_e are effective in carrying load. The probability of having an arc of length m on the other side of the interface is

$$p_m = \frac{1}{\bar{m}} \exp(-m/\bar{m}), \tag{3.33}$$

from which follows that the fraction of arcs of length greater than N_e should be

$$\varphi = \sum_{N_e}^{\infty} p_m \approx \exp(-\chi N_e). \tag{3.34}$$

It is therefore possible to write Σ_{eff} for each polymer as

$$\Sigma_{\text{eff}} = \Sigma_{\text{eff}}^{(\text{bulk})} \exp\left(-N_e(\chi - \chi_c)\right), \tag{3.35}$$

where we denoted with $\Sigma_{\text{eff}}^{(\text{bulk})}$ the bulk limit and with χ_c the critical interaction parameter for miscibility. The most important approximation contained in this scaling law is that all the monomers of effective strands are considered as located on the wrong side of the interface. This is not true in general, because effective strands cross the interface and we expect that only a part of them is on each side. Thus de Gennes' model overestimates the effect of energy interactions in preventing effective crossings and gives very low values for Σ_{eff}.

3.2.4 Numerical results

An accurate numerical evaluation of expression (3.19) has been obtained as follows. First we performed SCF calculations, as described in detail in chapter 2, to obtain the interface width, probability functions $q(x;i)$ and polymers mean fields. Then mean fields are inserted in the modified diffusion equation (3.3), which is solved numerically to obtain the needed Green functions. Finally, expression (3.19) is evaluated and the final result for Σ_{eff} is multiplied by $(n-2)/([n]-2)$ to consider the correct average number of entanglements, as discussed at the end of section 3.1.

In order to show the general dependence of Σ_{eff} on the interfacial width, we applied the method to the simple illustrative system, already introduced in chapter 2, simulating an interface between two materials with bulk parameters equal to those of PS and the same molecular weight 300k. For the interaction parameter χ we choose here values ranging from 0 to 0.05. The calculated values of Σ_{eff}, obtained for this system with equation (3.19), are showed in Figure 3.2 by joined full circles. For comparison in the same figure we show also the results obtained by

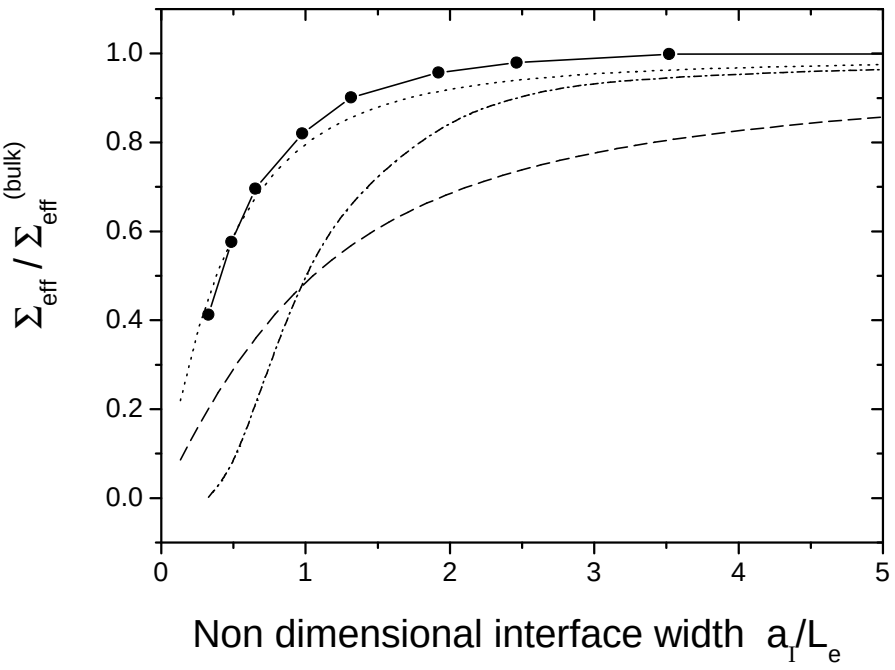

Figure 3.2: Areal density of effective entanglements as a function of the interfacial width a_I, for the illustrative system described in the text. Joined circles are obtained from equation (3.19), dotted line from approximate equation (3.25), dashed line from Brown's formula (3.29) and dash-dotted line from de Gennes' scaling law (3.35). Σ_{eff} is scaled with respect to its bulk value $\Sigma_{\text{eff}}^{(\text{bulk})} = 0.150$ nm^{-2}, and a_I with respect to the entanglement length of the system $L_e = 7.6$ nm.

applying Brown's equation (3.29)(dashed line), de Gennes' scaling law (3.35) (dash-dotted line) and those obtained with our long chain approximation (3.25) (dotted line). Noticing that the scale length over which Σ_{eff} varies is given by the distance between entanglements L_e, our model predicts a very quick saturation at relatively low interfacial widths, if compared with other approaches.

In Figure 3.3 variations of Σ_{eff} with the molecular weight, for the same illustrative system, are shown, assuming $\chi = 0.005$ and $N_A = N_B$. Moreover we used molecular weights being an integer multiple of M_e to avoid spurious effects due to our method of approximation. Increasing the molecular weight affects Σ_{eff} in two opposite ways: through the interface width by lowering it and through chain end effects by increasing

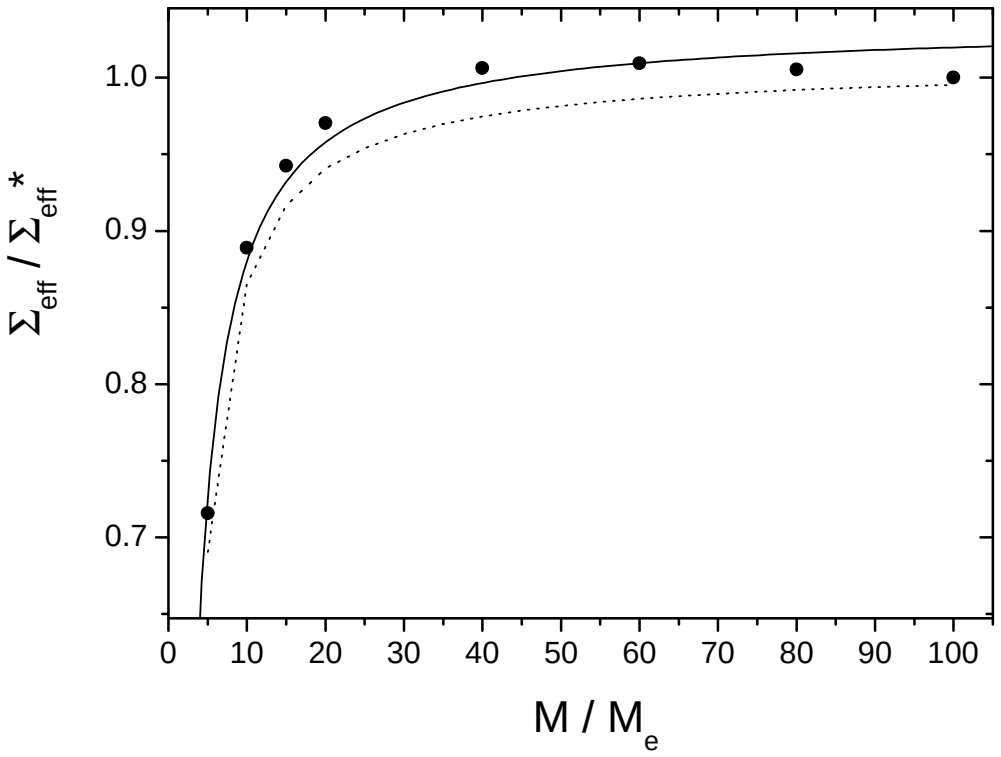

Figure 3.3: Areal density of effective entanglements as a function of the molecular weight of the two polymers, calculated for the illustrative symmetric system described in the text using equation (3.19) (full circles) and the approximate expression (3.25) (dotted line). Areal density is scaled with respect to $\Sigma^*_{\text{eff}} = 0.134\ \text{nm}^{-2}$, that is the value of Σ_{eff} calculated for $M/M_e = 100$. For comparison we plotted in solid line the function $(1 - 1.5M_e/M)$.

it. From the figure it is clear that chain end effects, that roughly contribute to Σ_{eff} with a factor $1-2M_e/M$, dominate, while the changes in width produce only a small correction. To demonstrate quantitatively that the chain end effects dominate, we fitted the calculated data with a function of the type $1 - pM_e/M$, and obtained $p \approx 1.5$. The corresponding function is plotted in Figure 3.1 as the solid line. This result is not surprising, since the dependence of the interfacial width from the molecular weight is weak. In fact only close to miscibility can a large change in the width be obtained by varying the molecular weight, but we have seen in Figure 3.2 that, for such large interfaces, Σ_{eff} has already reached saturation. We also plotted in the same figure the numerical results obtained with the long chain approximation (dotted line), that show an excellent agreement with the full calculations for all

molecular weights.

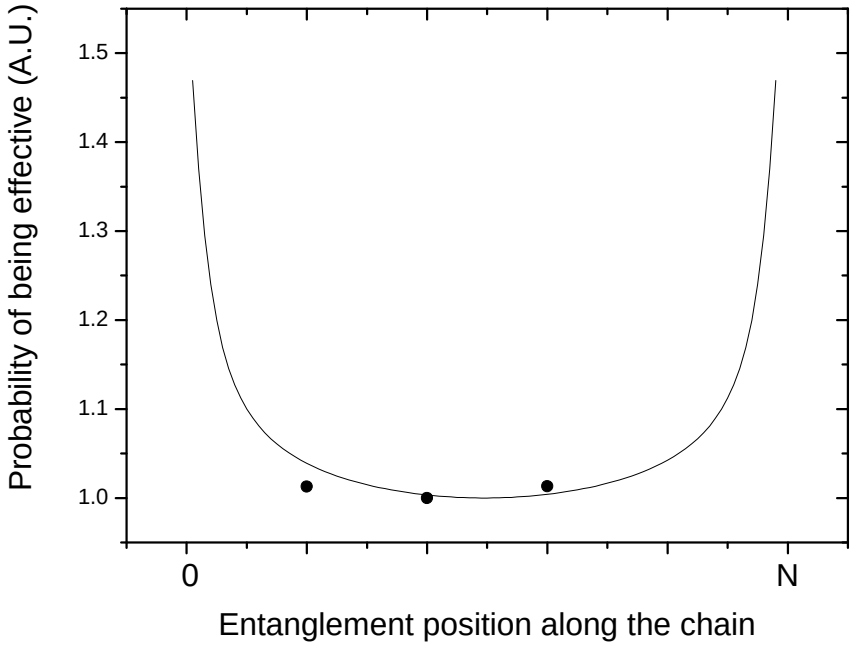

Figure 3.4: Probability of each segment of length N_e of forming an effective entanglement, as a function of its position along the chain. The probability of the innermost segment is taken as the unity. Two different chain lengths are considered: $N = 100N_e$ (solid line) and $N = 5N_e$ (circles), for which there are only 4 entanglements and therefore 3 strands in between.

Before ending this section we want to investigate also how entanglements localized at different positions along the chain contribute to the total Σ_{eff}. In Figure 3.4 we plot the quantity

$$\int_{-\infty}^{0} dx \int_{0}^{\infty} dx' q(x; i_k) G(x, x'; N_e) q(x'; N - i_{k+1}), \tag{3.36}$$

which is proportional, for every segment k, to its probability of crossing the interface and being effective in carrying load. The probability is normalized with respect to its value for the innermost segment and it is plotted for two different molecular weights, $M = 5M_e$ (circles) and $M = 100M_e$ (solid line). We see that segments closer to the chain end contribute most to Σ_{eff}, due to their greater freedom, and

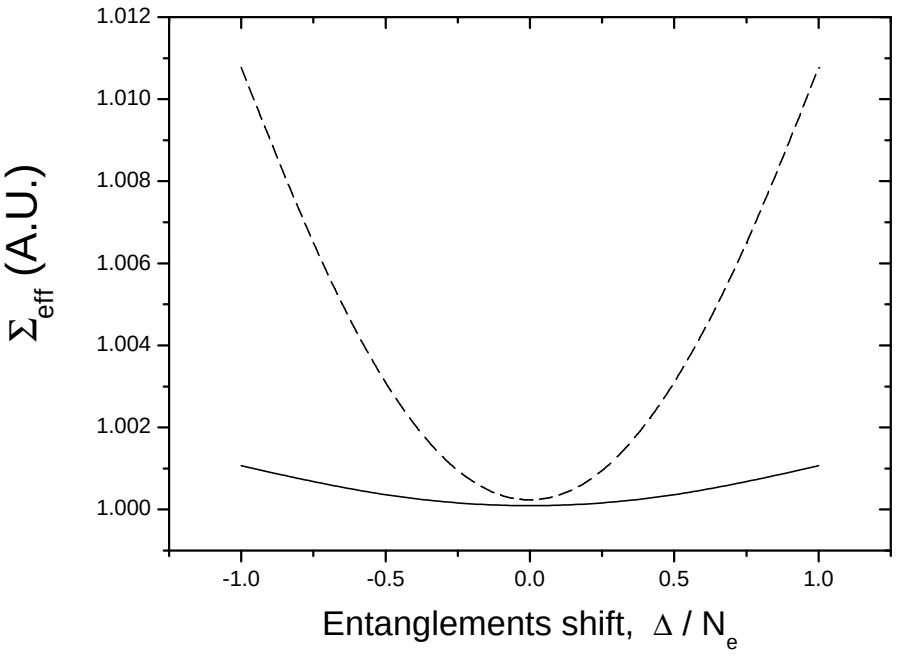

Figure 3.5: Effective density as a function of the entanglements shift along the chain Δ. Dashed and solid lines refer respectively to chains of length $N = 5N_e$ and $N = 100N_e$.

that the difference between different positions is more relevant for long chains. This observation could cast some doubts about our simple procedure to normalize Σ_{eff}, in which it is implicitly assumed that all entanglements are equivalent. Nevertheless it must be observed that for high molecular weights the effect on Σ_{eff} of adding (at most) one entanglement is very small. On the other hand, we see from Figure 3.4 that in shorter chains all the entanglements contribute to the same extent to the final Σ_{eff}.

In our simplified model we also assumed entanglements to be fixed in their positions and chose a symmetric distribution. We want to check what is the effect on Σ_{eff} of a shifting of all these positions along the chain. We therefore plot in Figure 3.5 the calculated Σ_{eff} as a function of Δ for chains with molecular weights $M = 5M_e$ (dashed line) and $M = 100M_e$ (solid line). Since the samples have an

integer number of segments, Δ can be varied between $-N_e$ and N_e, as it can be inferred from Figure 3.1a, and we see that the corresponding Σ_{eff} changes by about 1% for the shorter chains while it stays nearly constant for the longer ones. We can therefore conclude that our results are not strongly dependent on the choice of Δ.

3.3 Fracture mechanisms

In this section we describe how fracture energy of entangled interfaces can be calculated from Σ_{eff}. As done through the whole chapter we are only taking into consideration entangled chains, that, according to our model, have a molecular weight $M > 2M_e$. If chains are too short to be entangled, it is easy to pull them out from their surroundings, and such a process involves energies of the order of 1 J/m^2 or less. As discussed in the introduction for entangled chains we can distinguish two main regimes. At low densities, $\Sigma_{\text{eff}} < \Sigma_c$, there is no plastic deformation and chains fail by scission, originating fracture energies of the order of 1 to 10 J/m^2. When $\Sigma_{\text{eff}} > \Sigma_c$ crazing takes place and fracture energies higher than 100 J/m^2 are usually measured. These two regimes have been extensively studied and we report in this section the equations that are currently used to express fracture energy as a function of Σ_{eff}. We also show that it is important to introduce an intermediate regime, that we will call "partial crazing", to describe small plastic deformations.

3.3.1 Chain scission

At low densities, $\Sigma_{\text{eff}} < \Sigma_c$, and high molecular weights, $M > M_c$, the main failure mechanism is chain scission, as demonstrated by the studies on block copolymer reinforced interfaces already discussed in the introduction [56],[58]. Also computer simulations [75],[76] seem to confirm this prediction, showing that in highly entangled melts, the force needed to disentangle a chain is higher than the breaking force of covalent C-C bonds. The total fracture energy in this regime can be obtained following the classical Lake and Thomas approach [16]. It is assumed that, when pulling a strand between two subsequent entanglement, the supplied energy is shared between all bonds and, after breaking, it is dissipated. This leads to the following

expression for the fracture energy

$$G_c^{(\mathrm{sc})} = U_b \left(\Sigma_{\mathrm{eff}}^{(A)} N_e^{(A)} j^{(A)} + \Sigma_{\mathrm{eff}}^{(B)} N_e^{(B)} j^{(B)} \right), \tag{3.37}$$

where U_b is the energy needed to break a C-C bond, that is about 5×10^{-19} J, and all other quantities have already been defined. The expression obtained for $G_c^{(\mathrm{sc})}$ is linear in Σ_{eff} in agreement with experimental results [56],[58],[59] .

It is important to note that it cannot be excluded that some energy is also dissipated by chain pullout, but in our calculations we will assume that chain scission is the only process dissipating energy, and therefore it is completely responsible for fracture energy at low densities.

3.3.2 Crazing

If the interface is strong enough to sustain crazing stress σ_{craze}, then a plastic deformation occurs, capable of dissipating a huge amount of energy before the interface fails. The critical density for the onset of crazing is easily found as $\Sigma_c = \sigma_{\mathrm{craze}}/f_b$, where f_b is the maximum force that a C-C bond can sustain. Crazing regime was first described by Brown [17], and we briefly report his approach. At the microscopic level a craze is made by main fibrils, running perpendicular to the craze/bulk interface, and cross-tie fibrils, that connect main fibrils laterally, as schematically shown in Figure 3.6. Cross tie fibrils are essential in transferring stress in the lateral direction, with the result that there is a stress concentration at the crack tip. Brown modelled the crazed region, having a Young modulus much lower than the bulk material, as an elastic continuum between rigid boundaries; according to experimental results and to Dugdale model he also assumed the stress at the bulk/craze interface constant and equal to σ_{craze}. The tensile stress at a given distance x from the crack tip is then obtained as

$$\sigma(x) = k\sigma_{\mathrm{craze}} \sqrt{\frac{h}{x}}, \tag{3.38}$$

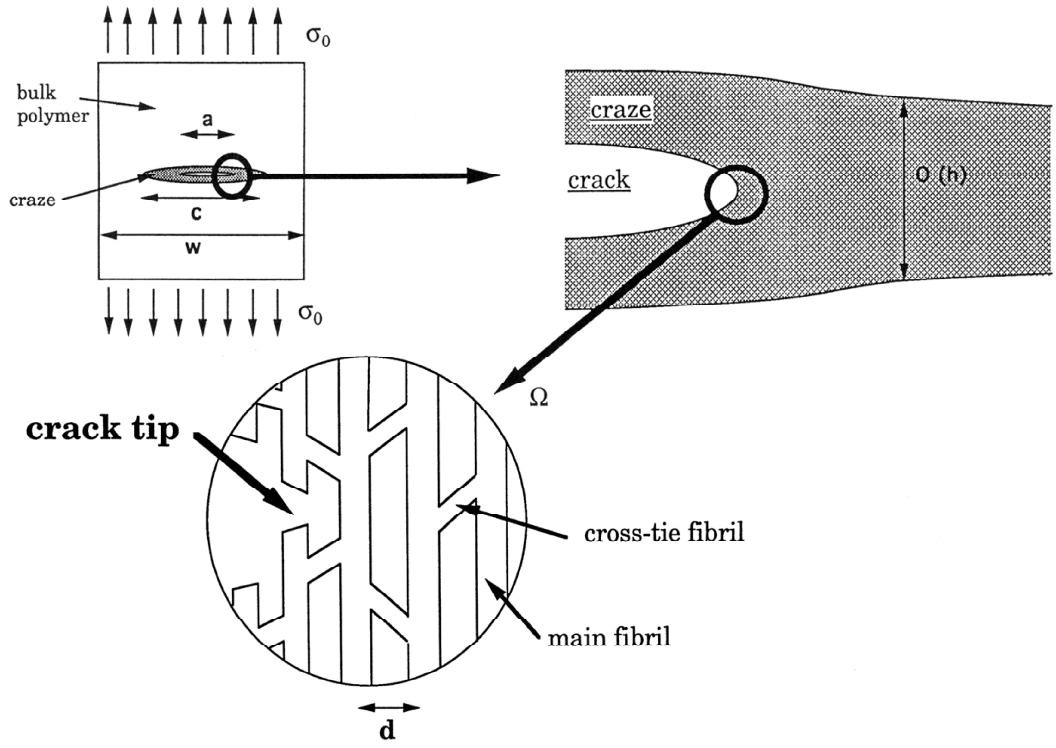

Figure 3.6: Schematic diagram illustrating the geometry of a crack inside a craze under external loading. Three different length scales are considered in order to show the quantities introduced in the text.

where k depends on the elastic properties of the craze and h is its maximum width. The stress will be maximum on the fibril closest to the crack tip, and it can be estimated as $\sigma_f = \sigma(d)$, where d is the fibril's spacing. The fracture criterion invoked by Brown states that a fibril breaks when $\sigma_f = \Sigma f_b$, where Σ is the density of load bearing strands in the fibril. From this relation the width h of the craze is given by

$$h = \left(\frac{\Sigma f_b}{k \sigma_{\text{craze}}} \right)^2 d \tag{3.39}$$

and the fracture energy is

$$G_c = h(1-v_f)\sigma_{\text{craze}} = \frac{\Sigma^2 f_b^2}{k^2 \sigma_{\text{craze}}} d(1-v_f), \tag{3.40}$$

where v_f is the fibrils volume fraction. The dependence of the fracture energy on Σ is quadratic, as confirmed by many experimental results [59],[56], [17],[57], some of which are reported in Figure 1.2. Note that the Σ appearing in the above fracture energy criterion is not exactly the same that we computed in the previous sections. In fact during craze formation some of the load bearing strands are broken, and only a fraction $q < 1$ survives [77]. We can however identify the effectively entangled strands that survive craze formation as the load bearing strands in the fibrils, and obtain $\Sigma = q\Sigma_{\text{eff}}$.

The continuum approach adopted by Brown fails for small crazes, this is why Sha and coworkers [78] developed a discrete version of Brown's model that predicts a fracture energy

$$G_c^{(\text{cr})} = \frac{\pi(1-v_f)\sigma_{\text{craze}} d}{-\alpha \log\left[1-\left(\sigma_{\text{craze}}/q\Sigma_{\text{eff}} f_b\right)^2\right]}, \tag{3.41}$$

where α is a dimensionless material constant depending on the effective Young modulus of the fibrils and on the angle between them, that is usually treated as a parameter of the model. Equation (3.41), where again we used $\Sigma = q\Sigma_{\text{eff}}$, is the one we will adopt in our numerical calculations together with expression (3.19). Note that $G_c^{(\text{cr})}$ is defined only if $q\Sigma_{\text{eff}} > \Sigma_c$, that can be interpreted as a condition for complete crazing.

3.3.3 Partial crazing

We have seen in the previous section that for $\Sigma_{\text{eff}} > \Sigma_c$ a plastic deformation takes place, but a discrete crazing model predicts that complete crazing is possible only if $\Sigma_{\text{eff}} > \Sigma_c/q$. What happens when $q\Sigma_{\text{eff}} < \Sigma_c < \Sigma_{\text{eff}}$? The interface is strong enough to sustain the crazing stress, but during craze formation some of the load bearing strands are broken and we know that the crazing formation is not complete. It is therefore advisable to introduce an intermediate regime, not yet taken into

consideration in the literature, that could be called "partial crazing". In this regime a craze starts, but it cannot fully develop. What happens is that a small plastic deformation takes place, but cross-tie fibrils are not yet created; this implies that lateral stress cannot be transferred and we expect fracture energy to be linear in Σ_{eff}, as for chain scission. In this section we propose a simple model to describe this partial crazing regime. When a craze develops, some of the load-bearing strands at the interface fail by chain scission. We assume that they are a constant fraction w of the total broken strands, including also those in the craze but away from the interface. The work per unit area needed to create a craze of width h is $\sigma_{\text{craze}} h(1-v_f)$. Assuming that the work is entirely spent to break entangled strands, which seems reasonable for the small craze widths we are considering, then the number of broken load-bearing strands per unit area is

$$\Sigma_{\text{broken}} = w \frac{\sigma_{\text{craze}} h(1-v_f)}{U_b N_e j}. \tag{3.42}$$

It is important to be careful in choosing N_e and j. For large widths h the majority of the broken strands probably belongs to the crazed material, while for small crazes there will be a consistent amount of strands of the other polymer. So it would be correct to write N_e and j as functions of L, but as a first approximation it is reasonable to take values relative to the material in which the craze grows. The fraction of broken load-bearing strands is probably a function of h too, but for the moment this complication will be neglected. The craze width can be calculated by imposing that its growth stops when the interface cannot sustain the crazing stress anymore, that is when $\Sigma = \Sigma_{\text{eff}} - \Sigma_{\text{broken}} = \Sigma_{\text{c}}$. From equation (3.42) the craze width is therefore

$$h = (\Sigma_{\text{eff}} - \Sigma_{\text{c}}) \frac{U_b N_e j}{w \sigma_{\text{craze}} (1-v_f)} \tag{3.43}$$

and consequently the fracture energy in the partial crazing regime is

$$G_c^{(\text{pc})} = G_c^{(\text{sc})}(\Sigma_{\text{c}}) + \sigma_{\text{craze}} h(1-v_f), \tag{3.44}$$

where $G_c^{(\mathrm{sc})}(\Sigma_\mathrm{c})$ indicates the fracture energy calculated for the scission mechanism at the critical density. This term is added because when Σ decreases to Σ_c the interface fails by chain scission. The derived expression for the fracture energy in the regime of partial crazing is linear in Σ_eff, as expected, and is steeper than the one obtained in the chain scission regime. The model also predicts that the critical width h_c, at which cross tie fibrils start to transfer load and a craze can fully develop, is obtained for $\Sigma_\mathrm{eff} = \Sigma_\mathrm{c}/q$ and is therefore given by

$$h_c = \left(\frac{1}{q} - 1\right) \frac{U_b N_e j}{w f_b (1 - v_f)}. \tag{3.45}$$

Using the values reported in Table 3.1 we obtain for PS $h_c = 113.6/w$ nm, where w is probably not smaller than 0.5 in such incomplete crazes. This value seems reasonable if compared with typical crazes width that are of the order of some μm. Moreover in their work Sha et al. [78] estimate that crazes with $h < 3l$, where l is the length of the main fibrils, are not fully developed, and give $l = 60$ nm for PS ; it follows that $h_c = 180$ nm, in agreement with our prediction.

Polymer	ρ (g cm^{-3})	C_∞	M_e [(a)] ($\times 10^{-3}$)	σ_craze (MPa)	α	q [(c)]	d [(c)] (nm)	v_f [(d)]
PMMA	1.15	9.1 [(a)]	10	100 [(b)]	0.015	0.63	17.7	0.25
PS	1.05	9.6 [(a)]	13.3	48 [(e)]		0.6	19.0	0.25
PpMS	1.015	17.6	13.3 *	31 [(e)]	0.027	0.6 *	19.0 *	0.25 *

Other parameters: f_b=1.115 nN, U_b=5$\times 10^{-19}$ J.

Table 3.1: Parameters used in the calculations. (a) From ref.[67]. (b) From ref.[14]. (c) From ref.[77]. (d) From ref.[78]. (e) From ref.[54]. (*) PS values.

3.4 Fracture energy calculations and comparison with experimental data

Not many experimental data are available in the literature to validate our method, because it is difficult to devise a system in which interfacial width can be changed over a wide range of values, while keeping all other experimental conditions constant. The experimental possibilities are mainly three. It is possible to anneal two beams of the same material for different times, as it has been done for PS [53], but in this case the sample is not in thermodynamic equilibrium and it cannot be described by our method. It is also possible to use two almost compatible materials and anneal them at different temperatures, as in the case of PS/PpMS [53]. Finally, for strongly immiscible polymers, a wide range of interfacial widths can be obtained by using a random copolymer; interfaces PMMA/P(S-r-MMA) have been studied by Brown [55], PS/PBr$_x$S by Schnell et al. [54], and PS/PS-r-PVP by Benkoski et al. [79]. In this section we apply our model to two of the above systems, namely PMMA/P(S-r-MMA) and PS/PpMS.

3.4.1 PS/P(S-r-MMA) interfaces

Interfaces between PMMA and a random copolymer P(S-r-MMA) have been experimentally investigated by Brown. He used thin layers of the copolymer to couple two sheets of PMMA, and changed the interface width by varying the PS fraction in the copolymer. The use of a thin layer ensured that the craze occurred mainly in the PMMA for every sample, and this is very important because the variations of fracture energy can be associated directly with a change in Σ_{eff}, without having to include corrections due to crazing details. Moreover Brown obtained a wide range of interfacial widths, compared with the entanglement lengths of the two materials, and performed the neutron reflectivity measurements on the same samples he used in the fracture tests. For all these reasons we believe that such an experiment can be used to test our model. Furthermore PS and PMMA are widely studied and there are many measurements available in the literature of their relevant bulk properties, as reported in Table 3.1. The random copolymer is treated as a homopolymer with

pre-averaged parameters and an empirical interaction parameter between PMMA and P(S-r-MMA) is introduced. This is simply an extension of Flory-Huggins theory and it is a widely used approach [80]-[83], that, even if it lacks a solid theoretical basis, could explain in many cases the enhanced miscibility of blends involving random copolymers [84]-[86]. Since we are working in a mean field approximation, the same approach is suitable for our calculation of Σ_{eff}, provided that the copolymer is "ideal", meaning that all correlations are lost between the chemical identity of successive monomers. When it is possible the effective parameters for the copolymer are extracted from experimental results, but this is not the case and we have to chose appropriate interpolations. In our calculations therefore we assume that the corresponding homopolymer has the same degree of polymerization of the copolymer, and is made of identical monomers with $M_0^{\text{h}} = xM_0^{\text{PS}} + (1-x)M_0^{\text{PMMA}}$, where x is the PS fraction in the copolymer. In a dense melt we can also assume that the mass density is given by the linear equation $\rho^{\text{h}} = x\rho^{\text{PS}} + (1-x)\rho^{\text{PMMA}}$. For the Kuhn segment length b the most widely used approach is the Gaussian interpolation. It is assumed that the copolymer behaves as a Gaussian chain with two different segment lengths for the two species, so that its squared radius of gyration is $R_g^2 = (xb_{PS}^2 + (1-x)b_{PMMA}^2)\, N/6$. It follows that the correct expression for the Kuhn segment length of the equivalent homopolymer is $b_{\text{h}}^2 = xb_{PS}^2 + (1-x)b_{PMMA}^2$. The molecular weight of entanglement can be related to the above quantities using the packing model of Fetters et al. [67], that will be discussed in more detail in chapter 4, predicting

$$M_e \propto \rho p^3, \tag{3.46}$$

where p is the packing length,

$$p \propto \frac{M_0}{b^2\rho}. \tag{3.47}$$

Considerable theoretical work has been done to derive an expression for the effective interaction parameter in blends involving random copolymers, but we prefer to choose an empirical χ so that the SCMF calculations would give experimental bare interfacial widths.

In Figure 3.7 we report the calculated Σ_{eff} as a function of the bare interfacial

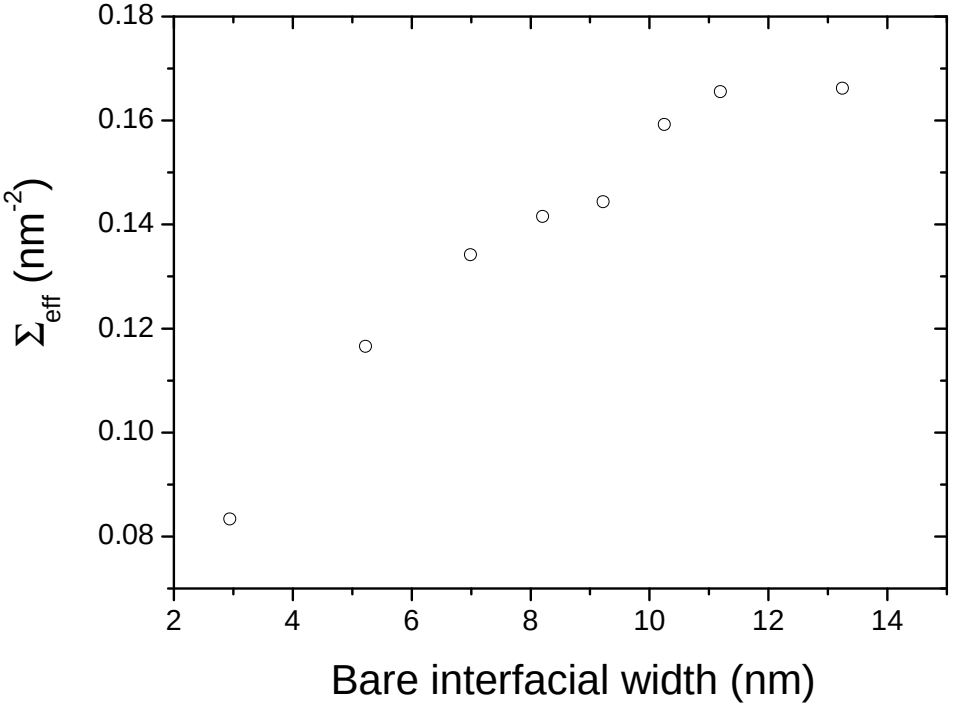

Figure 3.7: Areal density of effective entanglements as a function of the bare interfacial width, calculated with our model (eq.3.19) for the PMMA/P(S-r-MMA) samples investigated by Brown [55].

width for the PMMA/P(S-r-MMA) joints experimentally studied by Brown [55]. Bare interfacial width have been calculated by Brown using the relations suggested by Semenov [87] and Shull et al. [88]. The reason why the curve is not smooth is that in the experiments the molecular weight of the random copolymer was different for each sample. The measured and bare widths, together with the molecular weights of the polymers used in the experiment are reported in Table 3.2.

For the fracture energy calculations some of the craze parameters for PMMA, σ_{crazing}, v_f, d, q have been found in the literature, namely those reported in Table 3.1, while others have been chosen to fit the data. In particular the value for f_b was chosen such that it would give $\Sigma_c/q \approx 0.142$ nm^{-2}, and correspondingly a transition to complete crazing for widths around 9 nm, while α was chosen to fit the experimental fracture energy of the largest interface. The resulting fracture energy, calculated with our model, is compared with the experimental data by Brown [55] in Figure 3.8.

copolymer, % PS	M_w	measured a_I (nm)	bare a_I (nm)
20	165 000	15.7	13.0
30	300 000	13.7	11.1
40	265 000	12.9	10.3
55	125 000	12.0	9.5
68	160 000	10.7	8.2
78	173 000	9.5	7.0
89	180 000	7.6	5.2
100	330 000	5.0	2.9

Table 3.2: Interfacial widths between pure PMMA with $M_w = 127$ Kg/mol and different random copolymers P(S-r-MMA), as measured by Brown [55]. Bare widths have been obtained by Brown subtracting the effect of fluctuations due capillary waves [87],[88].

The fracture mechanisms predicted by the model are chain scission for the first pair, partial crazing for the following 3 samples and complete crazing for the others. In the partial crazing regime we used $w = 2/3$, that gives a critical length of about 120 nm, at which the cross-tie fibrils start to transfer load. This last result seems reasonable, since it is similar to the one already obtained for PS.

We notice that the agreement is good over the whole range of interfacial widths, agreement that is even more significant considering that we used literature values for most of the parameters.

A final comment should be made on the sigmoidal shape of the fracture energy as a function of the width. This is not directly related to Σ_{eff}, which is nearly linear below saturation, but is the result of a change in the fracture mechanism. For this reason it is not strange that the normalized fracture energy is not a universal function of the scaled width, a_I/L_e, as pointed out also by Benkoski et al. [89]. The width at which the transition to complete crazing occurs is in fact also a function of σ_{craze} and q.

3.4.2 PS/PpMS interfaces

The second system we studied is PS/PpMS, that has been experimentally investigated by Schnell et al. [53]. PpMS is very similar in structure to PS and, as

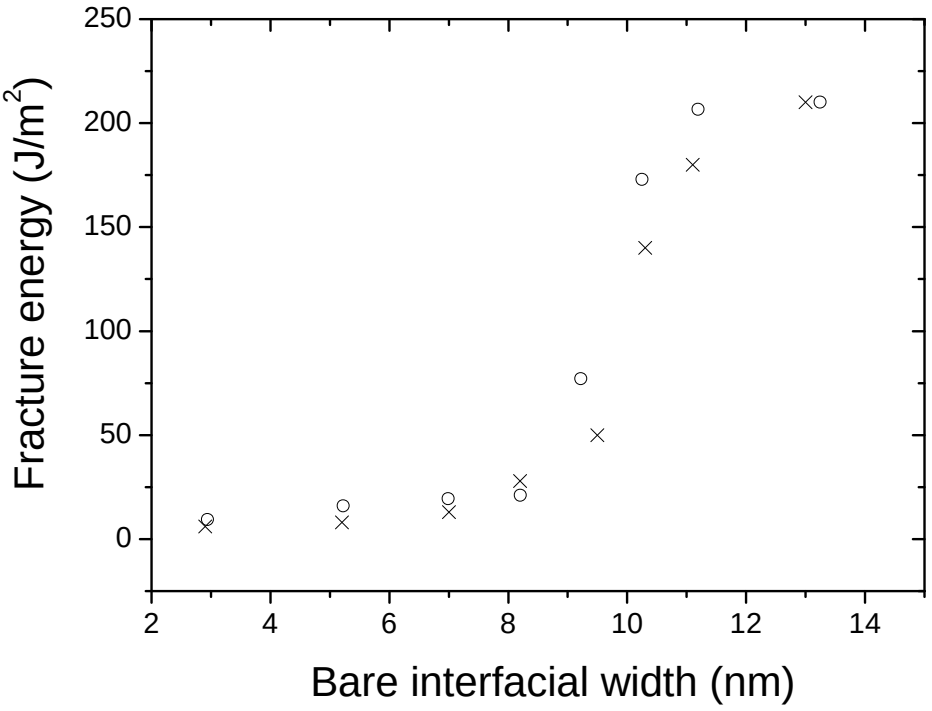

Figure 3.8: Fracture energy as a function of the bare interfacial width for PMMA/P(S-r-MMA), calculated from the Σ_{eff} given in Figure 3.7 (circles). Crosses represent experimental data by Brown [55].

a consequence, the two polymers are nearly miscible. In particular the width of the interface between them can be substantially changed by changing the annealing temperature of the sample or the molecular weight of the polymers. Schnell and coworkers performed neutron reflectivity tests on three different samples, namely PS(D) 105k / PpMS 131k, PS(D) 714k / PpMS 131k and PS(D) 714k / PpMS 613k, annealed at temperatures ranging from 120 to 180 °C and measured widths varying from 9 to 20 nm. These results were used to predict the interfacial widths of the samples that were used in the fracture energy tests, on which neutron reflectivity measurements were not performed. Some difficulties arise because the pairs used in the fracture tests have different molecular weights so that some theory must be used. The authors inverted the relation [38]

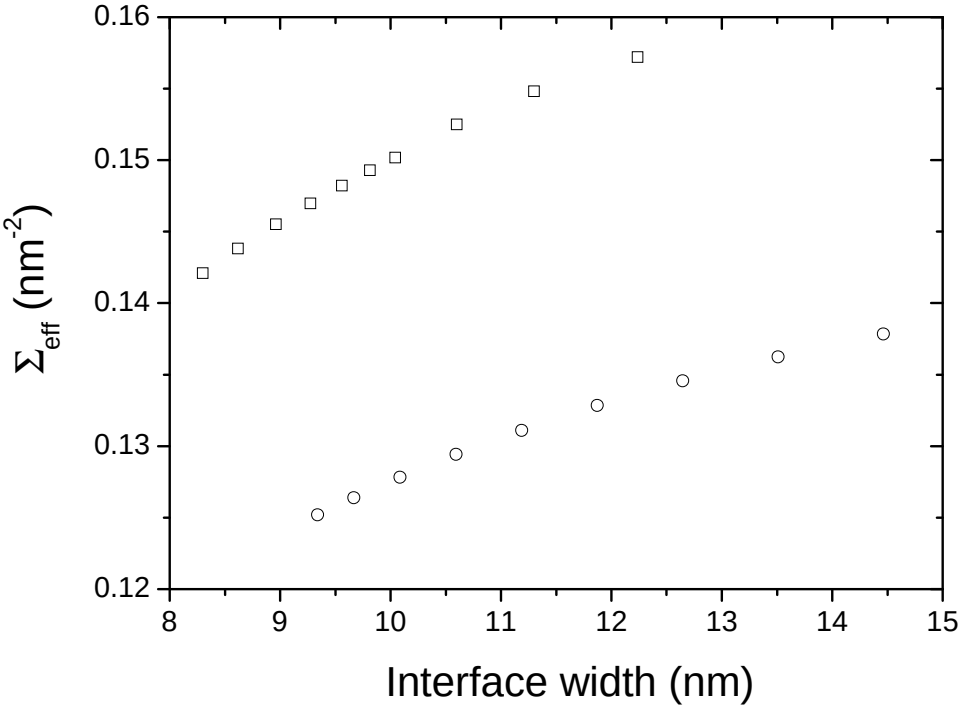

Figure 3.9: Areal density of effective entanglements as a function of the bare interfacial width, calculated with our model (eq.3.19) for two series of PS/PpMS interfaces: PS 1.25M/PpMS 570k (squares) and PS 139k/PpMS 157k (circles), at annealing temperatures ranging respectively from 120 to 210 °C and from 100 to 180 °C.

$$a_I = \frac{2b}{\sqrt{c\chi}} \left[1 - \frac{2\ln 2}{\chi} \left(\frac{1}{N_A} + \frac{1}{N_B} \right) \right]^{-1/2}, \tag{3.48}$$

to obtain χ as a function of the temperature, through the measured widths. Using $c = 7.5$ for the blends with the lowest molecular weights and $c = 6$ for the other two, and $b = 0.8$ nm they could obtain nearly the same function $\chi(T) = -0.011 + 6.8/T$ for all the three blends. Moreover the values of $\chi(T)$ were in agreement with the measurements of Jung and Fisher [90], so the authors decided to use such a χ and the relation (3.48) to predict the widths of the samples used in the fracture tests. We adopt here the same procedure, but the use $\chi(T)$ in our SCF calculation leads to slightly different widths with respect to the ones predicted by equation (3.48). The parameters used in the SCF calculations are reported in Table 3.1, but, while

for PS they have been measured by many different groups, for PpMS we could find only the values of the density and of the crazing stress in the literature. Since PpMS is very similar to PS for most of the other parameters we simply used PS values. PpMS stiffness C_∞, was chosen to obtain the proper value for the Kuhn segment length of the blend, $b_{\mathrm{PS/PpMS}} = \sqrt{(b^2_{\mathrm{PS}} + b^2_{\mathrm{PpMS}})/2} = 0.8\mathrm{nm}$, as found experimentally by Jung and Fisher [90] and assumed by Schnell et al.[53]. Since f_b was fixed by the previous fit, the only free parameter left is α. Again we used it to fit the highest experimental fracture energy.

The results for Σ_{eff} are displayed in Figure 3.9 for the pairs PS 1.25M/PpMS 570k and PS 139k / PpMS 157k. We note that for the investigated widths we are already in a saturation regime and that, fixing either width or temperature, the higher molecular weight sample shows the higher value of Σ_{eff}.

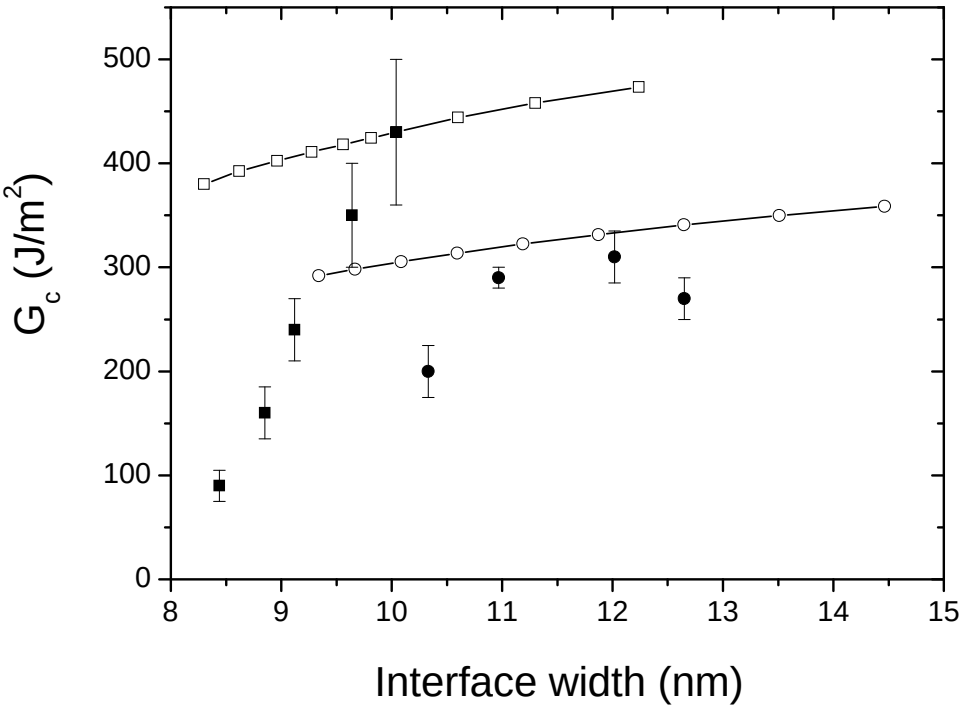

Figure 3.10: Fracture energy of PS/PpMS interfaces, calculated from the Σ_{eff} of Figure 3.9 (joined empty symbols). Experimental data from Schnell et al. [53] are also shown (full symbols). Two different pairs of molecular weights have been considered as in Figure 3.9: PS 1.25M/PpMS 570k (squares) and PS 139k/PpMS 157k (circles).

In Figure 3.10 we show the corresponding calculated fracture energies, compared with the experimental data by Schnell et al. [53]. As already discussed we derived the widths by using the measured temperature and the fitted χ in the SCF calculations; this is the reason why the experimental data in Figure 3.10 look a bit different from those in the original paper by Schnell and coworkers [53]. Notice that even if the ratio of the predicted saturation values for the two molecular weights seems to be correct, the experimental data show a rapid increase of the fracture energy for the two samples respectively around 9 nm and 11 nm, that is not reproduced by our model. As already discussed, the scale length over which saturation of Σ_{eff} is reached, is given in our model by the entanglements distance, that for this system is around 8 nm; in the experiments, instead, fracture energy saturates much more quickly. Such a behavior of G_c could be explained if the onset of crazing would arise for widths above 8.5 nm, but using the set of parameters discussed above we predict a much smaller value for the critical width. In fact for these samples crazing is the only predicted failure mechanism at all investigated temperatures. A more accurate estimate of PpMS parameters, would be needed to clarify this point.

In our calculations we neglected fluctuations due to capillary waves, that according to the work of Semenov [87] and Shull et al. [88], should correct all the measured widths of about 2 nm. This represent a correction of about 20 %, but, being the same for all the samples its inclusion cannot improve the comparison with experimental data. What we found, in fact, is that, including fluctuations, the plot of G_c as a function of the bare interfacial width is very similar to Figure 3.10, except that all the widths are about 2 nm smaller. Also Schnell and coworkers discussed the influence of capillary waves, but the agreement between the calculated χ and the measured one was so good, that they concluded fluctuations didn't play an important role and neglected it.

Chapter 4

Entanglements at polymer surfaces and interfaces

We have already stressed in the introduction how important is the concept of entanglement, and we showed in chapter 3 how M_e influences the fracture energy of a glassy polymer. In our numerical calculations we used values of M_e that have been measured for bulk polymers, but there are authors suggesting that M_e could be rather different at interfaces and surfaces [71]. A quantitative estimate of M_e in interfaces has been given by Ganesan and Pryamitsyn [72] and by Oslanec and Brown [73], who adopted a packing model of entanglements to predict M_e in interfaces. The two groups used different methods, but both found that M_e near a sharp interface can be as big as twice the bulk value.

In this chapter we describe the packing model of entanglements for bulk polymers, and propose a new method that extends this approach to inhomogeneous systems. The M_e is then computed numerically for interfaces and thin films; corrections to the fracture energy calculations of chapter 3 are presented.

4.1 Packing models of entanglements

The basic assumption of all packing models is that there is a relation between the size of the polymer coils and the degree to which they are entangled with each other. More precisely these models assumes that if a chain pervades a greater volume then

there is a greater probability that it forms an entanglement. This seems reasonable, since a chain that encounters many other chains is more likely to entangle than a closely coiled one, nevertheless there are authors having an opposite point of view. We mention here for example the models by Wu [62] and Wool [63] who predicted respectively $N_e \propto C_\infty^2$ and $N_e \propto C_\infty$, meaning that closely coiled chains should be more entangled than straighter chains. Recent data, collected by Fetters et al. [67] on a large number of polymers having very different chain stiffness, strongly support the packing model predictions, as we will show further down in this section. Therefore we shall base our analysis on the same premises.

In this section we present the quantitative descriptions of entanglements proposed by Fetters et al. [67] and Kavassalis and Noolandi [64], that are based on a static mean field description of dense chains and are appropriate for bulk polymers. We focus our attention on a chain, that we will call "test chain", and consider N_e consecutive monomers, which we will call "test segment". The test segment is assumed to form exactly one entanglement, and we will show how an entanglement criterion can be derived to determine N_e. First of all, the volume pervaded by the test segment, called hereafter V_p or "test volume", needs to be defined and estimated. The pervaded volume is usually defined as the volume of the smallest sphere containing entirely the segment and, one can assume that in the bulk this volume is proportional to the cube of the segment radius of gyration, i.e.

$$V_p = AR_g^3 = A\left(b\sqrt{N_e/6}\right)^3, \tag{4.1}$$

where A is a generic constant. The definition of V_p is somehow arbitrary and the choice of the radius of gyration is an approximation, but the scaling properties of V_p are correct, since we know that for Gaussian chains all the relevant lengths scale with $b\sqrt{N}$ in the bulk. We will see that this is not the case at interfaces and surfaces, for which it is not obvious how the above definition should be adapted.

The number of segments made of N_e monomers that would fill completely the pervaded volume is

$$N^* = V_p/V_0, \tag{4.2}$$

where

$$V_0 = N_e a^3 \tag{4.3}$$

is the packed volume of the test segment and $a^3 = M_0/\rho N_A$ is the volume occupied by one monomer. We can also interpret $N^* - 1$ as the number of segments of length N_e encountered by the test segment. Packing models assume that N^* is some universal number connected with the topological nature of entanglements, thus obtaining from equation (4.2) an entanglement criterion allowing to find scaling laws for N_e. In order to have a more physical picture, Witten et al. have defined a packing length p, that gives the number of individual chains in a given small volume of the melt, and that can be regarded as the fundamental quantity controlling M_e. For a chain with degree of polymerization N the packing length is defined as

$$p = \frac{M}{R_0^2 \rho N_A} = \frac{N a^3}{6 R_g^2}, \tag{4.4}$$

from which it can be seen that in the bulk p is independent of the chain length. From the above definition and the entanglement criterion (4.2) it follows that

$$N_e = \frac{6^3 N^{*2}}{A^2} p^3 / a^3, \tag{4.5}$$

a prediction that can be tested experimentally. Indeed the molecular weight of entanglement in the bulk is usually obtained from measurements of the plateau modulus G_N^0, which is related to M_e by

$$G_N^0 = \frac{4}{5} \frac{\rho k_B T N_A}{M_e} = \frac{4}{5} \frac{k_B T}{a^3 N_e}. \tag{4.6}$$

From the last equality one can predict that at constant temperature

$$G_N^0 \propto p^{-3}. \tag{4.7}$$

Such a scaling law has been tested by Fetters et al. [67] on a large number of polymers with very different properties. Their results are reported in Figure 4.1, where G_N^0, plotted against p^{-3}, exhibits a linear dependence. This behavior strongly supports to the validity of the packing model.

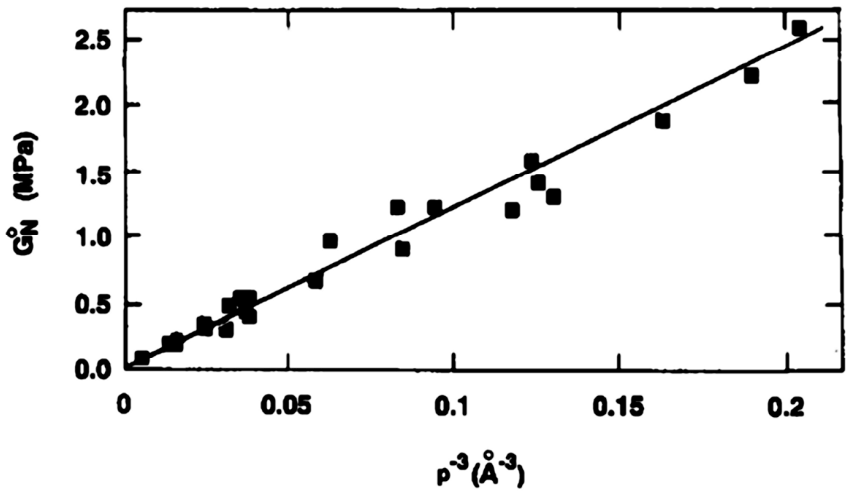

Figure 4.1: Linear plot of plateau modulus against the inverse cube of the packing length at 413 K for different polymers. After Fetters et al. [67].

A refined version of the packing model has been proposed by Kavassalis and Noolandi [64], who included chain end effects in their description. The fracture criterion (4.2) implies that on average $N^* - 1$ segments of length N_e should share the test volume with the test segment in order to form an entanglement. Kavassalis and Noolandi considered that the volume pervaded by the test chain can be occupied by segments of different lengths belonging to different chains. Moreover, they separated the contributions of tail segments, starting or ending inside the test volume, and non-tail segments, passing through it, in the belief that tail segments are not effective in forming entanglements. This observation is condensed in the following equation

$$V_p = a^3 \left[N_e + \sum_{m=1}^{N} (N_{\text{tails}}(m) + N_{\text{nontails}}(m))m \right], \tag{4.8}$$

where $N_{\text{tails}}(m)$ ($N_{\text{nontails}}(m)$) is the average number of tail (nontail) segments of length m contained in the test volume, excluding the test segment.

The entanglement criterion is finally written as

$$V_p = a^3 \left(N_e + \tilde{N} N_e + \sum_{m=1}^{N} N_{\text{tails}}(m) m \right), \tag{4.9}$$

where the coordination number $\tilde{N}$, defined by

$$\tilde{N} = N_e^{-1} \sum_{m=1}^{N} N_{\text{nontails}}(m) m, \tag{4.10}$$

has been introduced. $\tilde{N}$ can also be interpreted as the number of *nontail* segments of length N_e that a test segment must encounter to form an entanglement. The coordination number is therefore a measure of the topological constraints imposed on the test segment by other chains and it is analogous to $N^* - 1$, except that it excludes dangling ends. In this model $\tilde{N}$ is assumed to have a universal value, thus N_e can be computed from equation (4.10). This approach involves the calculation of the distribution of segments lengths, and it quite cumbersome; an alternative approximate method is the following. The average number of tails in the test volume is $2V_e/a^3N$ and their average length is $N_e/2$, leading to the relation

$$\sum_{m=1}^{N} N_{\text{tails}}(m) m \approx \frac{V_e N_e}{a^3 N}. \tag{4.11}$$

The entanglement criterion is then rewritten in the approximate form

$$\frac{V_p}{N_e a^3} \left(1 - \frac{N_e}{N} \right) = (\tilde{N} + 1), \tag{4.12}$$

from which N_e can be computed for $\tilde{N}$ known. Since the degree of polymerization N enters the above criterion, it follows that M_e depends on the molecular weight of chains; a typical dependence of N_e on N is shown in Figure 4.2.

We note that in the long chain limit the two criterions expressed by equations (4.2) and (4.12) are the same, provided that $\tilde{N}$ is identified with $N^* - 1$. In order to test their model, Kavassalis and Noolandi computed $\tilde{N} + 1$ from the molecular weights of entanglement measured experimentally for 13 different polymers with very high molecular weights. They found an average value of 9.1 with a standard deviation of 8% [65], thus confirming the validity of the packing model.

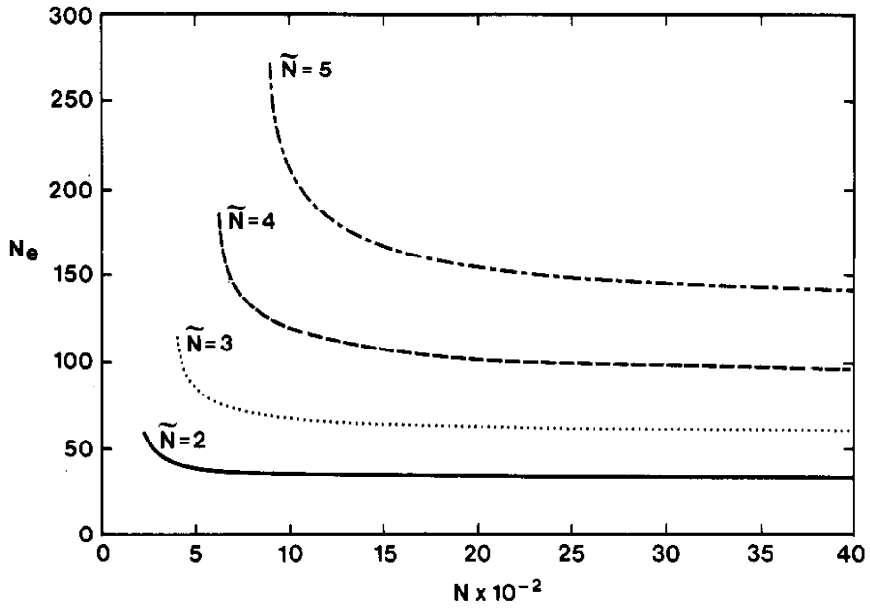

Figure 4.2: Mean spacing between entanglements versus degree of polymerization for several values of the coordination number and a typical chain stiffness. The curves terminate abruptly at $N = N_c$ and approach, in the long chain limit, a constant value given by equation (4.5) with $N^* = \tilde{N} + 1$. After Kavassalis and Noolandi [64].

4.2 Molecular weight of entanglement in inhomogeneous systems

The packing model has been proved to work for bulk polymers, it is then natural to apply it to inhomogeneous systems. We will work in a mean field approximation and for simplicity we will assume through the whole section that the inhomogeneity is only along one direction, denoted by x.

The first problem that we have to address in extending the packing model is the definition of the pervaded volume. We said that its exact definition is not essential in the bulk, since the final scaling law $V_p \propto \sqrt{N}$, is always obtained. On the contrary a precise definition of the pervaded volume is very important in interfaces or surfaces where, for example, the radius of gyration and the mean squared end-to-end distance vary differently with the dimensions of the inhomogeneity. Moreover, in a mean field description, the definition of the pervaded volume that we gave in the

previous section has no real meaning, since a chain can be entirely contained in the test volume only with a certain probability. Nevertheless we believe that the chain extension in one direction can still be considered proportional to the corresponding component of the radius of gyration, and we will adopt this assumption in our derivation.

In an interface or near a surface the components of the radius of gyration along the three directions are not the same, so that the shape that is more suitable to contain the test segment is not a sphere. It turns out that it is more appropriate the use of an ellipsoid, a parallelepiped or a cylinder, and we write the volume pervaded by the test segment as

$$V_p = A' R_{g,x} R_{g,y} R_{g,z}, \tag{4.13}$$

where A' is a constant and $R_{g,\alpha}$ is the component of the radius of gyration of the test segment along the $\alpha = \{x, y, z\}$ axis. Obviously, the squared radius of gyration is given by

$$R_g^2 = R_{g,x}^2 + R_{g,y}^2 + R_{g,z}^2, \tag{4.14}$$

and the packed volume of the test segment is the same as in the bulk, $V_0 = N_e a^3$. We now want to apply the entanglement criterion (4.2), which is suitable for high molecular weight chains, to find how N_e changes with respect to its bulk value. Since the external field varies only in the x direction, we can write

$$R_{g,y} = R_{g,z} = \frac{b}{\sqrt{18}} \sqrt{N_e}. \tag{4.15}$$

The x component of the radius of gyration instead will depend not only on the length, but also on the position of the segment. We write this latter dependence in terms of the starting point of the segment, x_0, and neglect for the moment the possible dependence on the position of the segment along the test chain. We then set $R_{g,x} \equiv R_{g,x}(x_0)$ and obtain

$$\frac{V_p}{V_0} = \frac{A' b^2}{18 a^3} R_{g,x}(x_0). \tag{4.16}$$

In the bulk $N_e = N_e^b$, $R_{g,x} = R_{g,x}^b = b\sqrt{N_e^b/18}$ and the criterion (4.2) leads to

$$\frac{A'b^2}{18a^3} = N^* \frac{\sqrt{18}}{b\sqrt{N_e^b}}. \tag{4.17}$$

In an inhomogeneous system the same entanglement criterion can therefore be written as

$$R_{g,x}(x_0) = \frac{b}{\sqrt{18}}\sqrt{N_e^b}. \tag{4.18}$$

This is an implicit equation for N_e through $R_{g,x}(x_0)$, and it is the one we will use in the following sections to determine the molecular weight of entanglement. In general it cannot be solved analytically, so that we will present only numerical evaluations of N_e for interfaces and thin films, but its main consequences can be already discussed from a qualitative point of view.

Near an interface or a surface, chains are known to be compressed in the perpendicular direction, thus their $R_{g,x}$ is smaller than in the bulk. In order to satisfy equation (4.18), the test segment should have the same $R_{g,x}$ as in the bulk, and this can be achieved only if N_e is larger than N_e^b. An analytical relation between the radius of gyration and N_e can be obtained if we assume that, even in an inhomogeneous system, each component of the radius of gyration is proportional to the square root of the chain length, that is if we can write

$$R_{g,x}(x_0) = c(x_0)\frac{b}{\sqrt{18}}\sqrt{N_e}, \tag{4.19}$$

where

$$c(x_0) = \frac{R_{g,x}}{R_{g,x}^b}. \tag{4.20}$$

In this approximation $c(x_0)$ is independent of N_e and from equation (4.18) we get

$$\frac{N_e}{N_e^b} = c(x_0)^{-2}, \tag{4.21}$$

that in general can be treated as an approximate relation to estimate N_e.

4.3 Radius of gyration

We found in the previous section that in an inhomogeneous system N_e can be obtained by inverting equation (4.18). We need then a method to compute the component of the radius of gyration along the x direction, $R_{g,x}$, as a function of N_e and x_0. Here we describe very quickly how this calculation can be performed in a mean field approximation.

The radius of gyration of a chain of length N is defined as

$$R_g^2 = \frac{1}{N}\sum_{i=1}^{N}\langle(\mathbf{r}_i - \mathbf{r}_G)^2\rangle, \tag{4.22}$$

where $\mathbf{r}_i$ is the position of the ith monomer along the chain and $\mathbf{r}_G$ is the chain center of mass

$$\mathbf{r}_G = \frac{1}{N}\sum_{i=1}^{N}\mathbf{r}_i. \tag{4.23}$$

For practical reasons it is better to introduce the equivalent definition

$$R_g^2 = \frac{1}{N^2}\sum_{i=1}^{N-1}\sum_{j=i+1}^{N}\langle(\mathbf{r}_i - \mathbf{r}_j)^2\rangle, \tag{4.24}$$

which is easier to evaluate numerically. Adopting a continuous notation for the monomer positions along the chain, the above definition becomes

$$R_g^2 = \frac{1}{N^2}\int_0^N dn\int_n^N dm\langle(\mathbf{r}_m - \mathbf{r}_n)^2\rangle. \tag{4.25}$$

It is well known that for a Gaussian chain in the bulk, where no external fields are present,

$$R_g^{b\,2} = \frac{1}{6}Nb^2. \tag{4.26}$$

In an inhomogeneous system the mean value of any physical quantity depending on the position of two monomers, while a chain end is held fixed at $\mathbf{r}_0$, is given by

$$\langle A(\mathbf{r}_n, \mathbf{r}_m)\rangle_0 = \int d\mathbf{r}_m \int d\mathbf{r}_n p(\mathbf{r}_0, \mathbf{r}_n; n)p(\mathbf{r}_n, \mathbf{r}_m; m-n)A(\mathbf{r}_n, \mathbf{r}_m), \tag{4.27}$$

where $m > n$ and $p(\mathbf{r}_n, \mathbf{r}_m; m-n)$ is the normalized probability of finding the mth monomer in $\mathbf{r}_m$ given that the nth is in $\mathbf{r}_n$. This quantity has already been found, in chapter 3, in terms of the Green function as

$$p(\mathbf{r}_n, \mathbf{r}_m; m-n) = G(\mathbf{r}_n, \mathbf{r}_m; m-n)\frac{q(\mathbf{r}_m; N-m)}{q(\mathbf{r}_n; N-n)}. \tag{4.28}$$

Substituting $A(\mathbf{r}_n, \mathbf{r}_m) = (\mathbf{r}_m - \mathbf{r}_n)^2$, we obtain

$$\langle(\mathbf{r}_m - \mathbf{r}_n)^2\rangle_0 = \int d\mathbf{r}_m \int d\mathbf{r}_n p(\mathbf{r}_0, \mathbf{r}_n; n) p(\mathbf{r}_n, \mathbf{r}_m; m-n) \left(\mathbf{r}_m - \mathbf{r}_n\right)^2, \tag{4.29}$$

where again $m > n$, and the radius of gyration is finally given by

$$R_g^2(\mathbf{r}_0) = \frac{1}{N^2}\int_0^N dn \int_n^N dm \langle(\mathbf{r}_m - \mathbf{r}_n)^2\rangle_0. \tag{4.30}$$

From the very definition it is evident how the radius of gyration can be decomposed into its three components along the principal axes. In our system the external field varies only in the x direction, so that we can write

$$R_{g,x}^2(x_0) = \frac{1}{N^2}\int_0^N dn \int_n^N dm \langle(x_m - x_n)^2\rangle_0, \tag{4.31}$$

$$R_{g,y}^2 = R_{g,z}^2 = \frac{1}{18} N b^2. \tag{4.32}$$

For the same reason $q(\mathbf{r}; n)$ will depend only on x, and

$$G(\mathbf{r}_n, \mathbf{r}_m; m-n) = G_0(y_n, y_m; m-n) G_0(z_n, z_m; m-n) G(x_n, x_m; m-n), \tag{4.33}$$

where

$$G_0(x, x'; N) = \frac{\sqrt{3/2\pi}}{b\sqrt{N}} \exp\left[-\frac{3\left(x - x'\right)^2}{2Nb^2}\right], \tag{4.34}$$

and $G(x_n, x_m; m-n)$ depends on the field. Using the above relations we find

$$\langle (x_m - x_n)^2 \rangle_0 = \int dx_m \int dx_n G(x_0, x_n; n) G(x_n, x_m; m-n) \frac{q(x_m; N-m)}{q(x_0; N)} (x_m - x_n)^2 . \tag{4.35}$$

The radius of gyration of a Gaussian chain in an external field can be computed finally from equations (4.31), (4.32) and (4.35).

As a matter of fact we are more interested in the radius of gyration of a segment of length N_e, belonging to a chain with degree of polymerization N, in which the first monomer, that we assume to be the Δth along the chain, is fixed at position $\mathbf{r}_0$. The relevant equations have then to be modified as follows

$$R^2_{g,x}(x_0) = \frac{1}{N_e^2} \int_0^{N_e} dn \int_n^{N_e} dm \langle (x_m - x_n)^2 \rangle_0, \tag{4.36}$$

$$\begin{aligned} &\langle (x_m - x_n)^2 \rangle_0 = \\ &= \int dx_m \int dx_n G(x_0, x_n; n) G(x_n, x_m; m-n) \frac{q(x_m; N-m-\Delta)}{q(x_0; N-\Delta)} (x_m - x_n)^2 , \end{aligned} \tag{4.37}$$

$$R^2_{g,y} = R^2_{g,z} = \frac{1}{18} N_e b^2. \tag{4.38}$$

4.4 M_e at interfaces

In this section we explicitly compute the molecular weight of entanglement at interfaces between immiscible polymers using the criterion (4.18) and the radius of gyration given by equations (4.36)-(4.37). The needed Green functions and probability distributions q are obtained from the SCF calculation, as already described in chapter 2. In this section we present the results obtained for a simple symmetric system, in order to show the main predictions of the model.

Similarly to the previous chapters we study the interface between two materials with bulk parameters equal to those of PS and the same molecular weight $M = 300k$. In particular for bulk PS $N_e^b \approx 128$ and the root mean square end-to-end distance

between entanglements is $L_e \approx 7.6$ nm, a value that can be taken as an estimate of the length of test segments. Arbitrary interfacial widths are obtained as usual by varying the interaction parameters χ at will. In such interfaces both polymers have symmetric concentration profiles and identical properties. It is therefore sufficient to consider only one of them, which we will call polymer A, whose bulk phase is located on the negative part of the x axis.

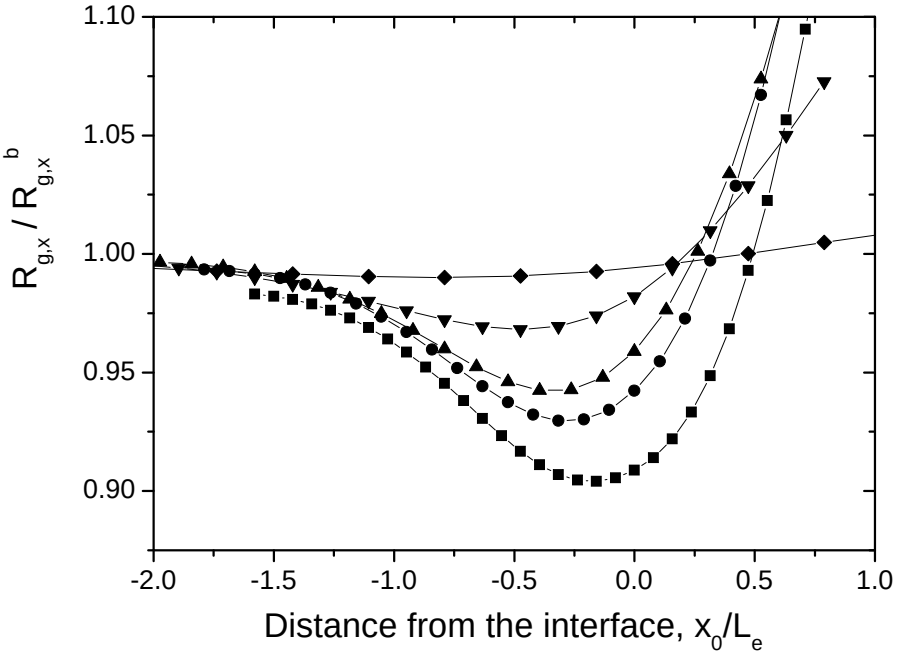

Figure 4.3: Scaled x component of the radius of gyration, $R_{g,x}/R^b_{g,x}$, calculated for a segment of length N^b_e as a function of the position x_0 of its first monomer, for the illustrative system described in the text. The interface is located at $x = 0$ and different interfacial widths are considered: $a_I = 2.5$ nm (squares), 3.75 nm (circles), 5 nm (upper triangles), 10 nm (lower triangles) and 27 nm (diamonds).

We computed $R_{g,x}$ for a test segment of length N^b_e as a function of the position x_0 of its first monomer, and show in Figure 4.3 the results obtained for different interfacial widths. In the numerical calculations we used $\Delta = N/2$, in order to avoid chain end effects and obtain meaningful results; the consequences of choosing

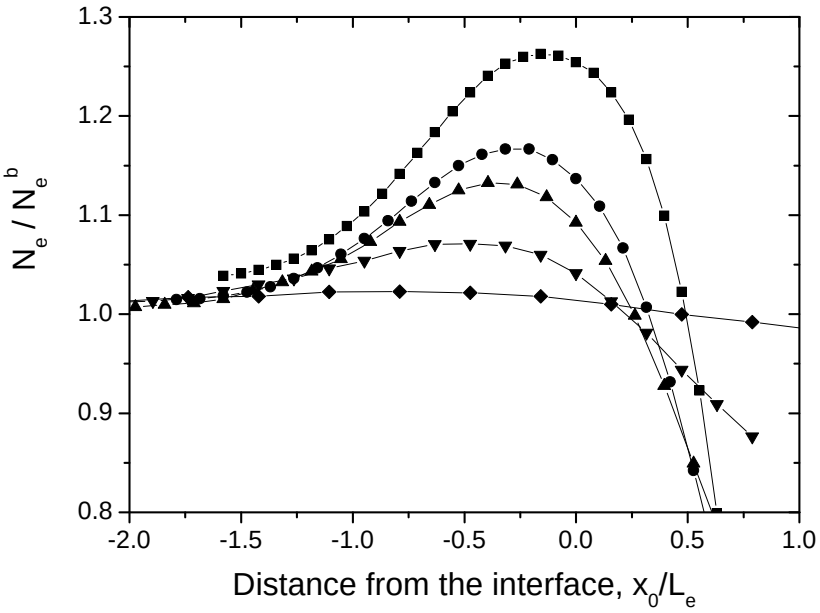

Figure 4.4: Scaled mean spacing between entanglements as a function of the starting position of the strand. Symbols and parameters are as in Figure 4.3.

a different Δ will be discussed further down. We note that an appreciable change in the radius of gyration is predicted only for widths $a_I < L_e$, because in wider interfaces the external field experienced by a segment is nearly constant. As the test segment position changes we distinguish three main regions. Segments starting at $x_0 < -2L_e$ seem to be unaffected by the interface for any width. Indeed, for widths $a_I < L_e$, the segments are too short to reach the interfacial region, while for $a_I > L_e$ we have already noticed that their radius of gyration changes very little. When $-2L_e < x_0 < 0$ the segments experience the highest gradient of the external field and are more coiled. We can imagine that a sharp interface acts like a surface or an impenetrable wall, reflecting the segments of polymer A starting on the A-rich side of the interface. We also notice that the radius of gyration reaches its minimum value when x_0 is very close to the interface, but not exactly at $x_0 = 0$. When $x_0 > 0$, segments start on the "wrong" B-rich side of the interface, and there is a high probability that they cross the interface. The larger x_0 the more they are stretched, until the radius of gyration equals its bulk value and eventually starts to

increase indefinitely. The critical distance $x_0 = x_c$, at which $N_e/N_e^b = 1$, depends on the interface width, and is larger for smaller widths. Figure 4.3 shows that a maximum value of $x_c \approx 4$ nm is found for $a_I = 2.5$ nm. We finally note that it is irrelevant to consider $x_0 >> a_I$, since in those regions the density of polymer A is practically 0.

The number of monomers between entanglements N_e has been numerically computed for different interfacial widths by inverting equation (4.18). In practice we first fix x_0 and then change N_e, until the corresponding $R_{g,x}$ satisfies the entanglement criterion. The resulting N_e are reported in Figure 4.4 as functions of x_0 for the same interfaces as in Figure 4.3. We see that, as expected, N_e is greater than in the bulk, at least in the regions where there is an appreciable density of A segments. The maximum correction to the bulk value is obtained for the narrowest interface, although it is only of about 25%. The three regions we described above are still present and all the comments we made remain valid.

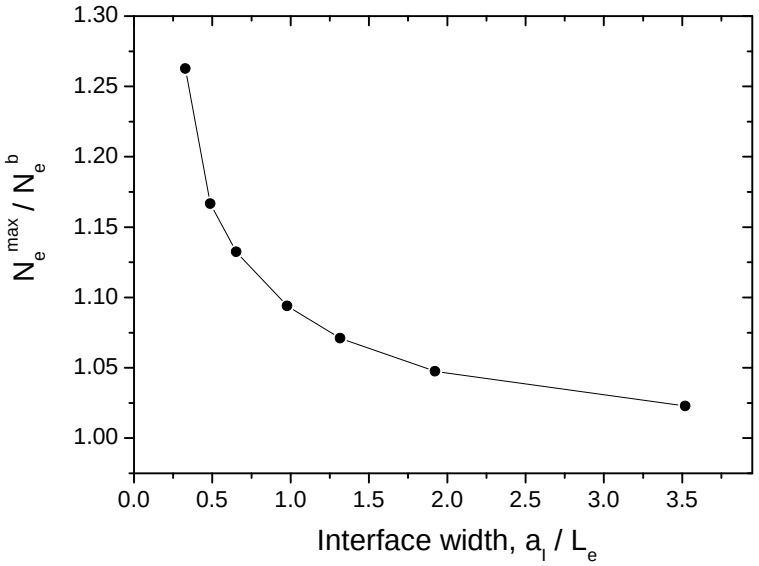

Figure 4.5: Maximum value of the mean spacing between entanglements as a function of the interface width. All parameters as in Figures 4.4 and 4.3.

An idea of how N_e depends on the interfacial width is given by the plot in Figure

4.5, where the maximum value of N_e/N_e^b is plotted against a_I in full circles. Our results show that, as a consequence of the packing model assumptions, an interface affects the entanglements only if its width is comparable with L_e.

We focus now our attention on the sample with the narrowest interface ($a_I = 2.5$ nm), and discuss the simplified formula (4.21) proposed in section 2. In Figure 4.6 we plot the N_e obtained from numerical inversion of equation (4.18) (solid line) and compare it with the values obtained from approximate equation (4.21) (dashed line). The two curves are similar, but not equal, meaning that the radius of gyration in an interface is not exactly proportional to $\sqrt{N}$.

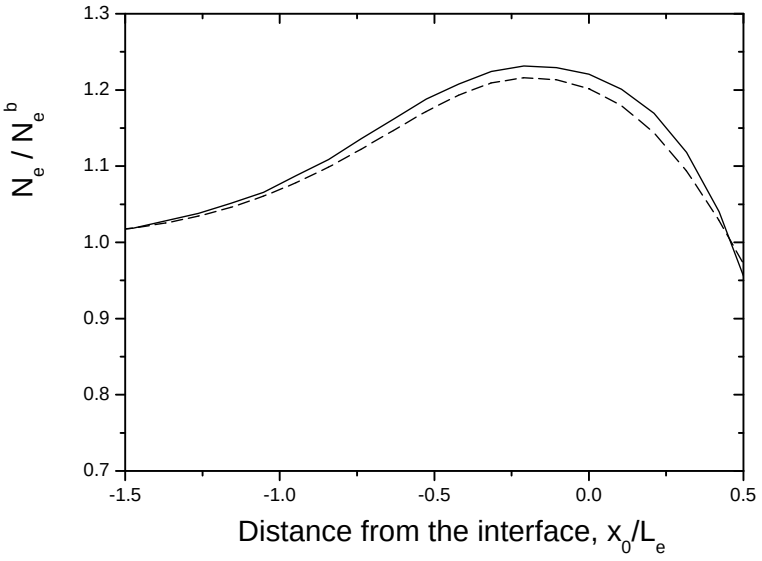

Figure 4.6: Scaled mean spacing between entanglements calculated from equation (4.18) for the sample with $a_I = 2.5$ nm as a function of the position of the first monomer of the strand x_0 (solid line). The dashed line is obtained from the radius of gyration plotted in Figure 4.3 with filled squares, using the approximate equation (4.21).

Finally we discuss the dependence of N_e on the position of the test segment along the chain. We changed Δ from 0 to $N - N_e$ for the sample with $a_I = 50$ nm and computed N_e as a function of x_0, obtaining the results displayed in Figure 4.7. A very different behavior is predicted for segments near the free chain end, that have a

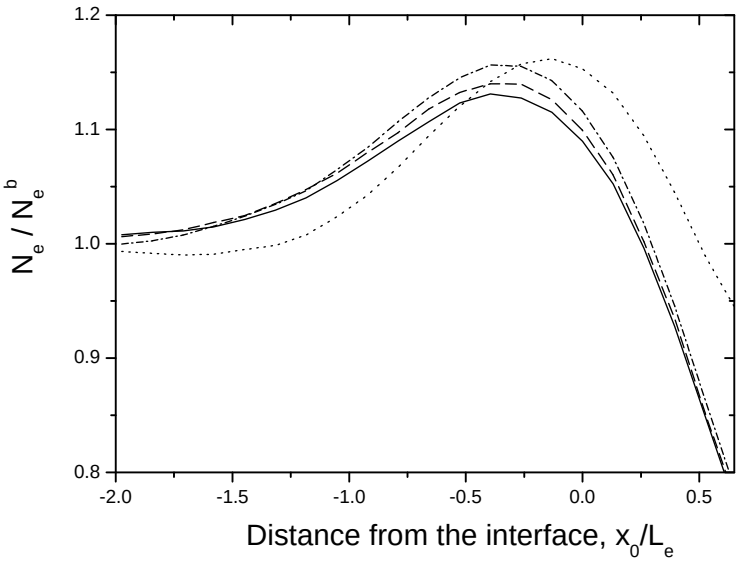

Figure 4.7: Scaled mean spacing between entanglements calculated from eq.(4.18) for the sample with $a_I = 5$ nm as a function of the position of the first monomer of the strand x_0. Different position of the strand along the chain are considered when computing the radius of gyration from eq. (4.36) and (4.37): $\Delta = 0$ (solid line), $N/2$ (dashed line), $4/5N$ (dash-dotted line) and $N - N_e$ (dotted line).

greater freedom. We remark that if we had considered a standing alone segment, we would have obtained the same curve plotted here for $\Delta = N - N_e$, and consequently a shift of the maximum toward the interface. From a practical point of view the choice of Δ has little importance, as long as the segment is chosen far from chain ends. Indeed we note that, except for the case $\Delta = N - N_e$, the curves are very similar. Moreover, in the model presented in section 3.1, we assumed that entanglements cannot be formed too close to chain ends, thus imposing $N_e < \Delta < N - 2N_e$.

To our knowledge no experiments have been proposed or performed to measure the molecular weight of entanglement in interfaces, and very few authors have considered the theoretical problem [71]-[73].

Oslanec and Brown [73] used an approach similar to the one we described and obtained comparable results. The only difference is that they implicitly assumed

that the test segment could not form effective entanglements with other segments of the test chain; consequently they find values of N_e which are slightly higher than the ones we showed.

We also mention the work of Ganesan and Pryamitsyn [72], who used a Monte Carlo technique to estimate N_e in the framework of the Kavassalis and Noolandi approach [64]. More precisely they were able to compute an average coordination number $\tilde{N}$ applying equation (4.10) to a segment of length N_e^b, as a function of the segment position and of the interface width. Unfortunately they could not invert the relation $\tilde{N}(N_e)$ and could only predict that $N_e/N_e^b < (\tilde{N}/\tilde{N}^b)^{-1}$ thus giving an upper limit to the correction. They investigated three different widths ranging from $a_I \approx 1.5L_e$ to $a_I \approx 2.6L_e$, and found that even for the narrower interface $N_e/N_e^b < 2$, in agreement with our results.

4.5 Corrections to fracture energy calculations

We want now to show how the results of the previous section affect the fracture energy calculations presented in chapter 3, but we need first to refine the entanglement model proposed in that chapter. In section 3.1 we assumed to know the exact position of the entanglements and showed that such approximation is good enough to compute Σ_{eff}. However, in such a simplified model, it is difficult to take into account the fact that M_e depends on the absolute position in space. For this reason a slightly different treatment of entanglements is required.

We consider a continuous chain and use the monomer number along the chain n as a curvilinear coordinate. To avoid confusion with the definition of n given in chapter 3, in this section we will always write explicitly N/N_e. We also define a density of entanglements along the chain $\rho_e(n)$, with the property that $\rho_e(n)dn$ is the number of entanglement between n and $n + dn$. As a first approximation we can imagine that all the positions are equivalent and that $\rho_e(n) \equiv 1/N_e$, except for monomers near the chain ends. For consistency with the discrete model of Mikos and Peppas [2], that we adopted in the calculation of Σ_{eff}, we assume that monomers within a distance of $N_e/2$ from the chain end cannot be entangled. We then write

$$\rho_e(n) = \frac{\theta(n - N_e/2) - \theta(n - (N - N_e/2))}{N_e}, \tag{4.39}$$

where $\theta(n)$ is the step function (3.31). It follows that the total number of entanglements is

$$\int_0^N dn\rho_e(n) = \frac{N}{N_e} - 1, \tag{4.40}$$

which is in agreement with our previous model. For the sake of clarity $\rho_e(n)$ is also plotted in Figure 4.8.

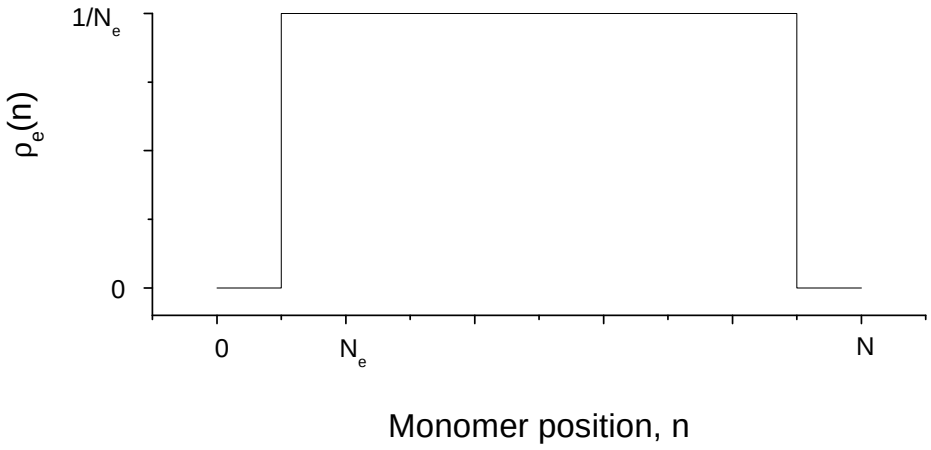

Figure 4.8: Density of entanglement along the chain used in the calculation of Σ_{eff}.

Moreover, in chapter 3 we assumed that two consecutive entanglements are always separated by N_e monomers, and we want to maintain this assumption. It follows that, as a consequence of equation (4.39), an effectively entangled strand can start only at positions $N_e/2 < n < N - 3/2N_e$. We then replace formula (3.19) with

$$\Sigma_{\text{eff}} = \frac{2\rho_b}{N} \int_{N_e/2}^{N-3/2N_e} dn\rho_e(n) \left[\int_{-\infty}^{0} dx \int_0^{\infty} dx' q(x; n) G(x, x'; N_e) q(x'; N - n - N_e) \right], \tag{4.41}$$

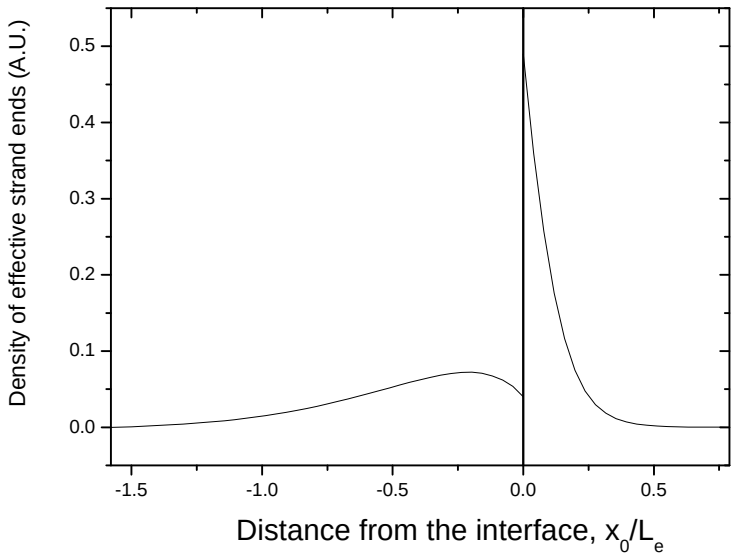

Figure 4.9: Typical density of the ends of effectively entangled strands. The total number of ends is, of course, the same on each side of the interface and equals Σ_{eff}.

where $\rho_e(n) \equiv N_e^{-1}$ within the limits of integration.

This formula has the advantage that it automatically gives the correct (real) number of entanglements along the chain and averages over all their possible positions. We note that the two expressions (3.19) and (4.41) are equivalent for the bulk case, where we used a real number of entanglements, while in general the first one is obtained from the second one by using a simple discrete approximation for the integral in dn, the only slight difference being in the treatment of chain end effects. For completeness we checked that, for the samples we studied, the Σ_{eff} computed with the two methods differ by less than 2 %, as it will be shown in Figures 4.11 and 4.12.

It is now easier to consider in the calculation of Σ_{eff} the appropriate value of N_e at the interface. We proved that N_e is significantly different from the bulk value only if the strand is within a distance $2L_e$ of the interface. Since all the effectively entangled strands cross the interface, they are likely to start very close

to the interface, as shown in Figure 4.9, where we plot a typical density of the ends of the effectively entangled strands on both sides of the interface. More precisely, we can estimate that more than 95 % of all the strands contributing to Σ_{eff} starts within a distance of L_e from the interface. Strands starting farther have a negligible probability of being effective. The correct N_e to be used in equation (4.41), that we will call $\bar{N}_e$, is therefore different from N_e^b and depends on the interface width. In principle $\bar{N}_e$ should be a function of the position of the strand in space, but as a first approximation we use a constant value. The simplest choice is to obtain $\bar{N}_e$ by weighting $N_e(x_0)$ with the volume fraction of the polymer over a small region around the interface, i.e.

$$\bar{N}_e = \int_{-L_e}^{L_e} N_e(x_0)\phi(x_0)dx_0 \Big/ \int_{-L_e}^{L_e} \phi(x_0)dx_0 \; . \tag{4.42}$$

We believe that the above expression is an appropriate value to estimate the order of magnitude of the corrections to Σ_{eff}, even if it contains many simplifications. The most important is probably the choice of using a single average value, but this is the most difficult to relax. In order to take into account that strands starting at different points in space have different lengths, a much more sophisticated treatment of entanglements would be required, but this is still a challenging problem for all the scientific community. Some comments must be made on our particular choice of $\bar{N}_e$. We have already explained why we are restricting ourselves to a particular region of space close to the interface, and we stress again that we are interested in the *local* density of entanglements. It follows that the $\bar{N}_e$ we use is not the correct average value for a whole chain, many monomers of which will be far from the interface, but it is correct for all the portions of chains that we are considering. Another simplification of equation (4.42) is that it ignores completely the position of the strand along the chain. In practice we compute N_e for the central segment of a chain, that is considering $\Delta = N/2$, and then weight it with the overall density of monomers. A more rigorous treatment would be take the average over all possible positions along the chain, but, recalling the discussions in the previous section, we believe that our simplified treatment is accurate enough and, even more, it is correct

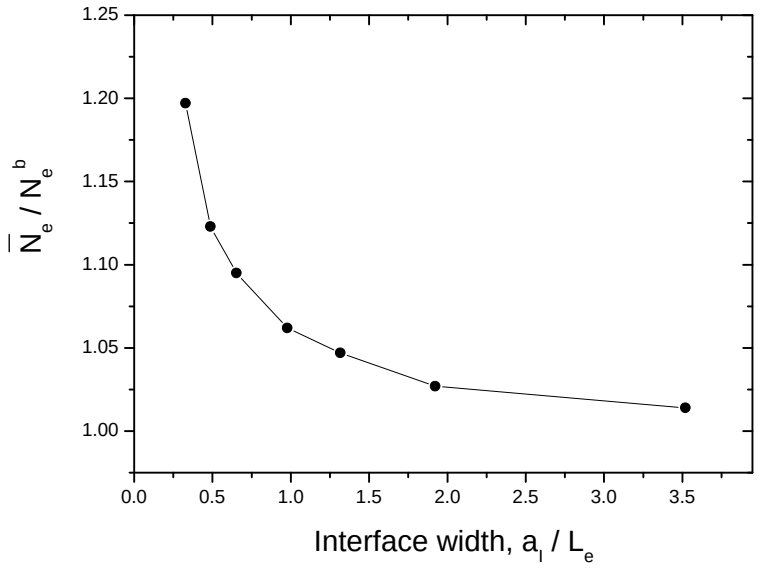

Figure 4.10: Mean value of the spacing between entanglements in the region of the interface, calculated from eq.(4.42), as a function of the interfacial width for the same illustrative systems system as in Figures 4.3, 4.4 and 4.5.

for long chains. We add here that a more sophisticated approach is probably useless, given the strong approximations made so far.

Before investigating the real systems, we perform numerical calculations on the same illustrative system for which Σ_{eff} and N_e have already been obtained respectively in chapter 3 and in the previous section. The $\bar{N}_e$ for this system has been computed by formula (4.42) and it is reported in Figure 4.10 as a function of the interfacial width.

In Figure 4.11 we plot the effective density Σ_{eff} obtained from equation (4.41), using $\bar{N}_e$ (solid line) and N_e^b (dashed line). Circles represent the curve obtained in chapter 3 from equation (3.19), that is plotted in order to show the agreement between the discrete and continuous descriptions of entanglements. We see that corrections to previous calculations are more significant for narrow interfaces, but they are present also in wider ones. Having in mind equation (4.41), we now discuss in detail how the final Σ_{eff} is affected by the use of $\bar{N}_e$ instead of N_e^b. The space

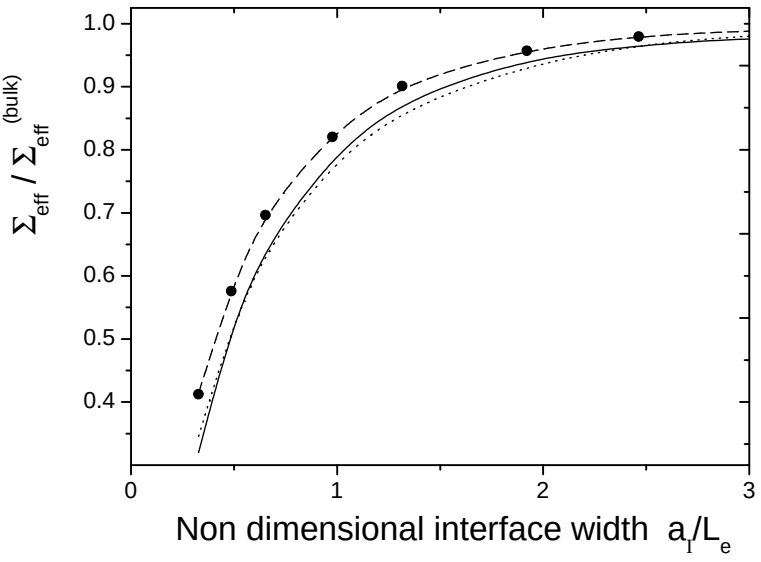

Figure 4.11: Density of effectively entangled strands as a function of the interfacial width, for the same illustrative system of the previous figure. Σ_{eff} has been computed from equation (4.41) using $N_e = \bar{N}_e$ (solid line) and $N_e = N_e^b$ (dashed line). In dotted line we plot the curve obtained for $N_e = N_e^b$ multiplied by a factor $N_e^b/\bar{N}_e$. Circles are taken from Figure 3.2.

integrals involving the Green function grows with the molecular weight of entanglement, but, even for narrow interfaces, we found that this effect produces corrections of less than 1% in the final density Σ_{eff}. The substitution of N_e in the integration limits has a comparable impact on the computed Σ_{eff}, but in the opposite direction, since a greater N_e tends to exclude the more mobile monomers from the integral. We therefore conclude that the greatest change in Σ_{eff} is due to a decreased average number of entanglements per chain. This is taken into account by $\rho_e(n)$, that corrects the bulk Σ_{eff} by a factor $N_e^b/\bar{N}_e$. This conclusion is confirmed by Figure 4.11 in which we plotted, as the dotted line, the Σ_{eff} obtained using N_e^b in equation (4.41) and multiplying the result by the factor $N_e^b/\bar{N}_e$. The curve seems to agree with the one obtained by the full calculations (solid line).

In real systems we found the same effects. In Figure 4.12 we report the Σ_{eff} cal-

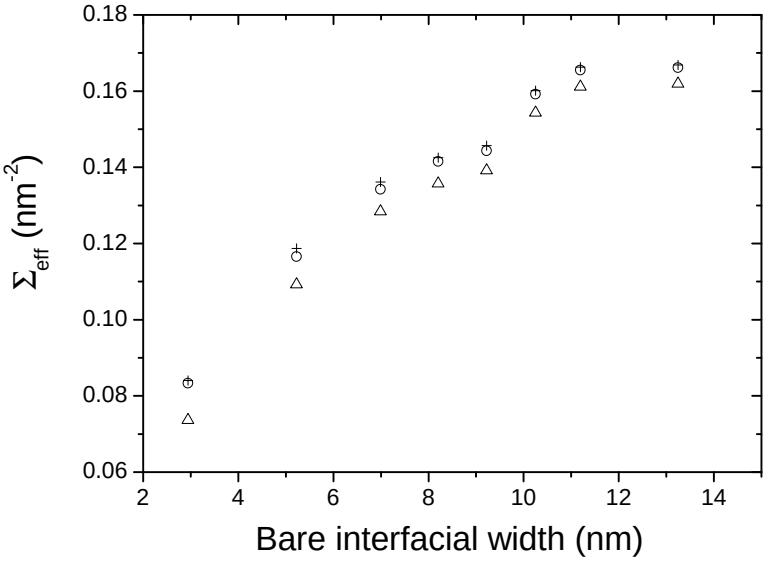

Figure 4.12: Areal density of effectively entangled chains Σ_{eff} for PS/P(S-r-MMA) interfaces. Circles represent the values calculated in chapter 3, pluses and triangles are obtained from equation (4.41) respectively for $N_e = N_e^b$ and $N_e = \bar{N}_e$.

culated in chapter 3 for PS-P(S-r-MMA) (circles) together with the curves obtained by equation (4.41) using N_e^b (pluses) and $\bar{N}_e$ (triangles). We see that the continuous and discrete approaches give nearly identical results, and that the corrections are significant for all samples.

The corresponding corrections to the fracture energy are shown in Figure 4.13 and, at first sight, are quite surprising: narrow interfaces seem to be unaffected, while for wider ones a significantly smaller fracture energy is predicted. From Figure 4.12 we can check that the corrections to Σ_{eff} are bigger for narrow interfaces, as expected, but this is not the case for the fracture energy. The explanation is simple if we recall that different failure mechanisms occur depending on the value of Σ_{eff}. The PS/PMMA interface, that is the narrowest sample, is predicted to fail by chain scission, implying that $G_c \propto N_e \Sigma_{\text{eff}}$. Since we showed that the density is approximately corrected by a factor inversely proportional to N_e, it is easy to conclude that the final fracture energy in the chain scission regime is practically unchanged. A

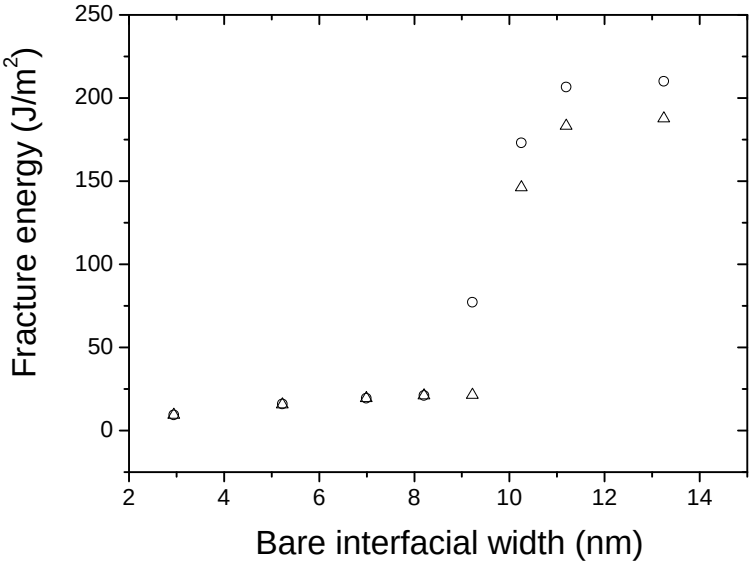

Figure 4.13: Fracture energy calculated for PS/P(S-r-MMA) interfaces from the Σ_{eff} showed in Figure 4.12 with the same symbols.

small effect can be seen in the samples that fail by partial crazing, but even in those cases the fracture energy is changed by less than 1 J/m^2, because the interfaces are larger and because the ultimate fracture mechanism is, again, the chain scission. In the case of failure by crazing the fracture energy is obtained from equation (3.41), and significant corrections are obtained even for small changes in Σ_{eff}. We also note that the biggest correction is observed at a width of about 9 nm and it is due to the fact that the corresponding sample is no longer predicted to fail by crazing, but by partial crazing.

We can conclude that considering an appropriate N_e for the interface does not change drastically the results obtained with N_e^b. The main corrections to this latter calculations are a lowering of the crazing fracture energies and a shift of the critical width at which transition to complete crazing occurs.

For these reasons in the case of PS/PpMS interfaces all the fracture energies are expected to be slightly lower than the ones obtained in chapter 3, without displaying

any other interesting effect.

4.6 M_e in thin films

Thin polymeric films are widely studied and their properties are expected to be greatly influenced by chain packing effects [71],[91],[92]. They are also interesting from a technological point of view, being commonly used as lubricants, or as dielectric layers in microelectronic devices. Moreover, Brown and Russell suggested that M_e could be measured by deformation tests on ultrathin films [71] and such experiments are currently being performed. We believe that their results will allow to test the main features of the approach proposed in this chapter. For these reasons we decided to apply the packing model of entanglements to thin films and to present in this section a quantitative estimate of M_e.

The problem of a solid-homopolymer melt interface has been treated by many authors [93]-[104], and it can be said that the conformation of surface chains is pretty well known. Many theoretical approaches are available to describe chain packing at surfaces [93]-[100] and computer simulations allow to test them with great accuracy [101]-[104]. We will adopt the simple approach proposed by Silberberg [99], which predicts the correct large scale features of chain conformations and is therefore suitable for our purposes. In Silberberg's model a solid surface is treated as a reflective barrier [105]-[108], and, from a mathematical point of view, this implies that the diffusion equation for the Green function satisfies a reflecting boundary condition at the interface [109]. In one dimension and in the absence of truly external fields, i.e. for $U_e \equiv 0$, it is easy to verify that the solution of equation (3.3) with additional reflective boundary conditions at $x = 0$, is

$$G(x', x; N) = \frac{\beta_N}{\sqrt{\pi}} \exp\left[-\beta_N^2 (x' - x)^2 - \beta_N^2 (x' + x)^2\right], \tag{4.43}$$

which satisfies

$$G(x', x; N) = G(x', -x; N). \tag{4.44}$$

Considering only the half space $x > 0$, we note that the above Green function is properly normalized to 1, implying that $q(x; n) \equiv 1$ and that the polymer density is constant everywhere. More sophisticated approaches have shown that, near the surface, the density is indeed different from the bulk value, but only in a small region, whose dimensions are comparable with the Kuhn statistical segment length. The magnitude and sign of this deviation from bulk density depend on the interaction energy between the polymer and the surface; constant density is obtained only when a specific small attractive energy is considered, compensating for the repulsion due to loss of entropy [100]. Nevertheless computer simulations [102] have demonstrated that conformational properties of chains longer than 5-6 statistical segments, are predicted with great accuracy by the simple treatment of Silberberg. Moreover they showed how, on the length scale of statistical segments, interfacial properties are independent of surface-segment energetics, compressibility and chain length.

Since we are mainly interested in conformational properties on the length scale of entanglements, that are usually made of about 100 monomers, it is reasonable to adopt a reflective surface statistics and to apply it to thin films. In this framework we describe a film of thickness L as a region of space included between two reflecting barriers placed at $x = 0$ and $x = L$. Considering multiple reflections, the appropriate one dimensional Green function for $0 < x < L$ can be obtained as

$$G(x, x'; N) = \frac{\beta_N}{\sqrt{\pi}} \sum_{i=-\infty}^{\infty} \exp\left[-\beta_N^2 \left(x - x' + 2iL\right)^2 - \beta_N^2 \left(x + x' + 2iL\right)^2\right], \quad (4.45)$$

and again produces a constant polymer density in the whole film. The radius of gyration of the test segment can be numerically computed for films of different thicknesses and for all the possible starting points using equations (4.31), (4.32) and (4.35). It is important to point out that, due to the use of Gaussian Green functions, the radius of gyration of the test segment is independent of its position along the chain.

Results for 4 different film widths are shown in Figure 4.14. The scaled radius of gyration is plotted as a function of the distance of the strand's starting point from one of the film surfaces. We note that strands are more packed only if they

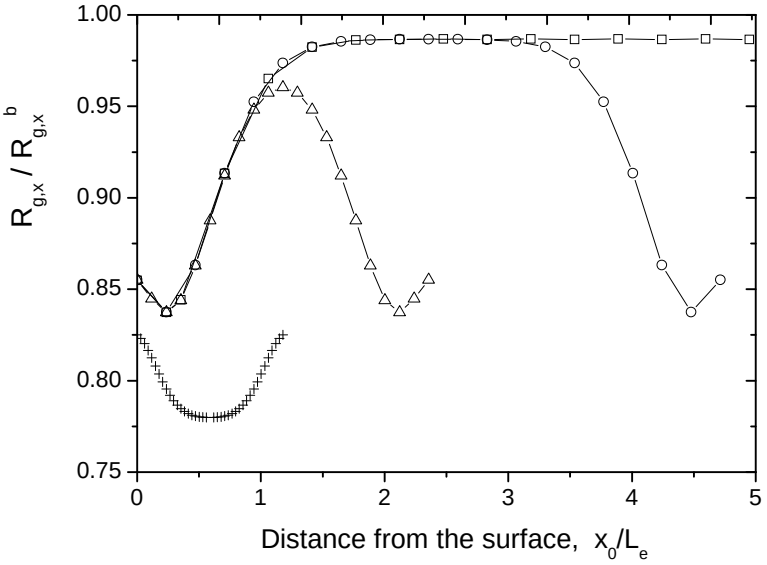

Figure 4.14: Scaled radius of gyration in the x direction calculated for a test segment made of N_e^b monomers as a function of its distance from the surface of a thin film. Four different film thicknesses are considered: L=7.2 (squares), 4.8 (circles), 2.4 (triangles) and 1.2 (pluses) L_e.

start within a distance of about L_e from the surface and that curves obtained for the three largest widths can be exactly superimposed. Consequently, in wide films the relative radius of gyration is significantly different from 1 only near the interface, while in very narrow films it tends to be constant and much smaller than 1. Two limiting cases can be studied analytically to check the numerical calculations. For an infinitely thick film, that is to say for a melt near an impenetrable wall, chains starting exactly on the surface satisfy $R_{g,x}/R^b_{g,x} = \sqrt{2(1-2/\pi)} \approx 0.85$, as confirmed by the numerical results. When $L \to 0$ the Green function is a constant, $G(x, x'; N) \equiv 1/L$, so that the radius of gyration in the x direction becomes independent of the position of the chain and satisfies $R_{g,x} = L/\sqrt{12}$. Since all the strand's monomers are involved in the calculation of the radius of gyration, this limit is properly reached only when the film thickness is comparable with the Kuhn segment length.

The mean entanglement spacing is found from the radius of gyration by numerical inversion of the criterion (4.18). The results are shown in Figure 4.15 for two

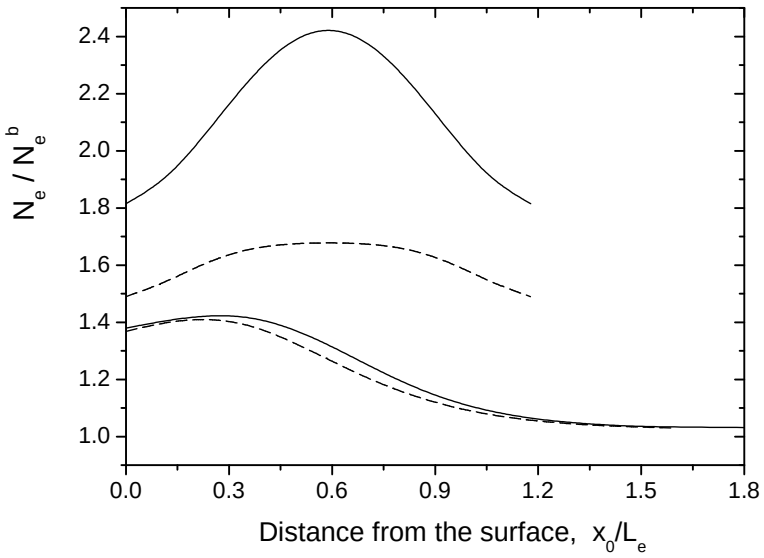

Figure 4.15: Scaled mean spacing between entanglements as a function of its distance from the surface of a thin film, calculated by inversion of equation (4.18) (solid lines). Dashed lines represent the same quantity, as obtained from approximate equation (4.21). Two different film thicknesses are considered: L=7.2 and 1.2 L_e.

representative film thicknesses $L = 7.2L_e$ and $L = 1.2L_e$. We note that for the former sample, the computed N_e has the same behavior and order of magnitude as the one previously obtained for narrow interfaces, confirming our expectations. In this situation equation (4.21) gives very similar results, from which we conclude that for chains starting exactly at the interface or very far from it the radius of gyration is still proportional to the square root of the chain length. Much higher values of N_e are found for a film thickness of $L = 1.2L_e$, in which case equations (4.21) and (4.18) give completely different results.

The behavior of very thin films is also shown in Figure 4.16, where we report the average value of N_e through the whole film. It can be observed that significant corrections to the bulk N_e are predicted when $L < 2L_e$. For films narrower than a certain critical width $L_c \approx L_e$ it is impossible to invert the entanglement criterion (4.18) because the radius of gyration is no longer a function of N_e, but only of the

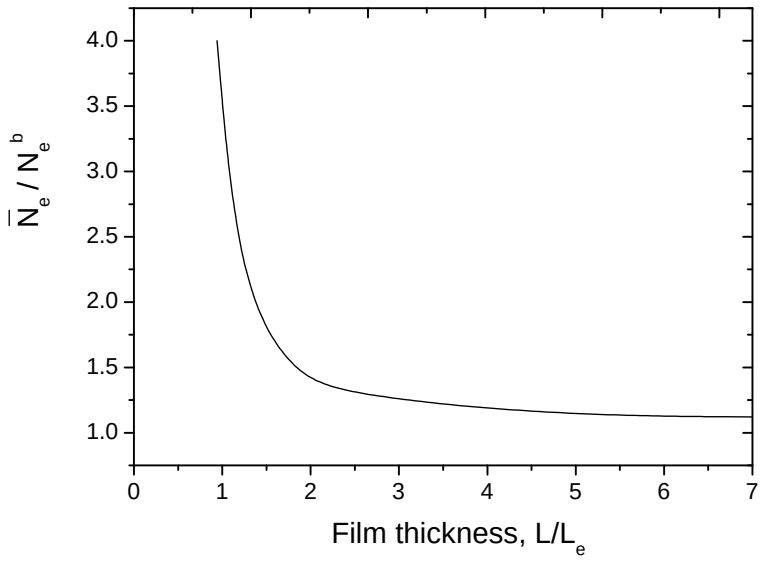

Figure 4.16: Average value of the mean entanglement spacing vs film thickness.

film thickness. For such small thicknesses it is then predicted that the chains cannot entangle.

Chapter 5

Conclusions

The theoretical investigation of the toughness of interfaces between glassy polymer undertaken in this thesis work lead to the formulation of a new model to calculate the dependence of the fracture energy on the interfacial width and on the molecular weight of polymer. Simulations produced with this model display a very good agreement with literature experimental data. Its main, and most original features with respect to previous literature models, are summarized below.

The model contains a new method to calculate the effective density of entangled strands across asymmetric interfaces, based on a main field description of chains.

A failure mechanism never taken into consideration before is properly taken into account. It consists in a "partial crazing", meaning an intermediate regime where craze formation starts but it cannot fully develop, resulting only in a small plastic deformation.

Properties of entanglements at interfaces and surfaces, scarcely known and generally assumed to be the same as in the bulk, were also studied. In particular the molecular weight between entanglements in inhomogeneous systems was studied, for which a new entanglement criterion derived from bulk packing models was proposed. This criterion was then adopted to compute M_e in interfaces and thin films, leading to some of the first estimates of this kind in the literature.

An alternative description of entanglements was developed, introducing an entanglement density distribution; in this way it was possible to take into account in

the calculations the appropriate value of M_e at interfaces, finding significant correlations to the fracture energies computed with the bulk value of M_e.

Future lines of work for the approach proposed in this thesis should include a refined description of entanglements treated as stochastic processes, thus relaxing some of the main approximation assumed in this thesis. In this context it would be extremely important to devise appropriate experiments to test these new entanglement theories.

List of publications

1. L. Silvestri, H.R. Brown, St. Carr and Se. Carr, *"Chain entanglements and fracture energy in interfaces between immiscible polymers"*, *J. Chem. Phys.*, to be published.

2. L.Silvestri, St. Carr and Se. Carr, *"A thermodynamic approach to the fracture energy of interfaces between glassy polymers"*, in *Proceedings of the 26th Annual Meeting of the Adhesion Society* (Adhesion Society, 2003).

3. F.Bassani , L.Silvestri and G.Czajkowski, *"Electromagnetically induced transparency in asymmetric double Quantum Wells"*, in *Radiation-Matter Interaction in Confined Systems - dedicated to the memory of Giovanna Panzarini.* Edited by L.C. Andreani, G.Benedek and E.Molinari (Italian Physical Society, Bologna, 2002).

4. L.Silvestri, F.Bassani, G.Czajkowski and B.Davoudi, *"Electromagnetically induced transparency in asymmetric double Quantum Wells"*, *The European Physical Journal B*, **27**, 89 (2002).

5. L.Silvestri, F.Bassani and G.Czajkowski, *"Electromagnetically Induced Transparency in Quantum Wells"*, *Physica Status Solidi (a)*, **190**, 683 (2002).

6. G.Czajkowski and L.Silvestri, *"Electric and magnetic field effects on optical properties of excitons in semiconductor nanostructures"*, in *Electrons and photons in solids - A volume in honour of Franco Bassani*, (Scuola Normale Superiore - Pubblicazioni della classe di scienze, Pisa, 2001).

7. G.Czajkowski, F.Bassani and L.Silvestri, *"Electric and magnetic field effects on optical properties of excitons in parabolic quantum wells and quantum dots"*, *Physica Status Solidi (a)*, **188**, 1281 (2001).

8. F.Bassani, L.Silvestri and G.Czajkowski, *"Electric and magnetic field effects on optical properties of excitons in Quantum Dots"*, in *Proceedings of the 25th International Conference on the Physics of semiconductors, 17-22 Sept. 2000, Osaka.* Edited by N.Miura and T.Ando (Springer Verlag, Berlin, 2001).

9. G.Czajkowski, F.Bassani and L.Silvestri, *"Magneto-optical properties of excitons in low dimensional semiconductor structures"*, in *Proceedings of the Conference: Atoms, Molecules and Quantum Dots in Laser Fields: Fundamental Processes, Pisa, Italy, June 12-16, 2000.* Edited by A. Rizzo (SIF, Bologna, 2000).

Bibliography

[1] L. Silvestri, H.R. Brown, St. Carrà, and Se. Carrà, *J. Chem. Phys.*, to be published.

[2] A.G. Mikos and N.A. Peppas, *J. Chem. Phys.* **88**, 1337 (1988).

[3] P.J. Flory, *Principles of Polymer Chemistry* (Cornell University Press, Ithaca, NY, 1953).

[4] P.G. de Gennes, *Scaling Concepts in Polymer Physics* (Cornell University Press, Ithaca, NY, 1979).

[5] M. Doi and S. F. Edwards, *The theory of polymer dynamics* (Clarendon, Oxford, 1986).

[6] R.P. Wool, *Polymer Interfaces* (Hanser, München, 1995).

[7] R. A. L. Jones and R. W. Richards, *Polymers at Surfaces and Interfaces*, (Cambridge University Press, Cambridge, 1999).

[8] *Polymer Data Handbook* (Oxford University Press, Oxford, 1999).

[9] R. P. Wool, B.-L. Yuan, and O. J. McGarel, *Polym. Eng. Sci.*, **29**, 1340 (1989).

[10] Benbow, J. J. Pr. Phys. SOC. 1961, 78, 970.

[11] Berry, J. P. J . Polym. Scz. 1961, 50, 313; Berry, J. P. J . Polym. Sci. A 1964, 2, 4069.

[12] Kusy, R. P.; Katz, M. J. J . Mater. Sci. 1976, 11, 1475.

[13] E.J. Kramer *Adv. Polym. Sci.* **52/53**, 1 (1983).

[14] W. Döll, *Adv. Polym. Sci.* **52/53**, 105 (1983).

[15] E.J. Kramer, and L.L. Berger, *Adv. Polym. Sci.* **91/92**, 1 (1990).

[16] G. J. Lake and A. G. Thomas, *"The strength of highly elastic materials", Proc. Roy. Soc. Lond.*, **300**, 108 (1967).

[17] H.R. Brown, *Macromolecules* **24**, 2752 (1991).

[18] E. Helfand and Y. Tagami *J. Chem. Phys.* **56**, 3592 (1972).

[19] E. Helfand and A.M. Sapse, *J. Chem. Phys.* **62**, 1327 (1975).

[20] E. Helfand, *J. Chem. Phys.* **62**, 999 (1975).

[21] E. Helfand, *Macromolecules* **8**, 552 (1975); E. Helfand, *J. Chem. Phys.* **63**, 2192 (1975); E. Helfand, S.M. Battacharjee, and G.H. Fredrickson, *J. Chem. Phys.* **91**, 7200 (1989).

[22] J.M.H.M. Scheutjens and G.J. Fleer, *J. Phys. Chem.* **83**, 1619 (1979); **84**, 178 (1980).

[23] K.M. Hong, and J. Noolandi, *Macromolecules* **14**, 727 (1981); K.M. Hong, and J. Noolandi, *Macromolecules* **14**, 736 (1981).

[24] K.M. Hong, and J. Noolandi, *Macromolecules* **14**, 1229 (1981).

[25] K. R. Shull and E.J. Kramer, *Macromolecules* **23**, 4769 (1990).

[26] K. R. Shull, *J. Chem. Phys.* **94**, 5723 (1991).

[27] K. R. Shull, *Macromolecules* **25**, 2122 (1992).

[28] K. R. Shull, *Macromolecules* **26**, 2346 (1993).

[29] G.H. Fredrickson, V. Ganesan, and F. Drolet, *Macromolecules* **35**, 16 (2002).

[30] J.W. Cahn, and J.E. Hilliard, *J. Chem. Phys.* **28**, 258 (1958).

[31] J.F. Joanny, and L. Leibler, *J. Phys. (Paris)* **39**, 951 (1978).

[32] K.M. Hong, and J. Noolandi, *Macromolecules* **16**, 1083 (1983).

[33] H. Nakanishi, and P. Pincus, *J. Chem. Phys.* **79**, 997 (1983).

[34] K. Binder, and H.L. Frisch, *Macromolecules* **17**, 2928 (1984).

[35] P.G. de Gennes, *J. Chem. Phys.* **72**, 4756 (1980).

[36] H. Tang, and K.F. Freed, *J. Chem. Phys.* **94**, 6307 (1991).

[37] H. Tang, and K.F. Freed, *J. Chem. Phys.* **94**, 1572 (1991).

[38] D. Broseta, G.H. Fredrickson, E. Helfand, and L. Leibler, *Macromolecules* **23**, 132 (1990).

[39] R.J. Roe, *Macromolecules* **19**, 728 (1986).

[40] I.C. Sanchez, and R.H. Lacombe, *J. Chem. Phys.* **80**, 2352 (1976);R.H. Lacombe, and I.C. Sanchez, *J. Chem. Phys.* **80**, 2568 (1976); I.C. Sanchez, and R.H. Lacombe, *Macromolecules* **11**, 1145 (1978).

[41] J. Dudowicz, and K.F. Freed, *Macromolecules* **24**, 5076 (1991); J. Dudowicz, M.S. Freed and K.F. Freed, *Macromolecules* **24**, 5096 (1991); J. Dudowicz, and K.F. Freed, *Macromolecules* **24**, 5112 (1991).

[42] J. Dudowicz, and K.F. Freed, *Macromolecules* **29**, 8960 (1996); K.F. Freed, J. Dudowicz, and K.W. Foreman, *J. Chem. Phys.* **108**, 7881 (1998).

[43] U.K. Chaturvedi, U. Steiner, *et al.*, *Phys. Rev. Lett.*, **63**, 616 (1989).

[44] S.H. Anastasiadis, T.P. Russell, S.K. Satija, and C.F. Majkrzak, *J. Chem. Phys.* **92**, 5677 (1990).

[45] M.L. Fernandez, J.S. Higgins, *et al.*, *Polymer*, **29**, 1923 (1988).

[46] M. Stamm, and D.W. Schubert, *Annual Review of Materials Science*, **25**, 325 (1995).

[47] S.H. Anastasiadis, I. Gancarz, and J.T. Koberstein, *Macromolecules* **21**, 2980 (1988).

[48] A.V. Ermoshkin, and A.N. Semenov, *Macromolecules* **29**, 6294 (1996).

[49] T.P. Russell, R.P. Hjelm, and P.A. Seeger, *Macromolecules* **23**, 890 (1990).

[50] H. R. Brown, *J.Mater. Sci.* **25** 2791 (1990).

[51] H.R. Brown, K. Char, V. R. Deline, and P.F. Green, *Macromolecules* **26**, 4155 (1993).

[52] P. J. Cole, R. F. Cook, and C. W. Macosko, *Macromolecules* **36**, 2808 (2003).

[53] R. Schnell, M. Stamm, and C. Creton, *Macromolecules* **31**, 2284 (1998).

[54] R. Schnell, M. Stamm, and C. Creton, *Macromolecules* **32**, 3420 (1999).

[55] H.R. Brown, *Macromolecules* **34**, 3720 (2001).

[56] C. Creton, E. J. Kramer, C.-Y. Hui, and H. R. Brown, *Macromolecules* **25**, 3075 (1992).

[57] H.R. Brown, *Annual Review of Materials Science* **21**, 463 (1991).

[58] C.-A. Dai, E. J. Kramer, J. Washiyama and C.-Y. Hui, *Macromolecules* **29**, 7536 (1996).

[59] C. Creton, H. R. Brown, and V.R. Deline, *Macromolecules* **27**, 1774 (1994).

[60] E.J. Kramer, L.J. Norton, *et al.*, *Faraday Discussions* **98**, 31 (1994).

[61] P. G. de Gennes, *C. R. Acad. Sci. Sèrie II* **308**, 1401 (1989).

[62] Souheng J. Wu, *J. Polym. Sci., Part B: Polym. Phys.* **27**, 723 (1989).

[63] R.P. Wool, *Macromolecules* **26**, 1564 (1993).

[64] T.A. Kavassalis, and J. Noolandi, *Macromolecules* **21**, 2869 (1988).

[65] T.A. Kavassalis, and J. Noolandi, *Macromolecules* **22**, 2709 (1989).

[66] T.A. Kavassalis, and J. Noolandi, *Phys. Rev. Lett.*, **59**, 2674 (1987).

[67] L. J. Fetters, D. J. Lohse, D. Richter, T. A. Witten, and A. Zirkerl, *Macromolecules* **27**, 4639 (1994).

[68] T.A. Witten, S.T. Milner, and Z.-G. Wang, in *Multiphase Macromolecular Systems*, edited by B.M. Culbertson (Plenum, New York, 1989).

[69] Y.-H. Lin, *Macromolecules* **20**, 3080 (1987); Y.-H. Lin, *Macromolecules* **23**, 5292 (1990); Y.-H. Lin, and J.-H. Juang, *Macromolecules* **32**, 181 (1999).

[70] N. Heymans, *Macromolecules* **33**, 4226 (2000).

[71] H. R. Brown and T. P. Russell, *Macromolecules* **29**, 798 (1996).

[72] V. Ganesan, and V. Pryamitsyn, *Macromolecules* **35**, 9219 (2002).

[73] R. Oslanec, and H.R. Brown, *submitted for publication.*

[74] S.F. Edwards, *Proceedings of the Physical Society, London* **85**, 613 (1965).

[75] A.R.C. Baljon, and M. O. Robbins, *Macromolecules* **34**, 4200 (2001).

[76] J. Rottler, S. Barsky, and M. O. Robbins, Phys. Rev. Lett. **89** , 148304 (2002).

[77] L. L. Berger, *Macromolecules* **23**, 2926 (1990).

[78] Y. Sha, C.Y. Hui, A. Ruina and E.J. Kramer, *Macromolecules* **28**, 2450 (1995).

[79] J. J. Benkoski, G. H. Fredrickson and E. J. Kramer, *J. Polym. Sci. B: Polymer Physics*, **39**, 2363 (2001).

[80] G.H. Fredrickson, and S.T. Milner, *Phys. Rev. Lett.*, **67**, 835 (1991).

[81] J. Dudowicz, and K.F. Freed, *Macromolecules* **31**, 5094 (1998).

[82] R.P. Kambour, J.T. Bendler, and R.C. Bopp, *Macromolecules* **16**, 753 (1983).

[83] G. ten Brinke, F.E. Karasz, and W.J. MacKnight, *Macromolecules* **16**, 1827 (1983).

[84] C. Dai, B.J. Dair, K.H. Dai, C.K. Ober, E.J. Kramer, C.-Y. Hui, and L.W. Jelinski, *Phys. Rev. Lett.*, **73**, 2472 (1994).

[85] R. Kulasekere, H. Kaiser, J.F. Ankner, T.P. Russell, H.R. Brown, C.J. Hawker, and A.M. Mayes, *Macromolecules* **29**, 5493 (1996).

[86] K.I. Winey, M.L. Berba, and M.E. Galvin, *Macromolecules* **29**, 2868 (1996).

[87] A.N. Semenov, *Macromolecules* **26**, 6617 (1993); *Macromolecules* **27**, 2732 (1994).

[88] K. Shull, A.M. Mayes, and T.P. Russell, *Macromolecules* **26**, 3929 (1993).

[89] J. J. Benkoski, G. H. Fredrickson and E. J. Kramer, *J. Polym. Sci. B: Polymer Physics*, **40**, 2377 (2002).

[90] W. G. Jung and E. W. Fisher, *Makromol. Chem., Macromol. Symp.*, **16**, 281 (1988).

[91] P.G. de Gennes, *Eur. Phys. J. E*, **2**, 201 (2000).

[92] A.N. Semenov, *Phys. Rev. Lett.*, **80**, 1908 (1998).

[93] A. Silberberg, *J. Chem. Phys.* **48**, 2835 (1968).

[94] C.A.J. Hoeve, *J. Polym. Sci.* **30**, 361 (1970); **34**, 1 (1971).

[95] R.J. Roe, *J. Chem. Phys.* **60**, 4192 (1974).

[96] E. Helfand, *Macromolecules* **9**, 307 (1976); T.A. Weber, and E. Helfand, *Macromolecules* **9**, 311 (1976).

[97] E.A. Di Marzio, and R.J. Rubin, *J. Chem. Phys.* **55**, 4318 (1971).

[98] J.M.H.M. Scheutjens and G.J. Fleer, *Macromolecules* **18**, 1882 (1985).

[99] A. Silberberg, *Colloid Interface Sci.* **90**, 86 (1982); **125**, 14 (1988).

[100] K.F. Freed, *J. Chem. Phys.* **105**, 10572 (1996).

[101] D.N. Theodorou, *Macromolecules* **21**, 1391 (1988); **21**, 1400 (1988).

[102] I.A. Bitsanis, and G. ten Brinke, *J. Chem. Phys.* **99**, 3100 (1993).

[103] T. Pakula, *J. Chem. Phys.* **95**, 4685 (1991).

[104] S.K. Kumar, M. Vacatello, and D.Y. Yoon, *Macromolecules* **23**, 2189 (1990).

[105] C.A.J. Hoeve, E.A. Di Marzio, and P. Peyser, *J. Chem. Phys.* **42**, 2558 (1965).

[106] C.A.J. Hoeve, *J. Chem. Phys.* **43**, 3007 (1965).

[107] R.J. Roe, *J. Chem. Phys.* **43**, 1591 (1965); **44**, 4264 (1966).

[108] A. Silberberg, *J. Chem. Phys.* **46**, 1105 (1967).

[109] E.A. Di Marzio, *J. Chem. Phys.* **42**, 2101 (1965).